UNIVERSIDADE ESTADUAL PAULISTA
"JÚLIO DE MESQUITA FILHO"
Campus de Ilha Solteira

PROGRAMA DE PÓS-GRADUAÇÃO EM ENGENHARIA MECÂNICA

José Camilo Carranza López

On the synchronization of two metronomes and their related dynamics

Ilha Solteira
2017

UNIVERSIDADE ESTADUAL PAULISTA
"JÚLIO DE MESQUITA FILHO"
Campus de Ilha Solteira

PROGRAMA DE PÓS-GRADUAÇÃO EM ENGENHARIA MECÂNICA

José Camilo Carranza López

On the synchronization of two metronomes and their related dynamics

Tese apresentada à Faculdade de Engenharia – UNESP – Campus de Ilha Solteira, para obtenção do título de Mestre em Engenharia Mecânica.
Área de Conhecimento: Mecânica dos Sólidos

Prof. Dr. Michael John Brennan
Orientador
Prof. Dr. Bin Tang
Co-orientador

Ilha Solteira
2017

FICHA CATALOGRÁFICA
Desenvolvido pelo Serviço Técnico de Biblioteca e Documentação

C312s

Carranza López, José Camilo.
On the synchrnization of two metronomes and their related dynamics / José Camilo Carranza. -- Ilha Solteira: [s.n.], 2017
106 f. : il.

Tese (doutorado) - Universidade Estadual Paulista. Faculdade de Engenharia de Ilha Solteira. Área de conhecimento: Mecânica dos Sólidos, 2017

Orientador: Michael J. Brennan
Co-orientador: Bin Tang
Inclui bibliografia

1. Synchronozation. 2. Metronomes. 3. van der Pol oscillator. 4. Instantaneous frequency. 5. Tracker video analysis. 6. Basins of attraction.

unesp

UNIVERSIDADE ESTADUAL PAULISTA

Câmpus de Ilha Solteira

CERTIFICADO DE APROVAÇÃO

TÍTULO DA TESE: On the Synchronization of Two Metronomes and their Related Dynamics

AUTOR: JOSE CAMILO CARRANZA LOPEZ
ORIENTADOR: MICHAEL JOHN BRENNAN
COORIENTADOR: BIN TANG

Aprovado como parte das exigências para obtenção do Título de Doutor em ENGENHARIA MECÂNICA, área: MECANICA DOS SÓLIDOS pela Comissão Examinadora:

Prof. Dr. MICHAEL JOHN BRENNAN
Departamento de Engenharia Mecânica / Faculdade de Engenharia de Ilha Solteira

Prof. Dr. GUSTAVO LUIZ CHAGAS MANHAES DE ABREU
Departamento de Engenharia Mecânica / Faculdade de Engenharia de Ilha Solteira

Prof. Dr. MARCIO ANTONIO BAZANI
Departamento de Engenharia Mecânica / Faculdade de Engenharia de Ilha Solteira

Prof. Dr. PAULO JOSÉ PAUPITZ GONÇALVES
Departamento de Engenharia Mecânica / Faculdade de Engenharia de Bauru

Prof. Dr. DIEGO FRANCISCO LEDEZMA RAMIREZ
Faculdad de Ingeniería Mecánica y Eléctrica / Universidad Autonoma de Nuevo León

Ilha Solteira, 05 de junho de 2017

To my parents Rosa and Rodolfo
My Sisters Deisy and Rocío
My brother Néstor

And the love of my life Paola

Max…

ACKNOWLEDGEMENTS

I feel lucky and grateful to life for allowed me to share the last five years under supervision of such an exceptional person, Prof. Mike Brennan. Many thanks for all your smart supervisions and conversations, and the wise advices which hardly would have found in other places. It was a pleasure working with you. I really enjoyed it!

I would like to extend this acknowledgement to my co-supervisor Prof. Bin Tang, who being a hardworking intellectual can be such a kind and smiling person. Thanks a lot for all your help and support.

My family deserves and special place in this acknowledgements. My parents: Rosa and Rodolfo, my nice sisters Deisy and Rocío, and my wonderful brother Néstor. There is no way this work could be finished without all your support. Thanks for believing in me and for helping me in all the possible ways one can imagine. I love you all…

Paola, thank you for all your sacrifice, patience and love, there is no way I can give you back all what I've received from you. I must to be the luckiest man in the world.

Thanks to all my friends in Ilha Solteira for making my life easier and so happy during all this time.

Finally, I want to thank the Mechanical Engineering department at Unesp – Ilha Solteira for having given me the opportunity of being part of your group. It has been an enriching experience. I also want to thank Capes for the economic support during these years.

RESUMO

Nesta tese são investigadas, teórica e experimentalmente, a sincronização em fase e a sincronização em anti-fase de dois metrônomos oscilando sobre uma base móvel, a partir de um modelo aqui proposto. Uma descrição do funcionamento do mecanismo de escapamento dos metrônomos é feita, junto a um estudo da relação entre este e o oscilador de van der Pol. Também uma aproximação experimental do valor do amortecimento do metrônomo é fornecida. A frequência instantânea das respostas, numérica e experimental, do sistema é usada na analise. A diferença de outros trabalhos prévios, os dados experimentais têm sido adquiridos usando vídeos dos experimentos e extraídos com ajuda do software Tracker. Para investigar a relação entre as condições iniciais do sistema e seu estado final de sincronização, foram usados mapas bidimensionais chamados 'basins of attraction'. A relação entre o modelo proposto e um modelo prévio também é mostrada. Encontrou-se que os parâmetros relevantes em relação a ambos os tipos de sincronização são a razão entre a massa do metrônomo e a massa da base, e o amortecimento do sistema. Tem-se encontrado, tanto experimental quanto teoricamente, que a frequência de oscilação dos metrônomos aumenta quando o sistema sincroniza-se em fase, e se mantém a mesma de um metrônomo isolado quando o sistema sincroniza-se em anti-fase. A partir de simulações numéricas encontrou-se que, em geral, incrementos no amortecimento do sistema levam ao sistema se sincronizar mais em fase do que em anti-fase. Adicionalmente se encontrou que, para dado valor de amortecimento, diminuir a massa da base leva a uma situação em que a sincronização em anti-fase é mais comum do que a sincronização em fase.

Palavras-chave: Sincronização em fase. Sincronização em anti-fase. Oscilador de van der Pol, Metrônomos. Frequência instantânea. Basins of attraction, Tracker video analysis.

ABSTRACT

This thesis concerns a theoretical and experimental investigation into the synchronization of two coupled metronomes. A simplified model is proposed to study in-phase and anti-phase synchronization of two metronomes oscillating on a mobile base. A description of the escapement mechanism driving metronomes is given and its relationship with the van der Pol oscillator is discussed. Also an experimental value for the damping in the metronome is determined. The instantaneous frequency of the responses from both numerical and experimental data is used in the analysis. Unlike previous studies, measurements are made using videos and the time domain responses of the metronomes extracted by means of tracker software. Basins of attraction are used to investigate the relationship between initial conditions, parameters and both final synchronization states. The relationship between the model and a previous pendulum model is also shown. The key parameters concerning both kind of synchronization have been found to be the mass ratio between the metronome mass and the base mass, and the damping in the system. It has been shown, both theoretically and experimentally, that the frequency of oscillation of the metronomes increases when the system reaches in-phase synchronization, and is the same as an isolated metronome when the system synchronizes in anti-phase. From numerical simulations, it has been found that, in general, increasing damping leads the system to synchronize more in-phase than in anti-phase. It has also been found that, for a given damping value, decreasing the mass of the base results in the situation where anti-phase synchronization is more common than in-phase synchronization.

Key words: In-phase synchronization. Anti-phase synchronization. van der Pol damping. Metronomes. Basins of attraction. Instantaneous frequency. Tracker.

LIST OF FIGURES

Appendix A

LIST OF TABLES

LIST OF SYMBOLS

Symbol	Name	Units
m_1	Mass of metronome 1	kg
m_2	Mass of metronome 2	kg
M	Base mass	kg
r	Length from the pivot point to the pendulum bob of a metronome	m
x_1	Horizontal displacement of m_1	m
x_2	Horizontal displacement of m_2	m
x_M	Horizontal displacement of M	m
$\ddot{x}_1$	Horizontal acceleration of x_1	m/s^2
$\ddot{x}_2$	Horizontal acceleration of x_2	m/s^2
$\ddot{x}_M$	Horizontal acceleration of x_M	m/s^2
t	Time	s
g	Gravity	m/s^2
c	Linear viscous damping coefficient	Ns/m
b	Nonlinear viscous damping coefficient	Ns^3/m
x_C	Center of mass	Kg
z_1	Relative horizontal displacement of m_1	m
z_2	Relative horizontal displacement of m_2	m
z_0	Relative horizontal displacement of M	m
k	Equivalent metronome stiffness	N/m
k_1	Equivalent stiffness for metronome 1	N/m
k_2	Equivalent stiffness for metronome 2	N/m
C_{vPol}	Non-dimensional damping parameter	-
$\dot{z}_1$	Relative horizontal velocity of m_1	m/s
$\dot{z}_2$	Relative horizontal velocity of m_2	m/s
$\dot{z}_0$	Relative horizontal velocity of M	m/s
$\ddot{z}_1$	Relative horizontal acceleration of m_1	m/s^2
$\ddot{z}_2$	Relative horizontal acceleration of m_2	m/s^2
$\ddot{z}_0$	Relative horizontal acceleration parameter	m/s^2
$\hat{z}_1$	Non-dimensional relative horizontal displacement of m_1	-
$\hat{z}_2$	Non-dimensional relative horizontal displacement of m_2	-
$\hat{z}_0$	Non-dimensional relative horizontal displacement parameter	-
$\hat{z}_1'$	Non-dimensional relative horizontal velocity of m_1	-
$\hat{z}_2'$	Non-dimensional relative horizontal velocity of m_2	-
$\hat{z}_0'$	Non-dimensional relative horizontal velocity parameter	-
$\hat{z}_1''$	Non-dimensional relative horizontal acceleration of m_1	-

$\hat{z}_2''$	Non-dimensional relative horizontal acceleration of m_2	-
$\hat{z}_0''$	Non-dimensional relative horizontal acceleration parameter	-
X	Horizontal amplitude	m
X_1	Horizontal amplitude for x_1	m
X_2	Horizontal amplitude for x_2	m
X_M	Horizontal amplitude for x_M	m
$\mathbf{x}_1$	Mode shape for x_1	-
$\mathbf{x}_2$	Mode shape for x_2	-
$\mathbf{x}_3$	Mode shape for x_M	-
T_n	Natural period of oscillation	s
$\tilde{x}$	Hilbert transform of x	-
A_1, A_2, R	Phasors	-

θ_1	Angle from vertical for m_1	rad
θ_2	Angle from vertical for m_2	rad
θ_0	Non-dimensional angle	-
σ	Mass ratio	-
τ	Non-dimensional time	-
ω_n	Angular frequency/natural frequency	(rad/s)
μ	Damping ratio	-
Ω	Non-dimensional frequency	-
η	Stiffness difference/metronomes difference	-
α, φ	Angle	rad
$\dot{\theta}$	Instantaneous frequency	Hz
ρ	Amplitude ratio	-

CONTENTS

1 INTRODUCTION

1.1 Historical Background

The most general meaning of synchronization is to be correlated, or corresponding in-time behaviour of two or more processes (BLEKHMAN, 1997). According to the Dictionary (MERRIAM-WEBSTER, 2017) synchronous means: happening, existing, or arising at precisely the same time, recurring or operating at exactly the same periods. The history of synchronization is related to the history of development and improvement of precision and accuracy of pendulum clocks. The first report known about synchronization was written by Dutch scientist Christiaan Huygens in 1665, who noted, while working in the longitude problem, that two pendulum clocks hanging from a common support, adjust their oscillation to be the same and the pendulums move in opposite direction, i.e. they synchronize in anti-phase (PIKOVSKY; ROSEMBLUM; KURTHS, 2011).

In the XVII century the longitude problem was one of the most challenging problems. The position on the earth surface is determined by two numbers corresponding to latitude and longitude. Accurate data would help to reduce the risk of increasingly longer sea voyages of European vessels, making navigation safer and more profitable (DUNN; HIGGIT, 2014, p. 12). Mistakes in the calculation of longitude sometimes ended in catastrophes for crew and losses of load. In fact, to solve the longitude problem was so important that in 1598 the King of Spain offered a considerable prize for a means of finding longitudes at sea. This was followed by a large offer by the Netherlands (BELL, 1950, p. 35). Later in 1714 in England, the Longitude Act was established which offered £20,000 (the equivalent of millions of dollars today) for a method to determine longitude to an accuracy of half a degree of a great circle (SOBEL, 1995).

To calculate latitude with acceptable accuracy at that time was relatively easy, and was based on the position of sun at midnight together with a table of corrections of the inclination of the sun each day. In the calculating of longitude, it is known that a day comprises 24 hours, and that a circumference, e.g. at equator, has 360 degrees, therefore an hour corresponds to 15 degrees. Fifteen degrees displacement to the east adds one hour to the previous time and the same displacement to the west subtracts one hour. Thus a relationship between time and longitude exists and from the knowledge of the local time of two points it is possible to calculate longitude from their difference. To calculate local time was not a

problem but to calculate the time measured at the reference point, e.g. the port, while on a ship was the real problem. Huygens, among others scientists, believed that pendulum clocks could serve that purpose, but he faced another problem. The precision of a pendulum clock depends on the motion of its pendulum, and any disturbance on the pendulum causes malfunction of the clock, in an inaccurate time. Although is usual to credit Christiaan Huygens as the inventor of pendulum clocks, they already existed in the XVII century. Even the first mechanical clock appeared in the middle of the fourteenth century (RUXU; KONGHAN, 2013, p. 5). What probably happened is that the pendulum clock was invented independently by more than one person and Huygens provided the first theoretical and practical account of a pendulum clock and how the pendulum improved its accuracy (POOK, 2011, p. 43).

Huygens first observation of synchronization occurred while he was sick in bed during the time he was trying to solve the longitude problem. He left two pendulum clocks hanging from a common support, which rested on the back of two chairs, as shown in Figure 1.1, and noticed that after some time their oscillations coincided while moving in the opposite direction. Here is part of a letter that Huygens wrote to his father in 1665, which is the first report known about synchronization.

> While I was forced to stay in bed for a few days and made observations on my two clocks of the new workshop, I noticed a wonderful effect that nobody could have thought of before. The two clocks, while hanging [on the wall] side by side with a distance of one or two feet between, kept in pace relative to each other with a precision so high that the two pendulums always swung together, and never varied. While I admired this for some time, I finally found that this happened due to a sort of sympathy: when I made the pendulums swing at differing paces, I found that half an hour later, they always returned to synchronism and kept it constantly afterwards, as long as I let them go (PIKOVSKY; ROSEMBLUM; KURTHS, 2011, p. 357).

The reasons why he was experimenting with two pendulums clocks can be found in his own *Instructions Concerning the Use of Pendulum-Watches, for Finding the Longitude at Sea*: “Those that intend to make use of pendulum-watches at sea, must have two of them at least, that, if one of them should by misshape or neglect come to stop, or (being by length of time become foul) need to be clean, there may likely always remain one in motion” (HUYGENS, 1669). As well as to where the pendulum clocks should be hung: “The watches on ship-board are to be hung in a close place, where they may be freest from moisture or dust and out of danger of being disordered by knocking or touching” (HUYGENS, 1669). Dust and moisture, as well as perturbations from the ship, could affect the precision of pendulum clocks.

Figure 1.1 – The original drawing of Huygens' experiment on synchronization of pendulum clocks.

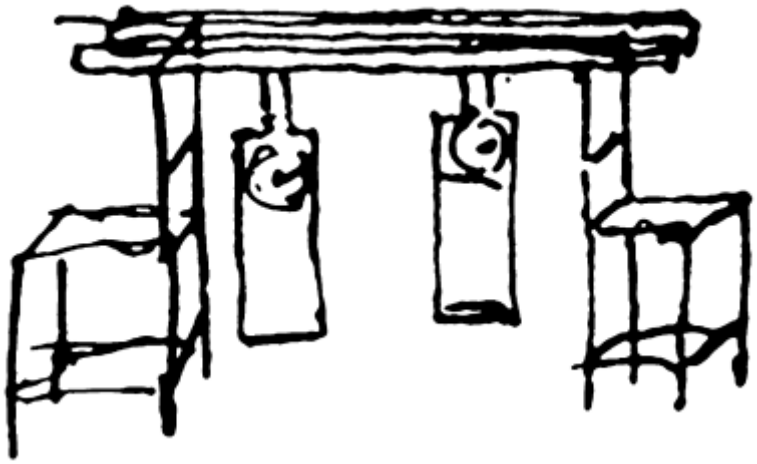

Source: Taken from (PIKOVSKY; ROSEMBLUM; KURTHS, 2011, p. 3)

The longitude problem was finally solved by John Harrison who invented a pocket chronometer for this purpose. However, the work of Huygens helped in the creation, improvement and understanding of pendulum clocks and his observations brought to light the synchronization phenomenon. After his observations, synchronization has been studied by many scientists and has been reported in several areas. Works about synchronization of biological systems are, for example (STROGATZ; STEAWARD, 1993; STROGATZ; STEAWARD, 2003).

1.2 Literature review

The first known work after the observations by Huygens was conducted by (ELLICOT, 1739, 1753) who carried out experiments mimicking the experiments by Huygens. He placed two pendulum clocks very close, sideway to one another (ELLICOT, 1739) and observed that if one clock is set to be at rest while the other is set to oscillate, the later transmits its motion to the former, while the motion of the first gradually decreases up to stop. Ellicot reported in short communications to the Royal Society, the conclusion that the two clocks mutually affected each other and. In common with Huygens, he observed that the influence from one to another was communicated by means of the common support.

Ellis (1873) also reported Huygens' experiments and published his observations in the form of a short communication. He also experimented with nine clocks at the same time.

After setting two clocks to oscillate in similar conditions as Huygens experiment, he verified the mutual influence, and that their oscillations modify and then keep the same frequency (the same difference in time shown by each clock day after day). He also found that pendulum clocks synchronized in anti-phase.

The first attempt to theoretically understand Huygens observations was provided by Korteweg (1906), based on a simplified undamped, undriven (without any escapement mechanism), 3DOF linear model consisting of two pendulums attached to a rigid frame. They were able to move in one direction, and represented some of the features of Huygens original system. Korteweg concluded from his model that anti-phase synchronization was much more dominant than in-phase synchronization.

Blekhman (1988) studied a laboratory reproduction of Huygens' coupled clock system, comprised of two pendulums connected to a rigid frame, which were constrained to oscillate in one dimension. He modeled the system as a three-degree-of-freedom system and used van der Pol damping (VAN DER POL, 1926, 1927; DEN HARTOG, 1985) to represent the escapement mechanism of the clocks. Bleckhman predicted that in-phase and anti-phase synchronization states are achievable and are stable under the same set of circumstances. The work by Blekhman is one of the most relevant concerning synchronization. Its importance comes from the absence in studies about synchronization in the area of mechanical engineering. Blekhman not only studied pendulum clocks but carried out in depth studies into synchronization of mechanical systems. In particular he studied coupled rotating vibro-exciters, e.g. coupled induction motors, for which it was known that they could synchronize under certain conditions (BLEKHMAN, 2000), and attempted to give a formal definition of synchronization (BLEKHMAN, 1997).

Bennett et al. (2002) studied a system composed of two pendulums hanging from a common movable frame free to move in one dimension. The pendulums were driven by an escapement mechanism. They found that the clocks synchronize in anti-phase when the system mass ratio is comparable with that reported by Huygens, and conclude from numerical simulations that in-phase synchronization is an unstable state, while anti-phase synchronization and oscillation-death are stable synchronization states. Shortly after, Pantaleone (2002) studied a system composed of two metronomes resting on a light wooden board resting on two empty soda cans. He modeled the metronomes using van der Pol oscillators and the coupling between them from an undamped motion of a mass-like base. In

contrast with Bennett et al. (2002) he concluded that the in-phase synchronization state is a stable state and suggested that anti-phase synchronization is unstable, he stated that anti-phase synchronization can be produced in a metronome system by either adding large damping to the base motion, or by having very large oscillation frequencies. Interestingly Veljko (2012) explained in detail the mathematical work necessary to understand the work by Pantaleone and included numerical simulations related to systems with more than two pendulums clocks. Senator (2006) studied a theoretical model following the Korteweg idea of analysing a related simplified system maintaining the main features of Huygens actual arrangement. His model included an escapement mechanism based on an adaptation of the model of Andronov and Chaikin (1949). Senator concluded that anti-phase synchronization is much more probable to occur than in-phase synchronization, for a wide range of parameters which include the possible parameters corresponding with Huygens original experiment.

More recently, additional work, including simulations and experiments, have been conducted by several researchers, for example (ULRICHS, 2009; CZOLCZYNSKI et al., 2007, 2009; DILÃO, 2009; PEÑA RAMIREZ, 2013) who have proposed systems intended to reproduce Huygens's original experience, and different models to analyze those systems. Most of them appear to be complex, leading to results and predictions which are difficult to understand and to compare with previous research.

In this thesis the conditions to obtain in-phase and anti-phase synchronization of two metronomes on a mobile base are investigated. For this purpose, a simplified three degree of freedom (3DOF) model has been proposed. This model has a more simple mathematical description compared with those of the previous works. It retains the important physics and is used to determine the main parameters concerning synchronization of the oscillators. Metronomes and pendulum clocks are nonlinear systems, specifically self-sustaining oscillators, since they can maintain a stable oscillation no matter (in theory) what the initial situation is (ANDRONOV; CHAIKIN, 1949, p. 116; STROKER, 1950) and their oscillation is entirely determined by the properties of the systems themselves (PIKOVSKY; ROSEMBLUM; KURTHS, 2011, p. 28). The escapement mechanism is the internal driven mechanism controlling the stable oscillation of metronomes and pendulum clocks (see Appendix 1). In this thesis the escapement mechanism is modelled as a van der Pol damping force (VAN DER POL, 1926, 1927) for convenience, which results in limit cycles (FIDLIN, 2006; NAYFEH; MOOK, 2002; THOMPSON; STEWART, 2002).

Theoretical and experimental displacement time histories from the in-phase and anti-phase synchronized system are processed by means of the Hilbert Transform (FELDMAN, 2011a, 2011b; BOASHASH, 1992; SHIN; HAMMOND, 2008) in order to determine the final synchronization state and to compare the frequencies of two metronomes. Measurements of the displacements of the pendulums bobs and the base are made with a camera and a freely available video analysis software.

To measure is the act of assigning a specific value to a physical variable. As such, a measurement system is used to extend the abilities of the human senses (FIGLIOLA; BEASLEY, 2011). For measuring high and middle range frequency oscillations it is usual to use accelerometers and velocity sensors (VENKATESHAN, 2015), which are contact measurement devices. Lasers displacement and proximity sensors which are non-contact measurement devices are also used e.g. for measuring vibration of rolling element bearings (TANDON; CHOUDHURY, 1999). However for the low frequencies of oscillation of metronomes a rather cheaper method can be employed to collect data based on videos and the use of image processing software.

Before the mass use of digital cameras, stroboscopic photography was used to collect data from bodies in motion. However the advances in technology in digital videos during the last two decades have enabled to easily collecting data from inexpensive cameras (BARBETA; YAMAMOTO, 2002), even those included in smartphones which allow the generation of short movies at rates of 15 and 30 frames per second (GIL; REISIN; RODRÍGUEZ, 2006). This is fast enough for the low frequencies of the metronome pendulums. Researchers have used these advances to improve experimental tests mainly for teaching purposes in physics (see e.g. (SIRISATHITKUL et al., 2013; GIL; REISIN; RODRÍGUEZ, 2006)).

In this work, data is extracted from videos of the experiments by means of video analysis software Tracker®. As its name implies, Tracker® analyses videos by tracking features of interest in the video image and then transforms the resulting data into real-world values and graphical overlays (BROWN, 2008). Examples of using Tracker® to extract data from images can be found in (GIL; REISIN; RODRÍGUEZ, 2006; SIRISATHITKUL et al., 2013; CHANPICHAI; WATTANAKASIWICH, 2010).

Finally in this thesis, the relationship between initial conditions (IC), main parameters and the final synchronization state of the system is investigated by means of basins of

attraction. More than ten thousand numerical integrations are used to construct such two dimensional maps. Basins of attraction have been seldom used in the investigation concerning synchronization, although they can be found in a few recent works. Czolczynski et al. (2009) used basins of attraction to show the possible final steady states of a system with 3 pendulums clocks. These steady states were: symmetrical synchronization, complete synchronization and desynchronous behaviour. Later they used basins of attraction to investigate how co-existing attractors of a 3DOF system, representing Huygens system of two clocks, are sensitive to the external perturbations. Once the system is synchronized either in-phase or in anti-phase, the system was perturbed and the final result is showed by the basins of attraction (CZOLCZYNSKI et al., 2011). Peña Ramirez (2013) also made use of a basin of attraction to investigate the relationship between coupling, parameters and initial conditions of its own nonlinear system used to investigate the synchronization of two pendulum clocks.

1.3 Objectives

The main aim of this thesis is to investigate the conditions to obtain in-phase and anti-phase synchronization of two metronomes on a mobile base. For this purpose the objectives are:

1. To develop a simplified model to investigate the in-phase and the anti-phase synchronization of two metronomes on a mobile base.
2. To investigate experimentally both kinds of synchronization and to verify the final frequency of each oscillator.
3. To investigate the relationship between initial conditions, parameters and the final synchronization states of the system.

1.4 Contributions to Knowledge

- A simplified lumped parameter model has been proposed to study in-phase and anti-phase synchronization of two metronomes on a mobile base. It has been shown that a relationship between this model and the previous pendulum model of Pantaleone (2002) exists. For the undamped system it has been shown that synchronization can be achieved provided that the ICs correspond exactly with their 2^{nd} and 3^{rd} normal modes of vibration. A detailed

description of the escapement mechanism of a metronome along with a description of the van der Pol oscillator and its common features are shown in appendixes. Also included is an experimental approximation of the damping coefficient for a metronome.

- A non-contact method to extract data from experiments concerning the synchronization of metronomes has been developed. The method is based on videos and the free software Tracker® available in internet. The instantaneous frequency extracted from measured data has been used to show that the frequency of oscillation of the coupled metronomes is the same, as for a single grounded metronome, when they synchronize in anti-phase, and when the metronomes synchronize in-phase their frequencies of oscillation increases, as predicted by the simplified model.

- The basins of attraction have been used to investigate the relationship between ICs, parameters and synchronization. Some insight has been given into how the system modifies its final synchronization state for some given sets of parameters.

- A value for the damping of the escapement mechanism has been calculated based on a perturbation method and experimental data.

1.5 Outline of Thesis

This thesis consists of 5 chapters and 2 appendixes. Chapter 1 introduces the topic of synchronization and provides a historical background, a literature review and specifies the main objectives of the thesis and the contributions to knowledge.

In chapter 2 the simplified lumped parameters model to investigate the in-phase and anti-phase synchronization of two metronomes on a mobile base is developed and analysed. The relationship between this model and the previous model by Pantaleone (2002) is discussed. Synchronization of an undamped system and later synchronization of a system with van der Pol damping, are investigated, both for similar and different natural frequencies of the metronomes. For both cases analytical expressions for the frequencies of oscillation of the undamped system when in-phase and anti-phase synchronization are derived.

In chapter 3 the Instantaneous Frequency (IF) of the metronomes is used to determine the final synchronization state of the system from both, numerical and experimental data. The methodology used to collect experimental data using videos, and the main features of the software used to extract time histories from the videos are described. Additionally, the relationship between the instantaneous frequency of a signal and the presence of higher harmonics in such a signal is discussed.

Chapter 4 investigates the relationship between initial conditions, system parameters and final synchronization states by means of the concept of basins of attraction, which are presented as two-dimensional colour maps. The axes of the maps correspond with the initial positions of the metronomes and a colour is used to each synchronization state of interest, so that for a given pair of initial positions, a coloured pixel is set in the map. The relationship between the final synchronization states and the ICs for various values of damping and ratios of metronome masses to base mass is investigated. Experimental results related to this investigation are shown.

Chapter 5 presents the summary and conclusions of the thesis. Some recommendations for further work are also given.

In Appendix 1 a detailed description of the escapement mechanism which drives the metronomes and two models to represent it are presented. The reasons on why the van der Pol oscillator has been chosen to model this system are also given.

In appendix 2 an approximation of the experimental damping value of a metronome is shown. It is calculated based on a comparison between the experimental and the theoretical envelopes of the time-domain displacements.

2 A SIMPLIFIED MODEL FOR TWO METRONOMES COUPLED BY A MASS

2.1 Introduction

The aim of this chapter is to introduce a simplified model to study the synchronization of two metronomes on a mobile base. Firstly, the relationship between the previous pendulum model of Pantaleone (2002) and the simple model is determined. Secondly, the simple model is used to study the in-phase and the anti-phase synchronization of the undamped system for similar and slightly different metronomes. Synchronization of the system with van der Pol damping is then studied for the same cases.

2.2 The Proposed Model and its Relationship with Previous Work

Figure 2.1 – Two metronomes supported by a mobile wooden base resting on empty soda cans to permit the base motion in the horizontal direction. (a) Sliding weight to set up the oscillation frequency, (b) pendulum bob, (c) wooden base and (d) empty soda can.

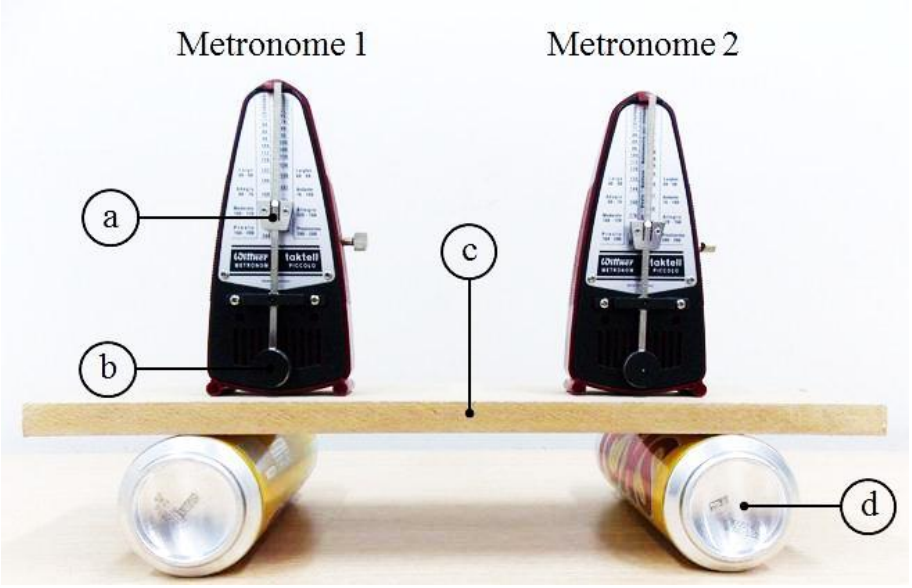

Source: Elaborated by the author

In 2002 Pantaleone proposed a simplified system with the aim of reproducing Huygens experiments, from which the first synchronization reports appear. Huygens original

set up was composed of two oscillating pendulum clocks hanging on a wooden base, resting on the top of two chairs capable of moving in the horizontal direction (see Figure 1.1 in Chapter 1). Pantaleone used two metronomes instead of pendulums clocks and placed them on top of a light wooden base resting on two soda cans, so that the base could move in the horizontal direction. Metronomes achieve synchronization much faster than pendulum clocks and are lighter and cheaper. Metronomes are driven by an escapement mechanism similar to that used in pendulum clocks, but instead of having weights it derives its energy from a spiral torsion spring. Figure 2.1 shows a picture of two metronomes on a wooden base, similar to Pantaleone's system which is of interest in this work (for a detailed description of the metronome and its escapement mechanism (see Appendix 1).

Figure 2.2 – Pantaleone's model for two metronomes oscillating on a mobile wooden base. The variables describing the dynamics of the system are the two angles that both pendulums bobs form with their own vertical axes and the horizontal displacement of the base.

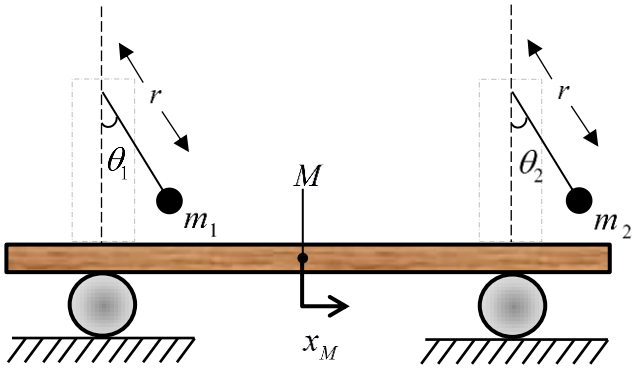

Source: Elaborated by the author.

Figure 2.2 depicts a model for the system shown in Figure 2.1. There are two angles θ_1 and θ_2 describing the positions of the pendulum bobs m_1 and m_2 from the vertical axis respectively, *r* is the constant length from the pivot point to the pendulum bob, and x_M is the horizontal displacement of the base of mass *M*, which includes the mass of the bodies of the metronomes. Figure 2.3 depicts the model for one metronome oscillating in a mobile base. Taking moments about *O* results in the equation of motion given by

$$m_1 r^2 \frac{d^2\theta_1}{dt^2} + m_1 g r \sin\theta_1 + m_1 r \frac{d^2 x_M}{dt^2} \cos\theta_1 = 0 \qquad (2.1)$$

Figure 2.3 – Force diagram for a single metronome of mass m_1 oscillating in a mobile base of mass *M*. The pendulum bob experiences the effect of the motion of the base as a horizontal force.

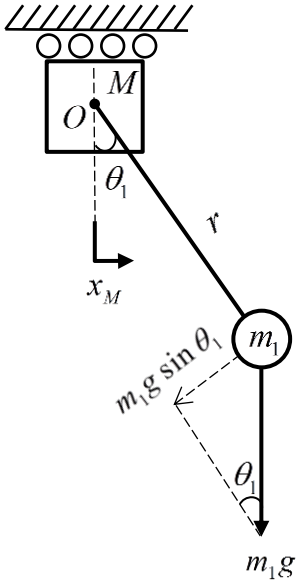

Source: Elaborated by the author.

where *g* is acceleration due to gravity. The two first terms are the usual terms describing the motion of a simple pendulum; they are related to the moment of inertia and the moment produced by tangential component of the gravitational force, which acts as the restoring force, acting on the pendulum bob. The third term is related to the moment of inertia of the pendulum bob due to the base motion. The escapement mechanism which drives the metronomes is crudely modelled as a damping mechanism (see Appendix 1). Together with inherent damping in the system it applies a damping moment given by

$$\text{Damping Moment} = \left(b\theta_1^2 - c\right) r^2 \frac{d\theta_1}{dt} \tag{2.2}$$

where c and b are the linear and the nonlinear viscous damping coefficients, respectively. Letting $\theta_0 = \sqrt{c/b}$, the tangential damping force acting on the pendulum bob can be written as $c\left(\left(\theta_1 \big/ \theta_0\right)^2 - 1\right) r \frac{d\theta_1}{dt}$. When θ is smaller than θ_0 energy is supplied to the system by the escapement mechanism, but when θ is larger than θ_0 energy is dissipated by the system (see Appendix 1). Inserting this into Eq. (2.1) and dividing Eq. (2.1) by *r* gives

$$m_1 r \frac{d^2\theta_1}{dt^2} + c\left[\left(\frac{\theta_1}{\theta_0}\right)^2 - 1\right] r \frac{d\theta_1}{dt} + m_1 g \sin\theta_1 + m_1 \frac{d^2 x_M}{dt^2} \cos\theta_1 = 0 \tag{2.3a}$$

Assuming the same form for the damping force, the equation of motion for the second metronome on the base can be written as

$$m_2 r\frac{d^2\theta_2}{dt^2}+c\left[\left(\frac{\theta_2}{\theta_0}\right)^2-1\right]r\frac{d\theta_2}{dt}+m_2 g\sin\theta_2+m_2\frac{d^2x_M}{dt^2}\cos\theta_2=0 \tag{2.3b}$$

It can be seen that the term coupling the equations is the acceleration of the base. It is desirable to write the displacement of the base mass x_M in term of θ_1 and θ_2. To do this, it is first noted that the center of mass for the system in Figure 2.2, x_C, is given by,

$$x_C=\frac{Mx_M+m_1\left(x_M+r\sin\theta_1\right)+m_2\left(x_M+r\sin\theta_2\right)}{M+m_1+m_2} \tag{2.4}$$

Assuming that m_1 and m_2 are equal and are given by *m*, then Eq. (2.4) can be written as

$$x_C=x_M+\frac{\sigma r}{1+2\sigma}\left(\sin\theta_1+\sin\theta_2\right) \tag{2.5}$$

where $\sigma=m/M$ is the mass ratio. Differentiating Eq. (2.5) twice with respect to time gives

$$\frac{d^2x_C}{dt^2}=\frac{d^2x_M}{dt^2}+\frac{\sigma r}{1+2\sigma}\frac{d^2}{dt^2}\left(\sin\theta_1+\sin\theta_2\right) \tag{2.6}$$

Now assuming no external forces are applied to the system, then $d^2x_C/dt^2=0$, so that

$$\frac{d^2x_M}{dt^2}=-\frac{\sigma r}{1+2\sigma}\frac{d^2}{dt^2}\left(\sin\theta_1+\sin\theta_2\right) \tag{2.7}$$

Substituting Eq. (2.7) into Eqs (2.3a) and (2.3b) gives

$$mr\frac{d^2\theta_1}{dt^2}+c\left[\left(\frac{\theta_1}{\theta_0}\right)^2-1\right]r\frac{d\theta_1}{dt}+mg\sin\theta_1-\frac{m\sigma r}{1+2\sigma}\cos\theta_1\frac{d^2}{dt^2}\left(\sin\theta_1+\sin\theta_2\right)=0 \tag{2.8a}$$

$$mr\frac{d^2\theta_2}{dt^2}+c\left[\left(\frac{\theta_2}{\theta_0}\right)^2-1\right]r\frac{d\theta_2}{dt}+mg\sin\theta_2-\frac{m\sigma r}{1+2\sigma}\cos\theta_2\frac{d^2}{dt^2}\left(\sin\theta_1+\sin\theta_2\right)=0 \tag{2.8b}$$

Equations (2.8a) and (2.8b) are the two equations describing the dynamics of the system in Figure 2.2 in terms of θ_1 and θ_2.

For $\theta_1 \ll 1$ and $\theta_2 \ll 1$, so that $\sin\theta_{1,2} \approx \theta_{1,2}$ and $\cos\theta_{1,2} \approx 1$ and letting $z_1 = r\theta_1$, $z_2 = r\theta_2$ and $z_0 = r\theta_0$ leads to

$$m\ddot{z}_1 + c\left[\left(\frac{z_1}{z_0}\right)^2 - 1\right]\dot{z}_1 + kz_1 - \frac{m\sigma}{1+2\sigma}\left(\ddot{z}_1 + \ddot{z}_2\right) = 0 \tag{2.9a}$$

$$m\ddot{z}_2 + c\left[\left(\frac{z_2}{z_0}\right)^2 - 1\right]\dot{z}_2 + kz_2 - \frac{m\sigma}{1+2\sigma}\left(\ddot{z}_1 + \ddot{z}_2\right) = 0 \tag{2.9b}$$

where the over dots means differentiation with respect to time and $k = mg/r$. Equations (2.9a) and (b) represent the system in Figure 2.4 for similar metronomes, such that $k_1 = k_2 = k$ and $m_1 = m_2 = m$, where $c\left[\left(z_{1,2}/z_0\right)^2 - 1\right]$ represents C_{vPol}, $z_1 = x_1 - x_M$ and $z_2 = x_2 - x_M$. The equation for the central mass is given by

$$M\ddot{x}_M - c\left[\left(\frac{z_1}{z_0}\right)^2 - 1\right]\dot{z}_1 - c\left[\left(\frac{z_2}{z_0}\right)^2 - 1\right]\dot{z}_2 - kz_1 - kz_2 = 0 \tag{2.9c}$$

Figure 2.4 – 3DOF system representing the masses of two metronomes coupled to a base in the centre by means of linear springs and van der Pol dampers.

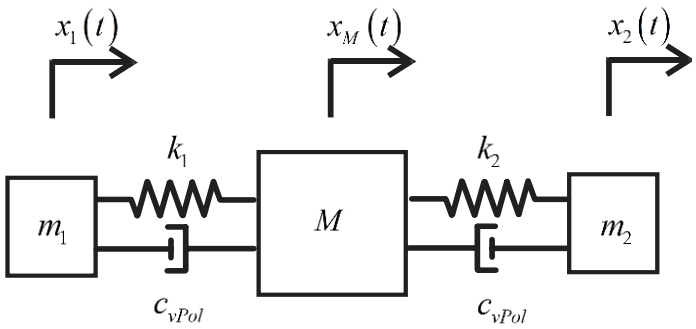

Source: Elaborated by the author.

The acceleration of the center of mass is given by

$$\ddot{x}_M = -\frac{\sigma}{1+2\sigma}\left(\ddot{z}_1 + \ddot{z}_2\right) \tag{2.10}$$

Equations (2.9a) and (b) show that the horizontal motion of the pendulum system can be captured by the model shown in Figure 2.4 provided that small angular displacements of the

pendulums are considered. Using the non-dimensional parameters $\hat{z}_1 = z_1/z_0$, $\hat{z}_2 = z_2/z_0$, $\hat{x}_M = x_M/z_0$ and $\mu = c/\omega_n m$, equations (2.9a, b, c) can be written as

$$\hat{z}_1'' + \mu\left[\hat{z}_1^{\,2} - 1\right]\hat{z}_1' + \hat{z}_1 - \frac{\sigma}{1+2\sigma}\left(\hat{z}_1'' + \hat{z}_2''\right) = 0 \tag{2.11a}$$

$$\hat{z}_2'' + \mu\left[\hat{z}_2^{\,2} - 1\right]\hat{z}_2' + \hat{z}_2 - \frac{\sigma}{1+2\sigma}\left(\hat{z}_1'' + \hat{z}_2''\right) = 0 \tag{2.11b}$$

$$\frac{1}{\sigma}\hat{x}_M'' - \mu\left[\hat{z}_1^{\,2} - 1\right]\hat{z}_1' - \mu\left[\hat{z}_2^{\,2} - 1\right]\hat{z}_2' - \hat{z}_1' - \hat{z}_2' = 0 \tag{2.11c}$$

where the primes denote differentiation with respect to $\tau = \omega_n t$. Note that μ and σ are the two parameters that control the behaviour of the system.

In the following sections, the system in Figure 2.4 is analysed for the synchronization of the system in Figure 2.1. Two cases are considered: in-phase and anti-phase synchronization. A simplified system with no damping is first studied, where it is shown that for such a system synchronization can be obtained whenever some particular initial conditions (ICs) are applied. A more general case of synchronization is also studied when the metronomes are different $\left(k_1 \neq k_2\right)$.

2.3 Undamped Synchronization

The simple model can be simplified even more by neglecting the damping (both positive and negative). This permits the exploration of the relationship between in-phase and anti-phase synchronization with the intrinsic features of the system, by means of a normal mode analysis. Consider the three degree of freedom (DOF) system shown in Figure 2.4 without any damping. It simply comprises three masses connected by two springs. The masses at the ends represent the metronome masses and the central mass represents the base mass. The motion of the system is free vibration restricted to the horizontal axis and the synchronization states depend only on the ICs.

The equations of motion for the system are given by

$$\begin{bmatrix} m_1 & 0 & 0 \\ 0 & M & 0 \\ 0 & 0 & m_2 \end{bmatrix} \begin{Bmatrix} \ddot{x}_1 \\ \ddot{x}_M \\ \ddot{x}_2 \end{Bmatrix} + \begin{bmatrix} k_1 & -k_1 & 0 \\ -k_1 & k_1+k_2 & -k_2 \\ 0 & -k_2 & k_2 \end{bmatrix} \begin{Bmatrix} x_1 \\ x_M \\ x_2 \end{Bmatrix} = 0 \tag{2.12}$$

2.3.1 *Synchronization for undamped and similar metronomes*

When the metronomes are considered to be similar such that $k_1 = k_2 = k$ and $m_1 = m_2 = m$, their natural frequencies of oscillation are similar too, and are given by $\omega_n = \sqrt{k/m}$. Eq. (2.12) then becomes

$$\begin{bmatrix} m & 0 & 0 \\ 0 & M & 0 \\ 0 & 0 & m \end{bmatrix} \begin{Bmatrix} \ddot{x}_1 \\ \ddot{x}_M \\ \ddot{x}_2 \end{Bmatrix} + \begin{bmatrix} k & -k & 0 \\ -k & 2k & -k \\ 0 & -k & k \end{bmatrix} \begin{Bmatrix} x_1 \\ x_M \\ x_2 \end{Bmatrix} = 0 \tag{2.13}$$

Assuming simple harmonic motion of the form $x = Xe^{j\Omega\tau}$ in which $j = \sqrt{-1}$, $\Omega = \omega/\omega_n$ and $\tau = \omega_n t$ is a non-dimensional time variable, Eq. (2.13) can be written as

$$\begin{bmatrix} 1-\Omega^2 & -1 & 0 \\ -1 & 2-\left(\Omega^2/\sigma\right) & -1 \\ 0 & -1 & 1-\Omega^2 \end{bmatrix} \begin{Bmatrix} X_1 \\ X_M \\ X_2 \end{Bmatrix} = 0 \tag{2.14}$$

where X_1, X_M and X_2 are the amplitudes of oscillation of m_1, M and m_2 respectively. Calculating the determinant of the matrix in Eq. (2.14) the *characteristic equation* of the system can be obtained and is given by (see e.g. Meirovitch (1975))

$$\Omega^2\left(1-\Omega^2\right)\left(\Omega^2-1-2\sigma\right) = 0 \tag{2.15}$$

Equation (2.15) has six roots; the three real solutions correspond to the three non-dimensional natural frequencies of the system

$$\Omega_1 = 0, \quad \Omega_2 = 1, \quad \Omega_3 = \sqrt{1+2\sigma} \tag{2.16a, b, c}$$

The subscripts refer to the three non-dimensional natural frequencies of the system. The corresponding three mode shapes of the system are given by

$$\mathbf{x}_1 = \begin{Bmatrix} 1 \\ 1 \\ 1 \end{Bmatrix},\ \mathbf{x}_2 = \begin{Bmatrix} 1 \\ 0 \\ -1 \end{Bmatrix},\ \mathbf{x}_3 = \begin{Bmatrix} 1 \\ -2\sigma \\ 1 \end{Bmatrix} \qquad (2.17a, b, c)$$

Each mode of vibration involves the amplitude of each mass undergoing sinusoidal motion.

The first vibration mode (Eq. (2.17a)) corresponds to a rigid-body motion and is not of interest here. The second mode (Eq. (2.17b)) corresponds to anti-phase motion of the metronome masses with no motion of the base where, according to Eq. (2.16b), the metronomes oscillate at the frequency when they are uncoupled from the rest of the system (i.e. on a rigid base). The third mode (Eq. (2.17c)) corresponds to the in-phase motion of the metronome masses with anti-phase motion of the base mass, the amplitude of which depends on the mass ratio σ. Thus, in-phase and anti-phase *synchronization* of this system corresponds to the second and third modes of vibration. Equation (2.16c) shows that the frequency of oscillation of the system is higher when the system synchronizes in-phase than when it synchronizes in anti-phase by a factor which depends on the mass ratio σ.

To obtain in-phase and anti-phase synchronization from this model (without the van der Pol dampers) it is necessary for the ICs to correspond exactly to the normal modes given by Eqs (2.17b) and (2.17c). When the ICs do not correspond to the normal modes, the system never achieves synchronization, instead it exhibits a beating behaviour which is the superposition of the 2nd and the 3rd normal modes (see e.g. (LUENBERGER, 1979, p. 44)). Numerically integrating Eqs (2.11a), (b) and (c), using the Runge-Kutta method of 4th order in Matlab®, the time-domain displacement can be obtained for each mass. Figures 2.5a and b show the anti-phase and in-phase synchronization, and Figure 2.5c the beating behaviour of the undamped 3DOF system with similar oscillators for ICs corresponding to the second, the third normal modes and ICs which do not correspond with the normal modes respectively, with a mass ratio $\sigma = 0.1$. The non-dimensional time in the figures is defined as t/T_n where $T_n = 2\pi/\omega_n$; the natural frequencies of oscillation are also given in Figures 2.5a and b.

Figure 2.5 – In-phase, anti-phase synchronization and beating phenomenon of the undamped 3DOF system with similar linear springs $\eta = 0$ with a mass ratio $\sigma = 0.1$. (a) Anti-phase synchronization when the ICs correspond exactly with the 2nd normal mode. (b) In-phase synchronization when the ICs correspond exactly with the 3rd normal mode. (c) Beating behaviour of the 3DOF system when the ICs are different to the normal modes, for this case [x_1 x_M x_2] = [0.5 1 -2] and all the initial velocities equal to zero. Solid blue line – m_1, red circle mark line – m_2 and dashed green line – M.

a)

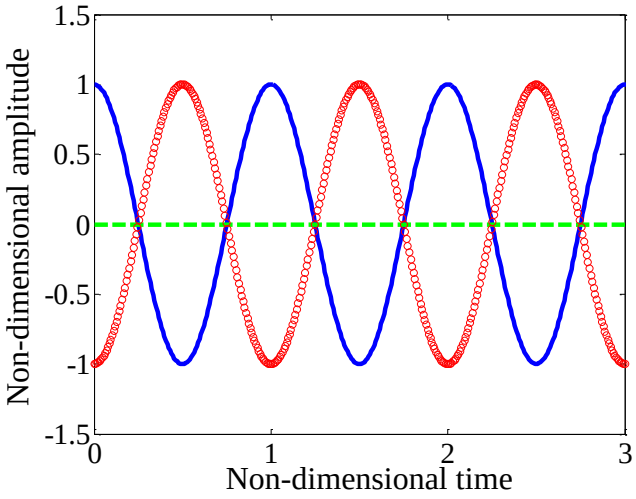

$\Omega_2 = 1$

b)

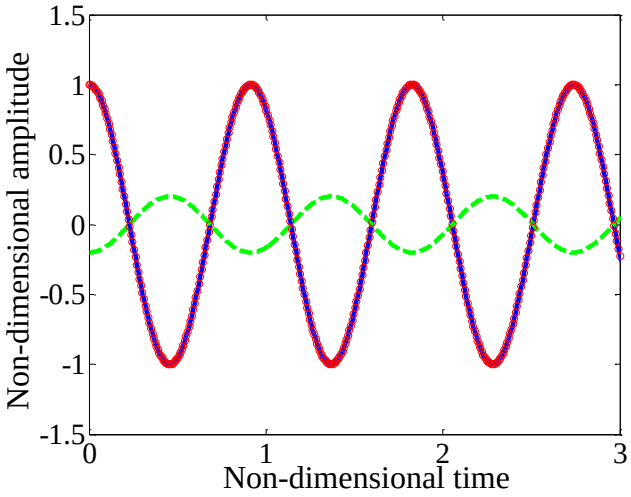

$\Omega_3 = 1.095 = \sqrt{1+2\sigma}$

c)

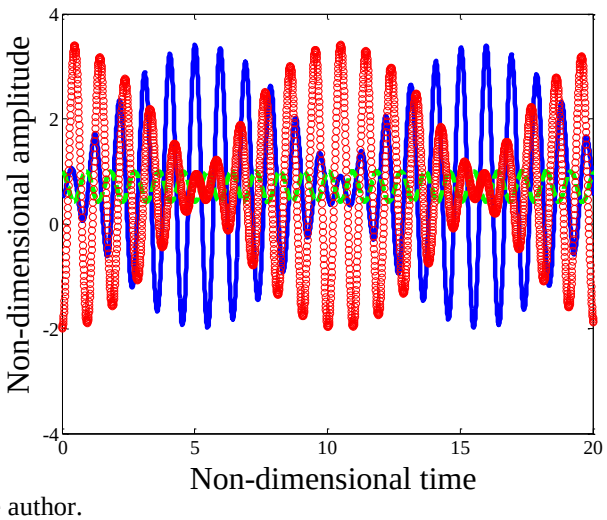

Source: Elaborated by the author.

2.3.2 *Synchronization for undamped and slightly different metronomes*

The undamped system facilitates a simple study into the case where the metronomes are slightly different. To make the metronomes different from one another, the case when $k_1 = k$ and $k_2 = k(1+\eta)$ is considered, where η is a constant, is studied. The equation of motion for this system is now

$$\begin{bmatrix} m & 0 & 0 \\ 0 & M & 0 \\ 0 & 0 & m \end{bmatrix} \begin{Bmatrix} \ddot{x}_1 \\ \ddot{x}_M \\ \ddot{x}_2 \end{Bmatrix} + \begin{bmatrix} k & -k & 0 \\ -k & k(2+\eta) & -k(1+\eta) \\ 0 & -k(1+\eta) & k(1+\eta) \end{bmatrix} \begin{Bmatrix} x_1 \\ x_M \\ x_2 \end{Bmatrix} = 0 \tag{2.18}$$

Assuming simple harmonic motion of the form $x = Xe^{j\Omega\tau}$ Eq. (2.18) becomes

$$\begin{bmatrix} 1-\Omega^2 & -1 & 0 \\ -1 & (2+\eta)-\Omega^2/\sigma & -(1+\eta) \\ 0 & -(1+\eta) & (1+\eta)-\Omega^2 \end{bmatrix} \begin{Bmatrix} X_1 \\ X_M \\ X_2 \end{Bmatrix} = 0 \tag{2.19}$$

From Eq. (2.19) the characteristic equation is obtained for the system. It contains a few more terms, but if only a slight difference between the stiffness is considered such that $\eta \ll 1$, then just first order terms in η can be considered. The natural frequencies of such a system are then given by

$$\Omega_1 = 0, \;\; \Omega_2 \approx \sqrt{1+\frac{\eta}{2}}, \;\; \Omega_3 \approx \sqrt{1+2\sigma+\frac{\eta}{2}} \tag{2.20 a, b, c}$$

and its normal modes by

$$\mathbf{x}_1 = \begin{Bmatrix} 1 \\ 1 \\ 1 \end{Bmatrix}, \;\; \mathbf{x}_2 \approx \begin{Bmatrix} 1 \\ -\eta/2 \\ -(1+\eta) \end{Bmatrix}, \;\; \mathbf{x}_3 \approx \begin{Bmatrix} 1 \\ -(4\sigma+\eta)/2 \\ (4\sigma+\eta)(1+\eta)/(4\sigma-\eta) \end{Bmatrix} \tag{2.21a, b, c}$$

Equation (2.21a) is not of interest because it corresponds to rigid-body motion. Eqs (2.21b and c) correspond to approximations for the 2nd and the 3rd normal modes of vibration of the system. Equations (2.21b and c) show that the normal modes depend on both the mass ratio σ and the stiffness difference η. Figure 2.6a shows the anti-phase synchronization of the system of Figure 2.4 with $\eta = 0.1$, when the ICs are chosen to be equal to the 2nd mode of vibration. Figure 2.6b shows the anti-phase synchronization of the same system when the ICs

are chosen to be equal the 3rd mode of vibration. Both figures were obtained by numerical integration of Eq. (2.18). The normal modes were calculated numerically too. Note that in both cases there is now motion of the center mass. For the second mode it is in-phase with mass m_2 and for the third mode it is in anti-phase with both masses as in the previous case.

Figure 2.6 – In-phase and anti-phase synchronization of the undamped 3DOF system with different springs $\eta = 0.1$ and with a mass ratio $\sigma = 0.1$. (a) Anti-phase synchronization when the ICs correspond exactly with the 2nd normal mode. (b) In-phase synchronization when the ICs correspond exactly with the 3rd normal mode. Solid blue line – m_1, red circle mark line – m_2, dashed green line – M.

a)

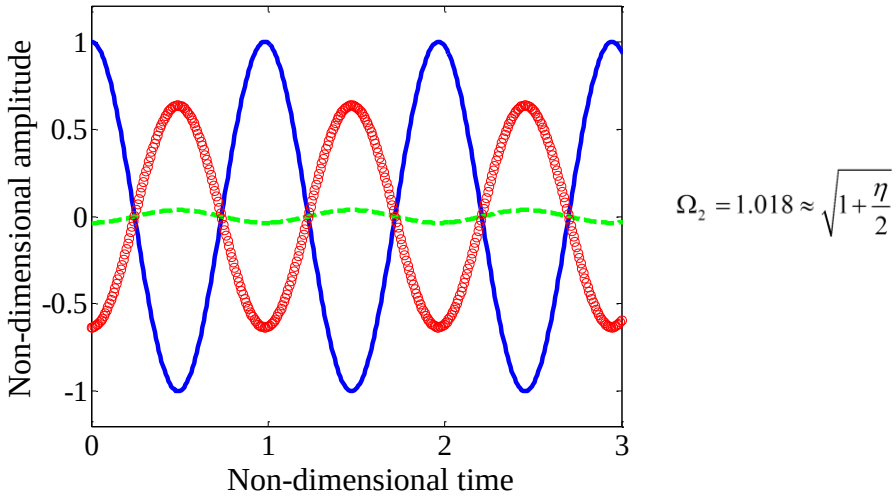

b)

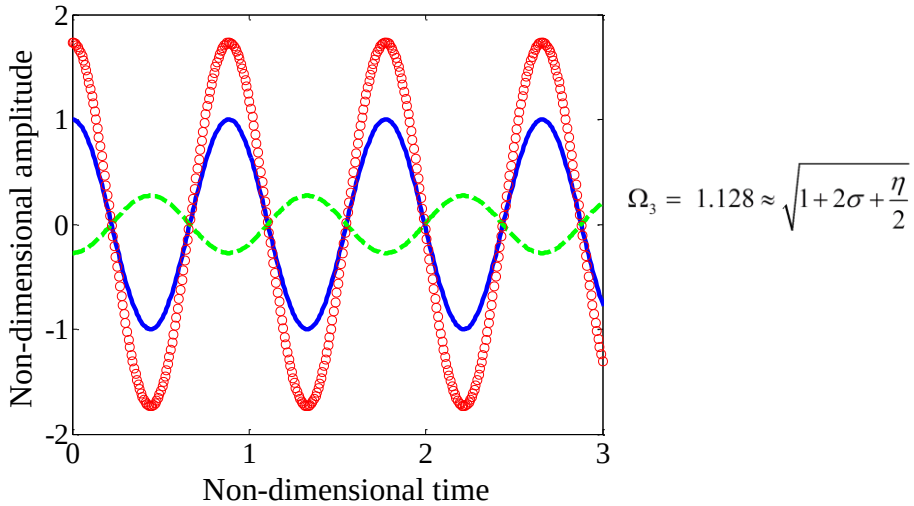

Source: Elaborated by the author.

2.4 Synchronization with van der Pol damping included

2.4.1 *Synchronization for similar metronomes*

In this section the effect of van der Pol damping on the simple model described in the previous section is studied. Two cases are considered. They are when the metronomes are similar and when they are slightly different.

Figure 2.7 – In-phase and anti-phase synchronization of the 3DOF system with van der Pol damping and similar springs $\eta = 0$ with a the mass ratio $\sigma = 0.1$ and the damping $\mu = 0.1$. (a) Anti-phase synchronization and zoom of its steady state respectively for ICs $\left[x_1(0)\ x_M(0)\ x_2(0)\right] = \left[0.5\ 0\ -2\right]$ and $x_i'(0) = 0$, where $i = 1, M, 2$. (b) In-phase synchronization and a zoom of its steady state for ICs of $\left[x_1(0)\ x_M(0)\ x_2(0)\right] = \left[-0.5\ 0\ -3\right]$ and $x_i'(0) = 0$. Solid blue line – m_1, red circle mark line – m_2, dashed green line – M.

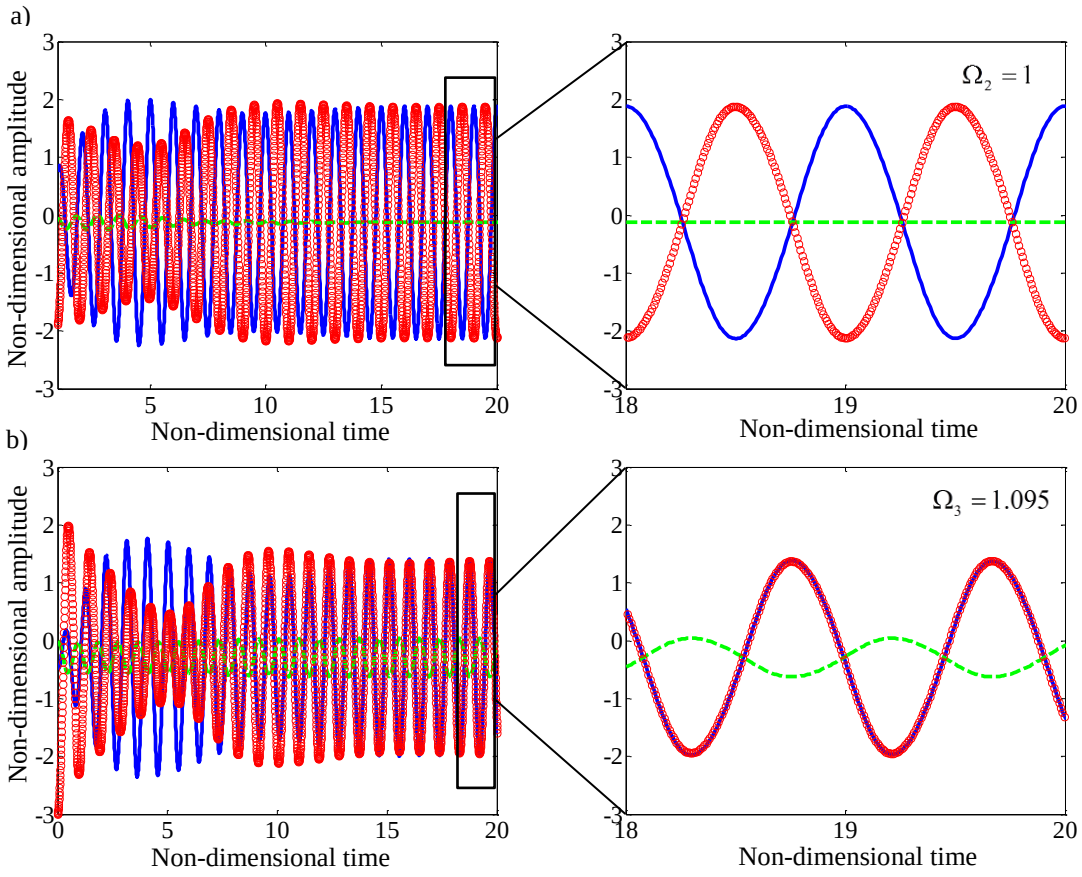

Source: Elaborated by the author.

Figure 2.4 shows the 3DOF system with linear springs with van der Pol dampers positioned between the central mass and each of masses at the ends. This model represents the two metronome system on a mobile wooden base, when small horizontal motion of the

pendulums is studied. The equations of motion for this system are given by Eqs. (2.11a, b, c). Figures 2.7a and b are obtained by numerical integration of Eqs (2.11a, b, c). They show anti-phase and in-phase synchronization respectively, with zooms, of the 3DOF system with similar oscillators $\eta = 0$ and van der Pol damping for $\mu = 0.1$ and $\sigma = 0.1$. Synchronization has been achieved from different ICs in each case. It is not necessary for the ICs to correspond to the normal modes of the system to achieve one or the other synchronization state.

In Chapter 4 the relationship between the main parameters in the system and the ICs leading the system to its final synchronization state are studied, with help of the concept of *Basins of Attraction* (see e.g (ENNS; MCGUIRE, 2001; STROGATZ, 1999)).

2.4.2 *Synchronization for slightly different metronomes*

Figures 2.8a and b show almost anti-phase and almost in-phase synchronization respectively and zooms of the 3DOF system with slightly different stiffness $\eta = 0.05$ and van der Pol damping for $\mu = 0.1$ and $\sigma = 0.1$. Here it is also not necessary for the ICs to correspond with normal modes. The difference in amplitudes comes from the difference in stiffness as shown by the approximations of Eqs. (2.21b and c). Additional simulations of Eqs. (2.11) when $k_1 \neq k_2$, $\mu = 0.1$ and $\sigma = 0.1$ suggest that for the same ICs used on Figures 2.8a and b for values of $\eta > 0.11$, synchronization is not achieved, instead a beating behaviour is obtained regardless the presence of van der Pol damping and this is maintained with even higher damping values. This is in agreement with previous work in which synchronization of oscillators was found only to occur when the difference between the uncoupled frequencies $\Delta\Omega$ of each metronome are within a certain range (PIKOVSKY; ROSEMBLUM; KURTHS, 2001, p. 18). For the system studied in this work this is given by $0 \leq \Delta\Omega \leq \sqrt{(1+\eta)} - 1$. For the ICs and values of μ and σ used in Figures 2.8a and b, the range for synchronization is $0 \leq \Delta\Omega \leq 0.053$ with $\eta \leq 0.11$. It should be noted that this range can change with the chosen ICs.

It can be seen in Figures 2.8a and b that there exists a phase shift between m_1 and m_2, this is due, and proportional to, the difference in stiffness. The phase shift between m_1 and

m_2 affects the central mass and reciprocally the central mass affects the motion of m_1 and m_2 so that, eventually, the final synchronization state changes, passing from almost anti-phase to almost in-phase synchronization and then to beating behaviour. Table 1 shows the relationship between the stiffness difference, the uncoupled frequency difference, and the final synchronization state for the same parameters and ICs used for Figure 2.8a. Note that given particular ICs and values for the parameters μ and σ the final synchronization state changes within the range of uncoupled frequency difference. The investigation to determine the relation among the ICs, parameters and the range of difference of natural frequencies

Figure 2.8 – Almost In-phase and almost anti-phase synchronization of the 3DOF system with van der Pol damping and slightly different springs $\eta = 0.05$ with a mass ratio $\sigma = 0.1$ and $\mu = 0.1$. (a) Anti-phase synchronization and zoom of its steady state respectively for ICs $\left[x_1(0)\ x_M(0)\ x_2(0)\right] = \left[0.5\ 0\ -2\right]$ and $x_i'(0) = 0$, where $i = 1, M, 2$. (b) In-phase synchronization and zoom of its steady state respectively for ICs of $\left[x_1(0)\ x_M(0)\ x_2(0)\right] = \left[-0.5\ 0\ -3\right]$ and $x_i'(0) = 0$. Solid blue line – m_1, circle marked red line – m_2, dashed green line – M.

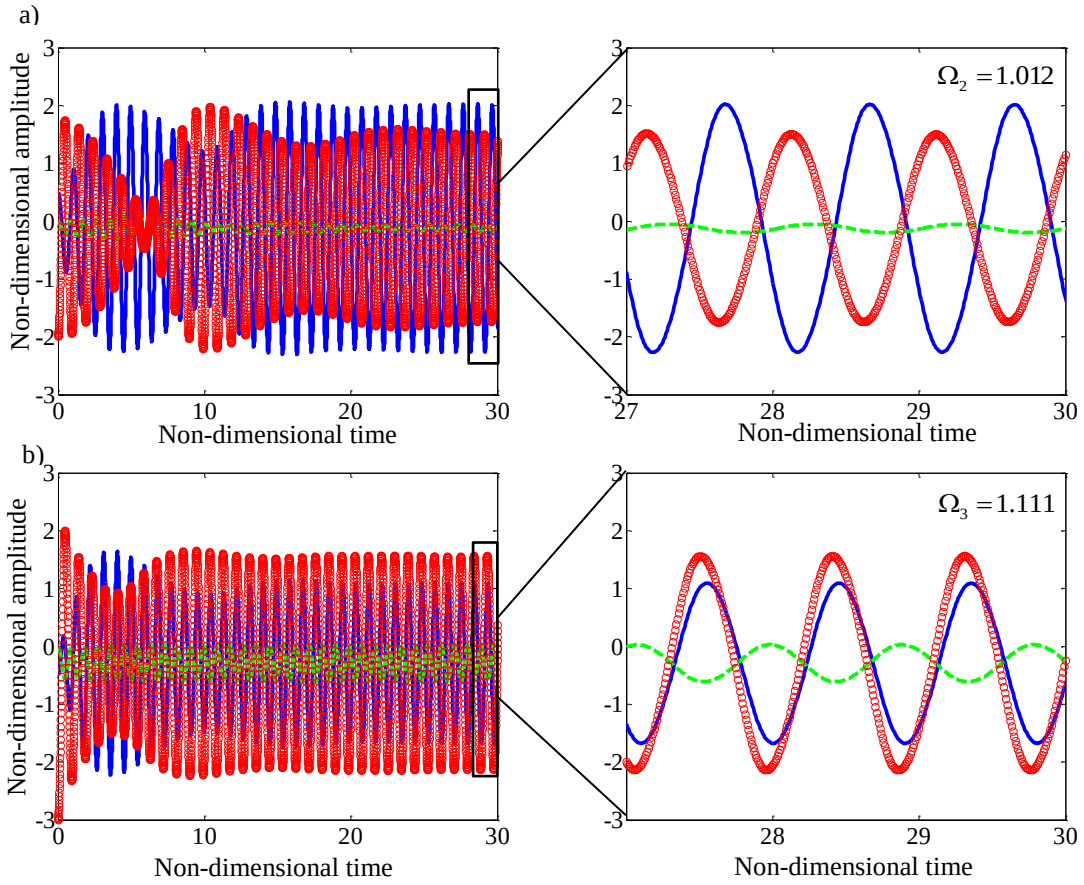

Source: Elaborated by the author.

leading to synchronization is outside the scope of this work, and is proposed as one of the topics for further work.

Table 1. Relationship between the difference in stiffness, uncoupled frequency difference, of the metronomes and the final synchronization state of the 3DOF system with a mass ratio $\sigma = 0.1$ and $\mu = 0.1$, for ICs $\left[x_1(0)\ x_M(0)\ x_2(0)\right] = \left[0.5\ 0\ -2\right]$ and $x_i'(0) = 0$, where $i = 1, M, 2$.

η	Non-dimensional time delay	Frequency difference percentage	Synchronization state
0	0	0.5%	Almost anti-phase
0.01	0.01	0.5%	
0.02	0.01	1.5%	
0.03	0.03	1.5%	
0.04	0.03	2%	
0.05	0.04	2%	
0.06	0.05	2.5%	
0.07	0.05	2.5%	
0.08	0.06	3%	Almost in-phase
0.09	0.06	3%	
0.1	0.1	4.9%	
0.011	0.1	4.9%	
beating			

Source: Elaborated by the author.

Figure 2.9 – Beating behaviour of the 3DOF system with van der Pol damping produced by the difference in the natural frequencies of each metronome for which $\eta = 0.12$, $\sigma = 0.1$ and $\mu = 0.1$, for ICs $\left[x_1(0)\ x_M(0)\ x_2(0)\right] = \left[0.5\ 0\ -2\right]$ and $x_i'(0) = 0$, where $i = 1, M, 2$. Solid blue line – m_1, circle marked red line – m_2, dashed green line – M.

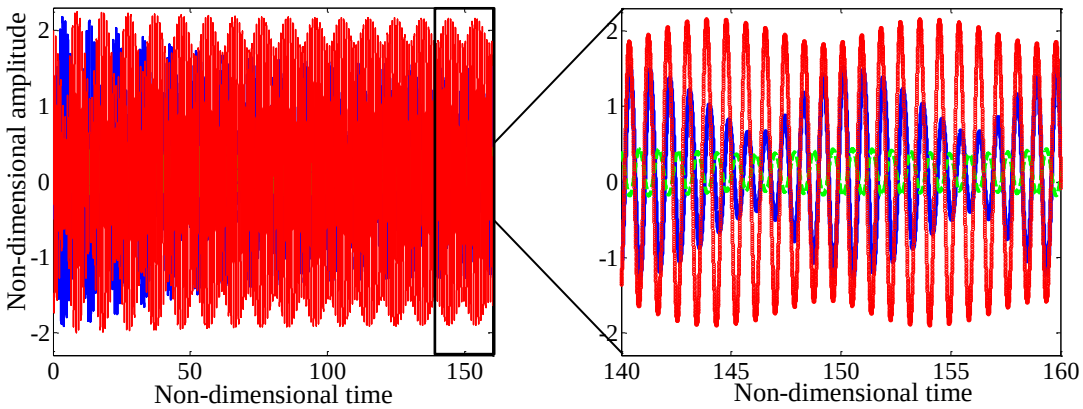

Source: Elaborated by the author.

Figure 2.9 shows the beating behaviour of the 3DOF system for $\eta = 0.12$ leading to a frequency difference outside the range of synchronization.

2.5 Conclusions

In this chapter a simplified lumped parameter model has been used to study in-phase and anti-phase synchronization of two metronomes on a mobile base. The relationship with this model and the previous pendulum model of Pantaleone (2002) has also been studied. Both types of synchronization have been analysed for the undamped system and when van der Pol damping is introduced in the system for similar and slightly different stiffness values in the metronomes. It has been shown that synchronization can be achieved for an undamped system provided that the ICs correspond exactly with their 2^{nd} and 3^{rd} normal modes of vibration, and when the ICs do not correspond to these modes, the system exhibits beating behaviour. It has also been shown that when van der Pol damping is considered in the system, it is not necessary for the ICs to correspond to the normal modes of vibration to synchronize either in-phase or in anti-phase. However they can never achieve synchronization if the natural frequency of oscillation of each metronome is very different.

3 THE INSTANTANEOUS FREQUENCY METHOD APPLIED TO NUMERICAL AND EXPERIMENTAL SYNCHRONIZATION OF TWO METRONOMES

3.1 Introduction

In chapter 2 a simplified model was introduced to represent the synchronization of two metronomes oscillating on a mobile base. In Appendix 1, the way in which the internal escapement mechanism of a metronome works was discussed. Two models that represent such a mechanism have also been discussed and the reasons for using the van der Pol oscillator in this work have been discussed. The principal aim of this chapter is to study the *Instantaneous Frequency* (IF) method to determine the final synchronization state of the 3DOF system studied in chapter 2. The methodology used to collect experimental data from videos is discussed, as is the application of the IF method to the collected data from experiments, so that the final synchronization state can be determined.

In section 3.2 the concept of the IF is introduced. Section 3.3 shows the relationship between the IF and the presence of harmonics in signals. In Section 3.4 the IF concept is applied to numerical data for both synchronization states of interest. Section 3.5 summarizes the main features of the software used to collect data from videos of the experiments. In section 3.6 the IF method is applied to experimental data from in-phase and anti-phase synchronization tests and section 3.7 presents the conclusions for this chapter.

3.2 The Instantaneous Frequency

This section presents a method to identify the synchronization of metronomes by means of the IF concept. The IF is based on the Hilbert Transform (HT) and the instantaneous phase.

The Hilbert transform $\tilde{x}(t)$ of a time-domain signal $x(t)$ is the convolution integral of the functions $x(t)$ with $(\pi t)^{-1}$ and is defined by (FELDMAN, 2011a)

$$\tilde{x}(t) = \frac{1}{\pi}\int_{-\infty}^{\infty} \frac{x(\tau)}{t-\tau} d\tau \tag{3.1}$$

The singularity $t = \tau$ is to be avoided. For this, a method for assigning a definite value to the improper integral (3.1), called the Cauchy principal value, is applied (JOHANSSON, 1999; FELDMAN, 2011; LEITHOLD, 1996). The HT of a signal $x(t)$ has the effect of leaving the amplitudes of $x(t)$ unaltered and shifting its phase by $\pi/2$. Thus, if the original signal is a sine function, its HT is a cosine function. Additionally, with the HT of a signal a new complex signal can be formed, where the real part is the original signal $x(t)$ and the imaginary part is the HT $\tilde{x}(t)$. This is called the *Analytical Signal* and is given by

$$h(t) = x(t) + j\tilde{x}(t) \tag{3.2}$$

Considering, for example, a harmonic signal $x(t) = A\cos\varphi$ and its HT $\tilde{x}(t) = A\sin\varphi$, the analytical signal could be represented in polar coordinates by

$$h(t) = Ae^{j\varphi} \tag{3.3}$$

Figure 3.1 shows the polar representation of the analytic signal of Eq. 3.3. The instantaneous phase of an analytical signal is given by

$$\varphi(t) = \arctan\left(\frac{\mathrm{Im}(h(t))}{\mathrm{Re}(h(t))}\right) = \arctan\left(\frac{\tilde{x}(t)}{x(t)}\right) \tag{3.4}$$

Figure 3.1 – Polar representation of an analytic signal, where the real part, is the original signal and the imaginary part, is the Hilbert transform of the original signal.

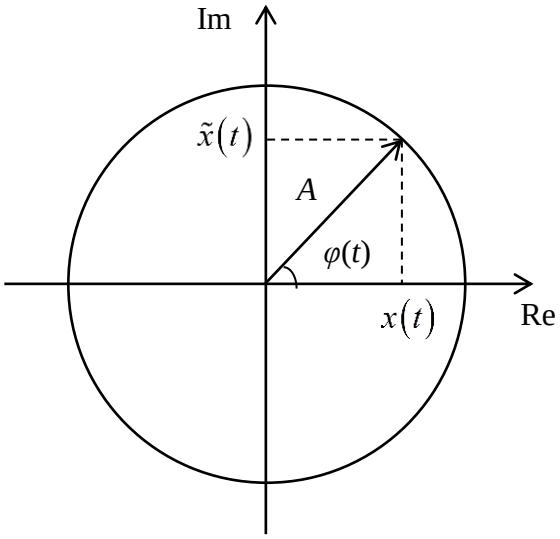

Source: Elaborated by the author.

and the *Instantaneous Frequency* (IF) is calculated by means of the difference between the phases of two adjacent points at time t_1 and t_2, and is given by

$$\dot{\varphi}(t) = \frac{\varphi_2 - \varphi_1}{t_2 - t_1} = \frac{\arctan\left(\tilde{x}_2(t)/x_2(t)\right) - \arctan\left(\tilde{x}_1(t)/x_1(t)\right)}{t_2 - t_1} \tag{3.5}$$

Figures 3.2a shows a 2 Hz sinusoidal signal with amplitude of unity in the time-domain and a signal composed of the sum of a 2 Hz sinusoidal signal, also with amplitude 1, and its third harmonic (6Hz) with an amplitude 1/20. Figure 3.2b shows the respective IFs for the signals in Figure 3.2a. The IF for the sinusoidal signal is almost a straight line with a value of 2Hz, while the IF for the composite signal oscillates around the value 2Hz, corresponding to the frequency of the fundamental harmonic, with a frequency equal to twice this frequency. This phenomenon is discussed in the next section.

Figure 3.2 – Illustration of the instantaneous frequency (a) Solid black line – 2 Hz sinusoidal signal with amplitude of 1, circled red line – A signal composed of a fundamental sinusoidal signal of 2 Hz and its third harmonic, the amplitude of which is 1/20. (b) Solid black line – IF for the sinusoidal signal, circled red line – (rippled) IF for the composite signal.

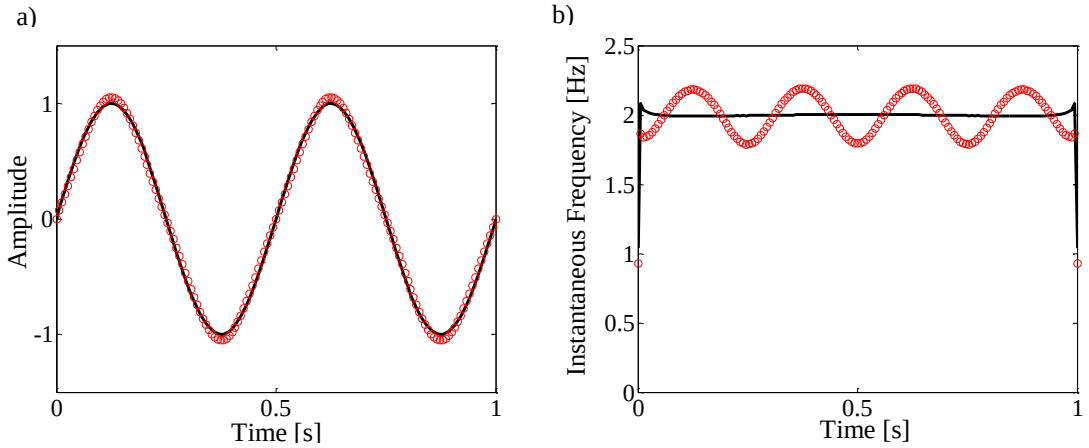

Source: Elaborated by the author.

3.3 The Instantaneous Frequency and the Presence of Higher Harmonics in a Signal

The aim of this section is to discuss the behaviour of the IF of a signal which consists of a fundamental frequency and a small higher harmonic. Figure 3.2b shows that such a signal produces an oscillation of the IF around the value of the fundamental frequency. The

frequency of the oscillation is twice the fundamental frequency for the case in which the third harmonic has been added to a sinusoidal signal.

Figure 3.3a depicts the the sum of two harmonics in the complex plane, where phasors A_1 and A_2 represents the fundamental and the third harmonic, respectively. Thus, A_2 rotates at three times the angular velocity of A_1. If the phase of A_1 at a given time is $\varphi(t)$, the phase of A_2 will then be given by $3\varphi(t)$ at the same instant in time. The IF of the composite signal, represented by the resultant phasor *R*, is given by the time derivative of the phase angle $\theta(t)=\varphi(t)+\alpha(t)$. To determine $\alpha(t)$ the complex plane axes can be positioned on A_1, by rotating the reference frame axes by $\varphi(t)$, as shown in Figure 3.3b, so that the angle that A_2 forms with the horizontal is given by the difference $3\varphi(t)-\varphi(t)=2\varphi(t)$. The amplitude of the vectors can be normalized by $|A_1|$ so that $|A_2|/|A_1|=\rho$. The phase angle θ is then given by

$$\theta(t)=\varphi(t)+\arctan\left(\frac{\rho\sin 2\varphi(t)}{1+\rho\cos 2\varphi(t)}\right) \tag{3.6}$$

Figure 3.3 – Complex representation of the sum of two signals. (a) Sum of a fundamental sinusoidal signal and its third harmonic with amplitude $|A_2|=1/20|A_1|$ (*The vectors have not scaled to clearly illustrate the behaviour*), where $|A_1|$ is the amplitude of the fundamental signal, $|R|$ the resultant amplitude, $\varphi(t)$ the instantaneous phase of the fundamental signal, $\theta(t)$ the instantaneous phase of the resultant and $\alpha(t)$ the phase difference between the resultant and the fundamental signals. (b) Representation in (a) when the axes are rotated by $\varphi(t)$. The amplitudes have been normalized dividing by $|A_1|$ so that $\rho=|A_2|/|A_1|$.

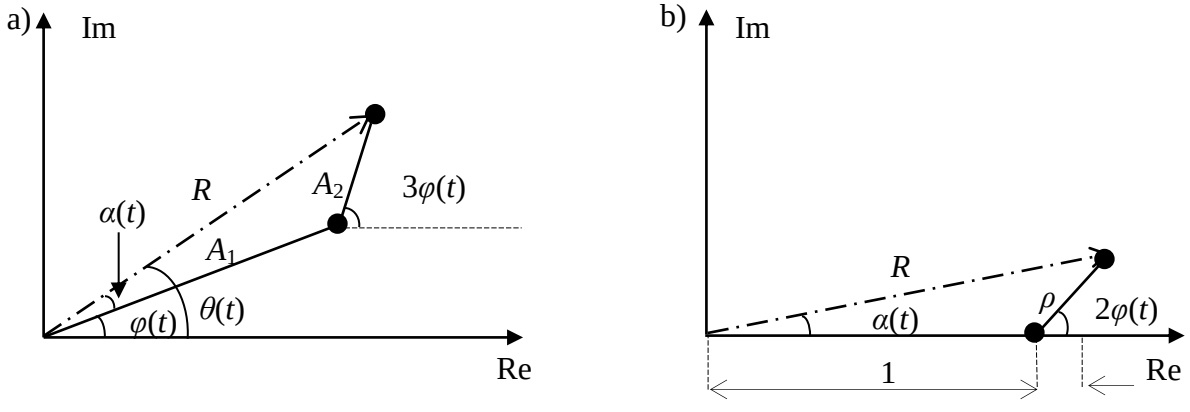

Source: Elaborated by the author.

For a small amplitude third harmonic such that $\rho \ll 1$, then $\rho \cos 2\varphi(t) \ll 1$. $\theta(t)$ is then given approximately by

$$\theta(t) \simeq \varphi(t) + \rho \sin 2\varphi(t) \tag{3.7}$$

Setting $\varphi(t) = \omega t$, where ω is the angular frequency corresponding to the fundamental frequency, the time derivative of Eq. (3.7) leads to the IF, given by

$$\dot{\theta}(t) \approx \omega + 2\omega\rho \cos 2\omega t \tag{3.8}$$

Equation (3.8) is thus the expression for the IF of a signal composed by a sinusoidal signal and a small third harmonic of this signal. Eq. (3.8) shows that this IF comprises a constant value, corresponding to the frequency of the first harmonic, and an oscillatory term with a frequency equal twice the fundamental frequency, the amplitude of which depends upon the amplitude ratio and the fundamental frequency. When the amplitude of the third harmonic is such that the approximation in Eq. (3.7) is not valid, or when the signal consists of more than two harmonics, the simpler way of determining the IF is by using Eq. (3.5).

The general result from Eq. (3.8) can be written as

$$\dot{\theta}(t) \approx \omega + (n-1)\rho\omega \cos(n-1)\omega t \tag{3.9}$$

where *n* is the number of the harmonic being added to the fundamental. In the case of Eq. (3.8) $n = 3$.

3.4 Instantaneous Frequency for In-phase and Anti-phase Synchronization of the 3DOF Model

The aim of this section is to apply the IF concept to signals from the 3DOF system described in chapter 2, which has van der Pol damping and similar metronomes (Figure 2.4). The final synchronization state can then be verified by means of the IFs of each of the masses in the steady-state. The time domain displacements of the masses when the system is synchronized in both in-phase and anti-phase states, are used to calculate the analytical signals. These are then used to calculate the instantaneous phases and later the IFs, employing Eqs (3.2), (3.4) and (3.5).

Figures 3.4a and c show the time-domain displacements and the IFs of the masses m_1, m_2 and M when the system synchronizes in anti-phase, respectively, for ICs $\left[x_1(0)\ x_M(0)\ x_2(0)\right]=\left[3\ 0\ -2.8\right]$ and $\dot{x}_i(0)=0$. Figures 3.4b and d show their respective zooms. The IF is plotted in non-dimensional units corresponding to the value of the IF divided by the natural frequency of a single oscillator ω_n. Figure 3.4d shows that when the system synchronizes in anti-phase, masses m_1 and m_2 have the same frequency of oscillation while M remains static and therefore its frequency is zero in the steady-state. Note that the IF of m_1 and m_2 oscillates around 1 with a frequency which is nearly more than twice this value (counting the number of peaks).

Figure 3.4 – (a) and (b) Anti-phase synchronization (simulation) of the 3DOF system and zoom of the steady-state, respectively, for ICs $\left[x_1(0)\ x_M(0)\ x_2(0)\right]=\left[3\ 0\ -2.8\right]$ and $x_i'(0)=0$. (c) and (d) IFs for each mass and zoom at the steady-state, respectively. Solid blue line – m_1, red circle mark line – m_2, dashed green line – M.

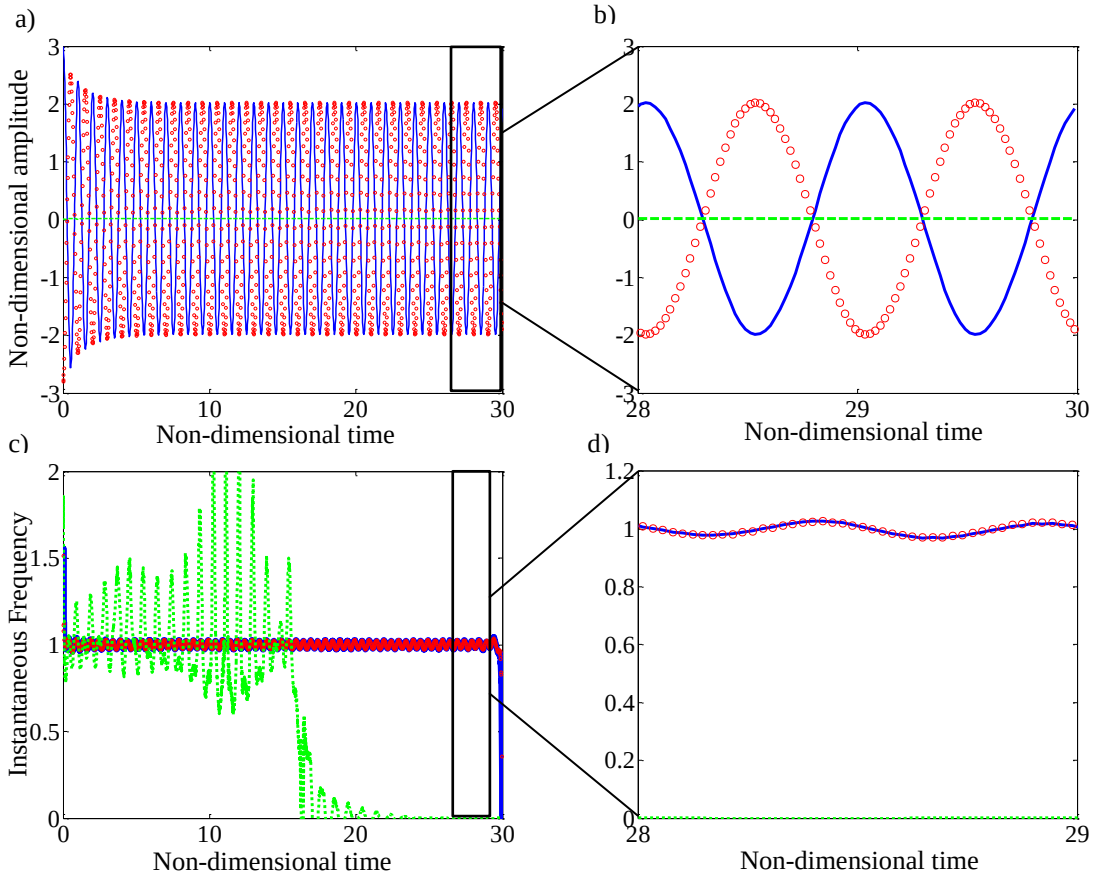

Source: Elaborated by the author.

This means that when the system synchronizes in anti-phase, m_1 and m_2 oscillate at the natural frequencies of the individual oscillators describing motions which are almost sinusoidal. Their motion is composed of a large fundamental harmonic and small higher harmonics (see Section 3.3).

Figure 3.4c shows that the IF for *M* undergoes large changes around the value 1 and has considerable noise while the system passes from transient to the steady-state and while *M* comes to rest. This is caused by the way the IF is calculated. Due to the fast small motions of the base, the difference of the phases between two adjacent points is large, compared with the same phases for the motion of the metronomes (see Eq. (3.5)), and this is amplified when this amount is divided by the lapse of time for calculating the IF. Figure 3.3c shows that at the beginning of the motion, the base mass *M* oscillates with a frequency similar to the frequency of the metronomes but with very small amplitude, and later the oscillation of the base stops.

Figure 3.5a and 3.5c show the time-domain displacements and the IFs of the masses m_1, m_2 and *M* when the system achieves in-phase synchronization, respectively, for ICs $\left[x_1(0)\ x_M(0)\ x_2(0)\right]=\left[1.5\ 0\ 1.3\right]$ and $x_i'(0)=0$. Figures 3.5b and d show their respective zooms. Figure 3.5b and d show that when the system achieves in-phase synchronization, the three masses share the same frequency of oscillation. Comparing the IFs in Figure (3.5d) and (3.4d) it can be seen that the frequency of oscillation of the masses is higher when the system synchronizes in-phase than when synchronizes in anti-phase, a fact observed in section 2.3.1 of chapter 2 when a simpler model has been analysed. The oscillation of the IFs reveals the presence of very small higher harmonics in the time-domain displacement of the masses in Figure (3.5b)

Figure 3.5 – (a) and (b) In-phase synchronization (simulation) of the 3DOF system and zoom of the steady-state, respectively, for ICs $\left[x_1(0)\ x_M(0)\ x_2(0)\right]=\left[1.5\ 0\ 1.3\right]$ and $x_i'(0)=0$. (c) and (d) IFs for each mass and zoom at the steady-state, respectively. Solid blue line – m_1, red circle mark line – m_2, dashed green line – M.

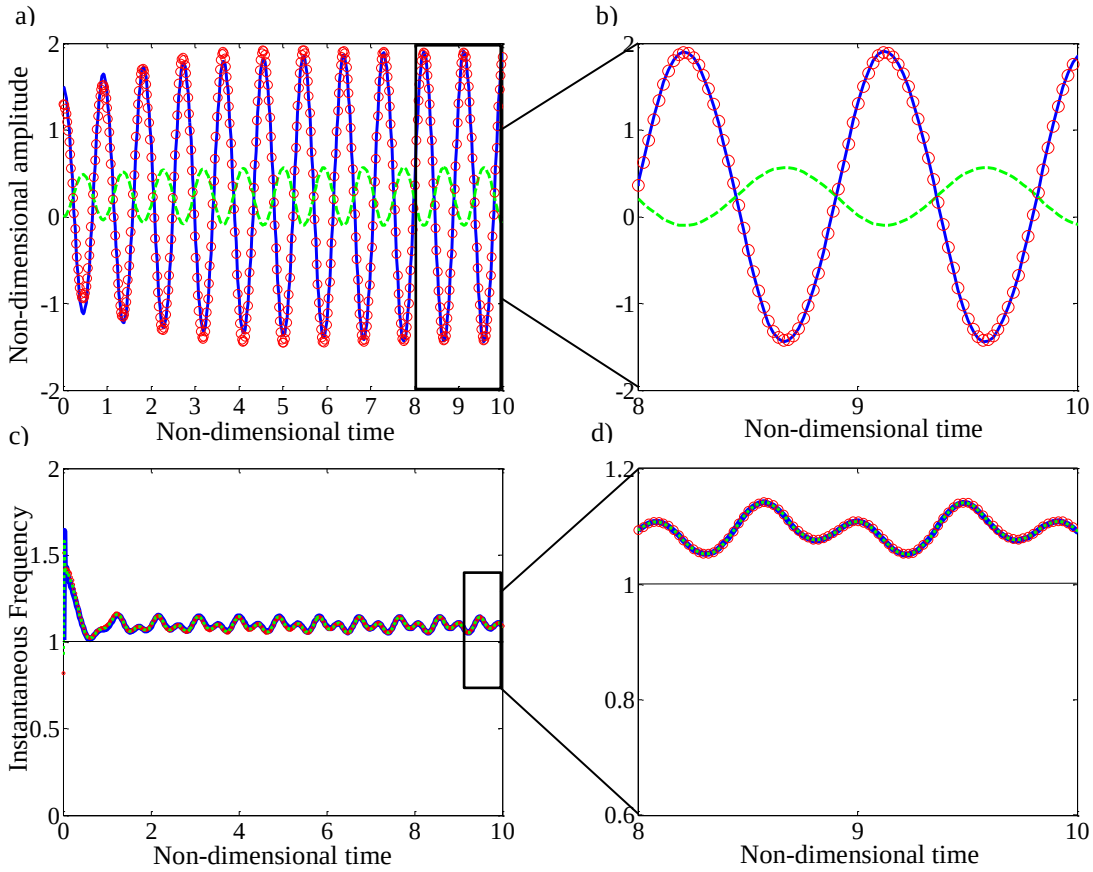

Source: Elaborated by the author.

3.5 Collecting Experimental Data with Tracker®

In this thesis, data collection has been carried out by means of videos of the experiments with two metronomes oscillating on a mobile base, where the final state is anti-phase or in-phase synchronization, as well as videos of each metronome oscillating alone (uncoupled). The horizontal displacements of the metronomes and the displacement of the base were extracted from each frame of the video with help of the software Tracker® (2016). This section describes the main features of the software used in this work for collecting data.

Tracker® is a free video analysis and modelling tool available to download from the internet (BROWN, 2008). It is easy to use and is especially useful for collecting data in two

dimensions. Because the frequencies of oscillation of the metronomes are low, it is possible to use commercial cameras to record the experiments. Tracker® exploits the fact that videos capture frames at a certain rate of time to calculate position, velocity and all the variables which are related to them. It is also possible to introduce new formulas into Tracker® based on actual variables and to obtain outputs, which can be copied to different formats (e.g. excel).

The video needs to be uploaded in Tracker®, then the center of the axes and its inclination needs to be chosen, so that it is not necessary for the camera to be fixed horizontally while recording. A calibration bar is also available to calibrate the size of the motion. It is necessary just to know the real length of one of the elements in the video (or previously have marked a length in the video) and introduce it by means of the calibration bar to obtain output data in the chosen units (e.g. meters).

Each position at a given frame can be collected manually by clicking on the target (e.g. the pendulum bobs) keeping the [Shift] button pressed, then the position is saved and the next frame is shown so that the new position of the target can be saved. This process can be repeated frame by frame up to the end of the video. There is an automatic option to collect the positions of the target. In this option a template of the region near the target is chosen by Tracker® at the first click on the target. Then the software will start to search the position which best fit the previous template within a certain area around the target. This process is repeated frame by frame. For using this option, it is necessary to choose the option *punctual mass* and keep [Shift] + [Ctrl] pressed during the first time the target is chosen, and then the software will automatically start the tracking process. Although this is the best option when the numbers of desired output positions is high, care is needed and the process supervised because Tracker® could fail to track the target. If this happens, a new template needs to be created at the incorrect point and the previous correct point will be already saved. Once the data or the points have been collected and saved, they will always be available when the Tracker® file is open. Figure 3.6 shows the screen of Tracker® while collecting data automatically from an experiment of a metronome oscillating alone. In the center is the pendulum bob with a target being tracked automatically and the previous collected points, there is an area around the target used by the software to compare and choose the best point which fits the template. This template chosen by Tracker® can be seen at the bottom right side square. The data collected and the plot obtained from them can be seen in the center and upper right side, respectively.

Figure 3.6 – Tracker® screen while collecting data in automatic mode from a single metronome. The area around the target at the pendulum bob is the template search area. In the bottom right side is a square with a template for automatic tracking. In the center right side are the collected data and above is the plot generated by the tracker data. In the center of the screen is the recent history of points collected, which can be manually changed.

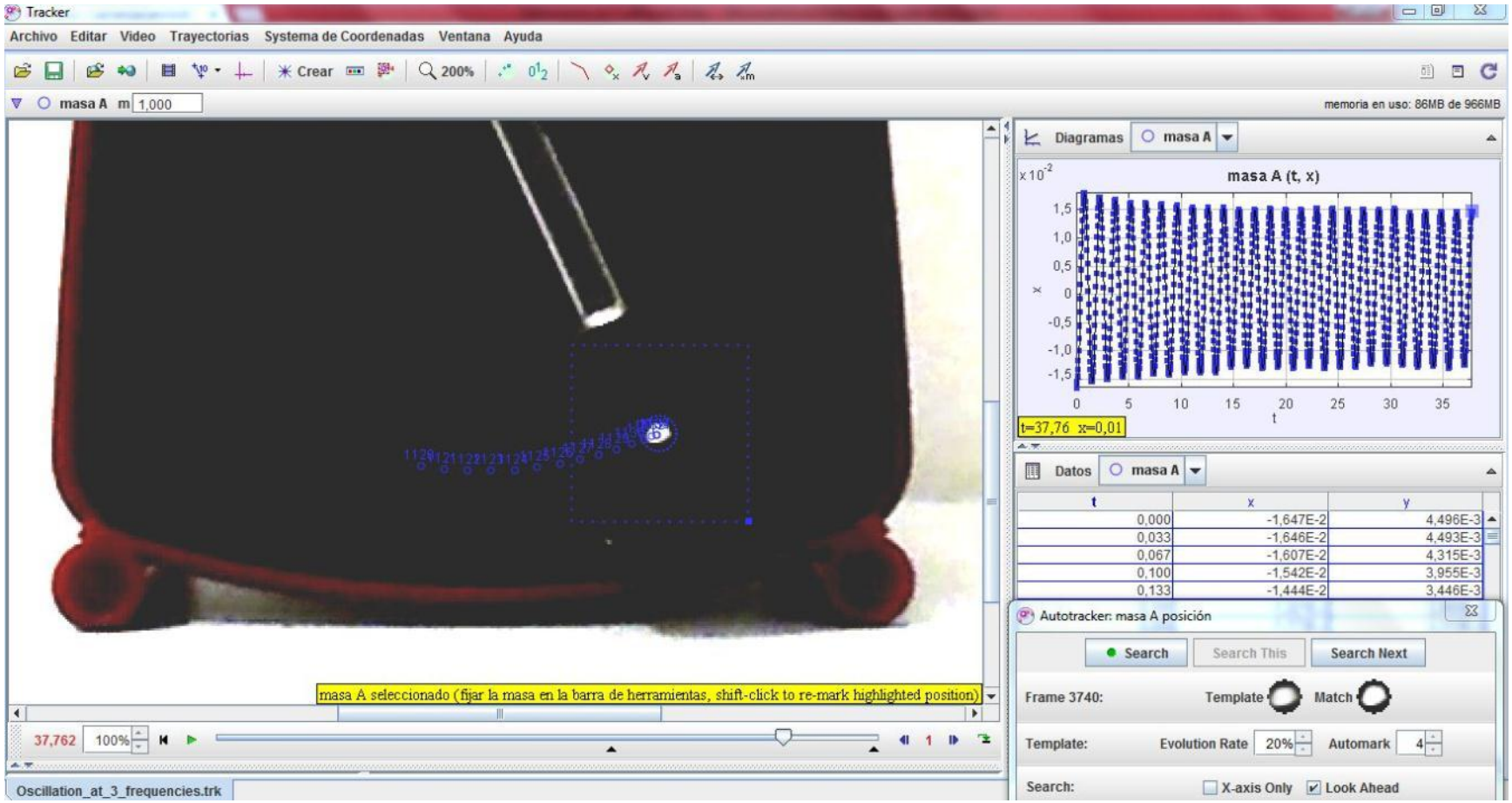

Source: Elaborated by the author.

For videos with problems of brightness, contrast and colour, several filters are available to improve the quality of the templates, so that the quality of the images can be improved. Zoom can also be used in the areas of interest to improve the accuracy of the points on the target. Figure 3.7 shows the screen of Tracker® during the collect of data of three points: the pendulum bobs and the center of the base. A filter has been used to improve the quality of the video and to facilitate the tracking process. It is also possible to see the axes in cyan and the calibration bar at the bottom of the metronome at the right side.

Figure 3.7 – Tracker® screen with a *negative* filter while collecting data from the whole experiment, one mass displacement at a time. It is possible to seen the axis in purple and the calibration bar in blue at the bottom of the metronome on the right.

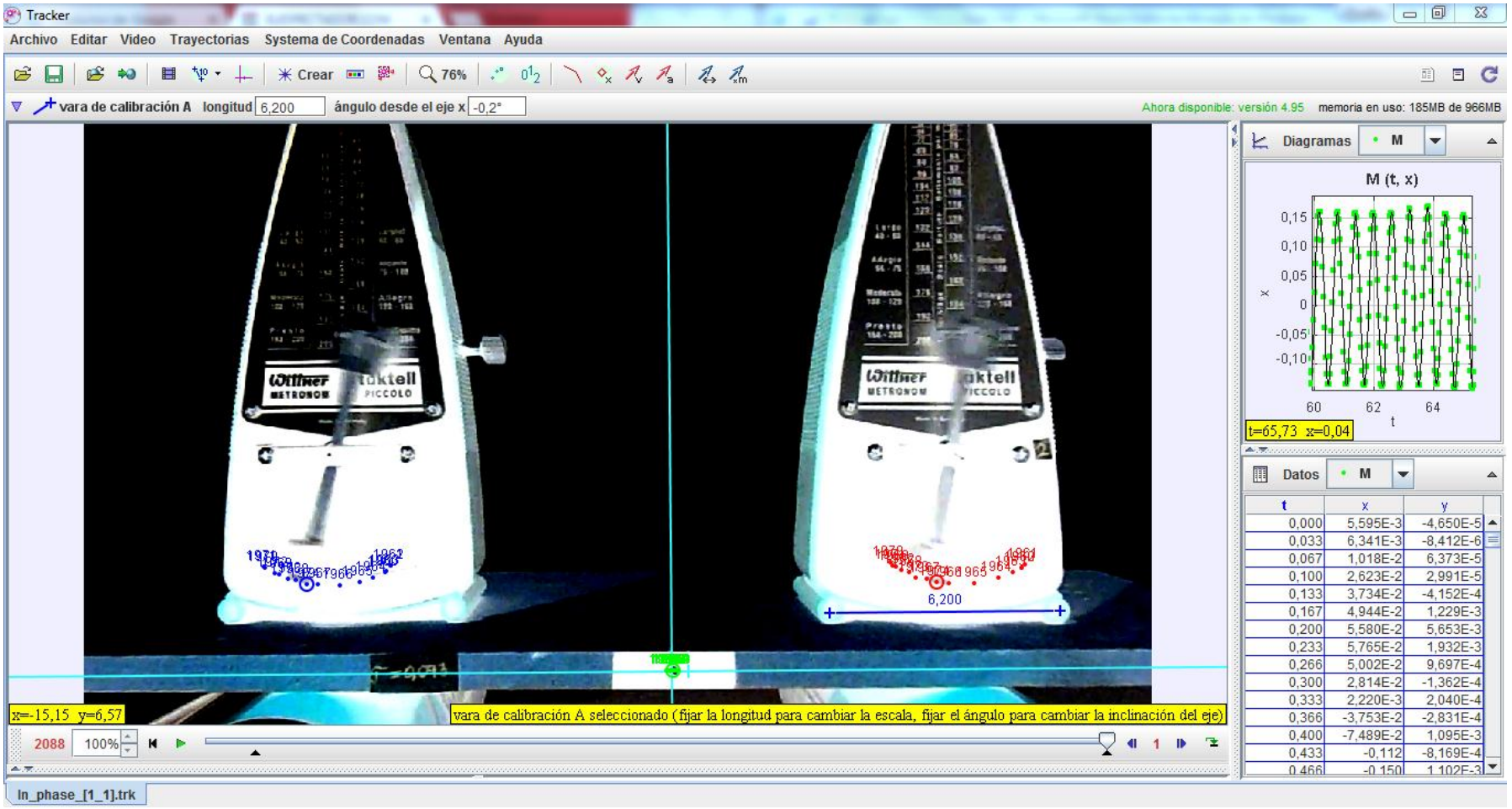

Source: Elaborated by the author.

3.6 Experimental Synchronization Analysis

In this section the experiments on anti-phase and in-phase motion of the metronomes are described. The data is extracted from videos using Tracker®. The IF method is then applied to the data which is then presented and discussed.

The metronomes used in the experiments are *Wittner® Taktell-Piccolo (Serie 830)*, the frequencies of which can be set from 40 to 200 bpm (see Appendix 1 for a detailed description of the metronomes). A metronome has 146g of mass, but the oscillating mass of it, the mass of the pendulum is 30g, which is called in this work the *metronome mass* (m_1 for the metronome at the left side and m_2 for the metronome at the right side in Figure 2.1 and Figure 3.8). The difference between these two masses is the casing mass and this difference is added to the mass of the wooden base, as they move together during the experiments. The result of this addition is called the *base mass M* and is 438.4g, leading to a mass ratio $\sigma = 0.068$ for the experiments described in this chapter.

The experiments were recorded with a Nikon Coolpix L320 camera at 30 frames per second (fps) with a resolution of 1280×720 pixels. The horizontal displacements of the pendulums bobs are of interest and not the angle described by the pendulums with respect to the vertical axis, since the approximation $r\sin\theta \approx r\theta = x$ (with an error about 5.5% for an angle of 40º) is assumed; where *r* is length of a pendulum, θ its angle from the vertical and *x* its horizontal displacement for small angles. The maximum measured angle described by a metronome at the steady-state in these experiments was approximately 32º.

Three sets of experimental results are shown. In the first experiment, the oscillation frequencies of two metronomes oscillating separately on a rigid base were measured. In the second and the third experiments anti-phase and in-phase synchronization were investigated respectively. The frequencies of the metronomes in each experiment are compared.

In the first experiment an isolated metronome was set to oscillate on a table at 192 bpm (1.6 Hz), its motion was recorded and its horizontal displacement was extracted with Tracker®. Later a second experiment was carried out with a second metronome, which was set to oscillate in an isolated condition at the same frequency. Figure 3.8a shows two pictures corresponding to each experiment. The IFs were calculated from the displacement data and plotted. The ICs are not taking into account in this first experiment as the interest is on the frequency of oscillation at the steady-state and the metronomes are isolated from each other.

Figure 3.8 – Actual pictures of the experimental setups. a) Experiment 1, b) Experiment 2, c) Experiment 3.

a)

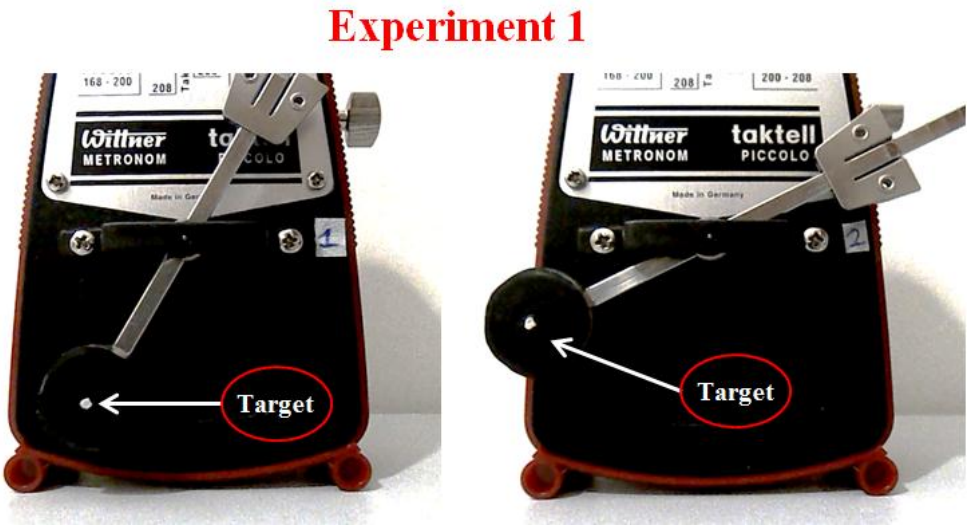

b)

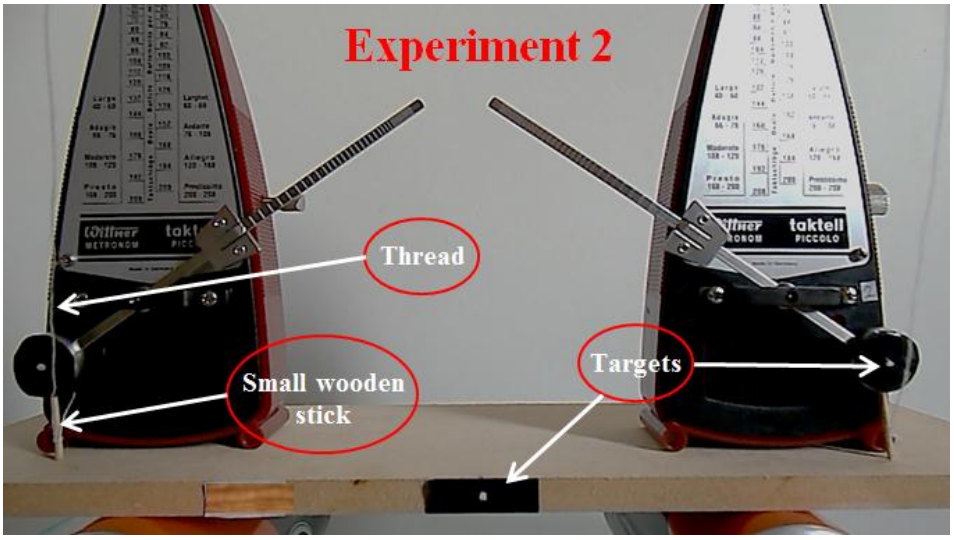

c)

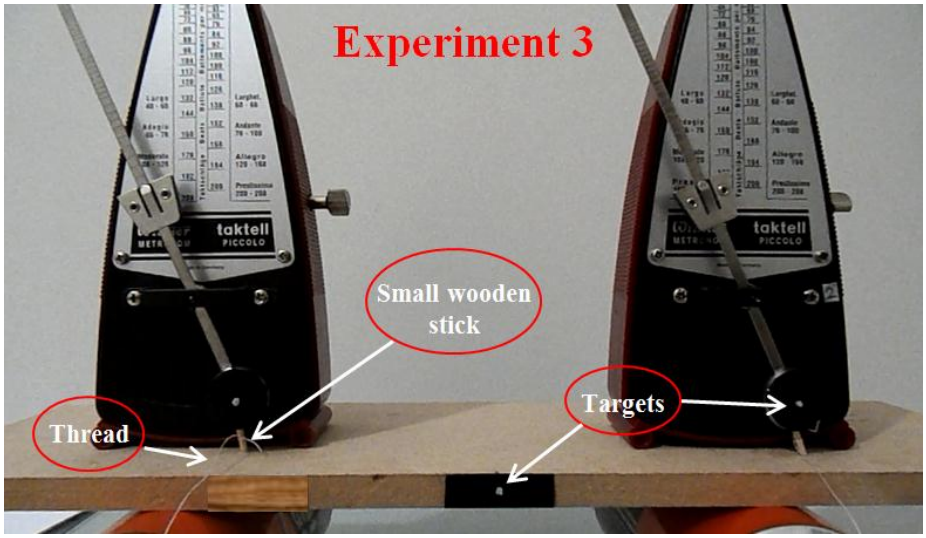

Source: Elaborated by the author.

Figures 3.9a and c show the horizontal time-domain displacement of both metronomes and the IFs, respectively. Figures 3.9b and d show their respective zooms at the steady-state. It is important to stress that although the data of both metronomes are plotted in the same graph, they correspond to separate experiments. Figure 3.9c and d shows that the IFs of both metronomes oscillate about the value 1.6 Hz. This is the frequency at which both metronomes where set to oscillate. The oscillation of the IFs in Figure 3.9d reveals the presence of higher harmonics in the displacement of the metronomes; some noise is also present in the signals.

Figure 3.9 – Experimental time-domain displacements of two metronomes alone (uncoupled) with different ICs and their IFs. (a) and (b) displacement of each metronome and zoom at their steady-state. (c) and (d) IFs for each metronome and zoom at the steady-state, respectively. Solid blue line – m_1, red circle mark line – m_2, dashed green line – M.

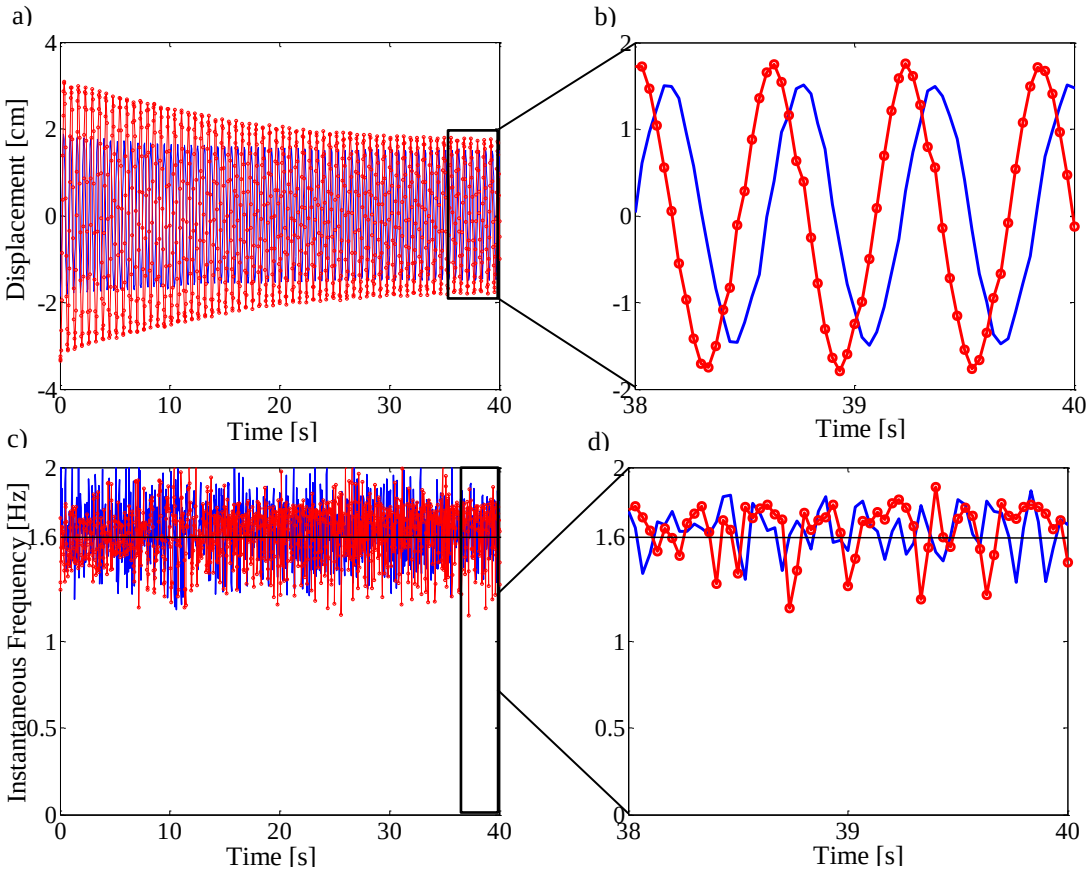

Source: Elaborated by the author.

In the second experiment, anti-phase synchronization of two metronomes on top of a mobile base was studied. Figure 3.8b shows a picture of the experimental setup. The metronomes are located on a wooden base which sits on two soda cans. This enables the wooden base to move in the horizontal direction (see also Figure 3.7). For the synchronization

experiments small wooden sticks joined by a thread were placed between the wooden base and pendulum bobs and removed at the same time to start the metronomes moving. This was done to ensure the ICs were those required. In particular the initial velocities were set to zero. To track the motion of the pendulum bobs and the base, small white targets were adhered to their centers (Figure 3.8b).

The ICs for the system in Figure 3.8b were $\left[x_1(0)\ x_M(0)\ x_2(0)\right]=\left[3.02\ 0\ -2.87\right]$ [cm] and $\dot{x}_i(0)=0$ where i can take the values $1, M, 2$. Anti-phase synchronization of the system is observed for a mass ratio $\sigma=0.068$, which corresponds to $M=14.7m$. Figures 3.10a and c show the time-domain displacements of each mass and their IFs, respectively. Figures 3.10b and d show their respective zooms. Figure 3.10b shows the anti-phase motion of m_1 and m_2 and the almost zero motion of *M* in the steady state; some noise can also be seen.

In Figure 3.10c it is possible to see that the calculation of the IFs amplifies the effect of the noise present in the displacement signals, and this effect is larger for *M* (Figure 3.10 shows a mean value of the IF for *M*). Note that the noise present in the experimental data contributes to the noise in the experimental IFs. This effect is present in simulations too and has been discussed in section 3.4. Figure 3.10d shows that when the system is synchronized in anti-phase, the IFs of m_1 and m_2 oscillate around their natural frequencies of oscillation (or initial set up oscillation frequencies), 1.6 Hz, while the base *M* remains static. The oscillation of the IFs reveals the presence of higher harmonics in the displacements.

In the third experiment, in-phase synchronization of the system in Figure 2.1 is studied. The IFs of the metronomes alone are compared with those obtained from the synchronization experiments at the steady-state. Figure 3.8c shows an actual picture of the in-phase experiment. The ICs are $\left[x_1(0)\ x_M(0)\ x_2(0)\right]=\left[1.35\ 0\ 1.33\right]$ [cm] and $\dot{x}_i(0)=0$. Figures 3.11a and c show the time-domain displacement of the metronomes and the base, and their IFs, respectively. Figure 3.11b and d show their respective zooms. Figure 3.11b shows that m_1 and m_2 oscillate in-phase while *M* oscillates in anti-phase in relation to m_1 and m_2. Figures 3.11c and d show that the three masses oscillates at a frequency which is little higher than 1.6 Hz, the mean value of the IFs in these figures is 1.65 Hz. This shows that when the

system synchronizes in-phase, the frequency of the oscillators is increased, compared with the

Figure 3.10 – Experimental anti-phase synchronization and their IFs. (a) and (b) Anti-phase synchronization of the system and zoom of the steady-state, respectively, for $\sigma = 0.068$ and ICs $\left[x_1(0)\ x_M(0)\ x_2(0)\right] = \left[3.02\ 0\ -2.87\right]$ [cm] and $x_i'(0) = 0$. (c) and (d) IFs for each mass and zoom at the steady-state, respectively. Solid blue line – m_1, red circle mark line – m_2, dashed green line – M.

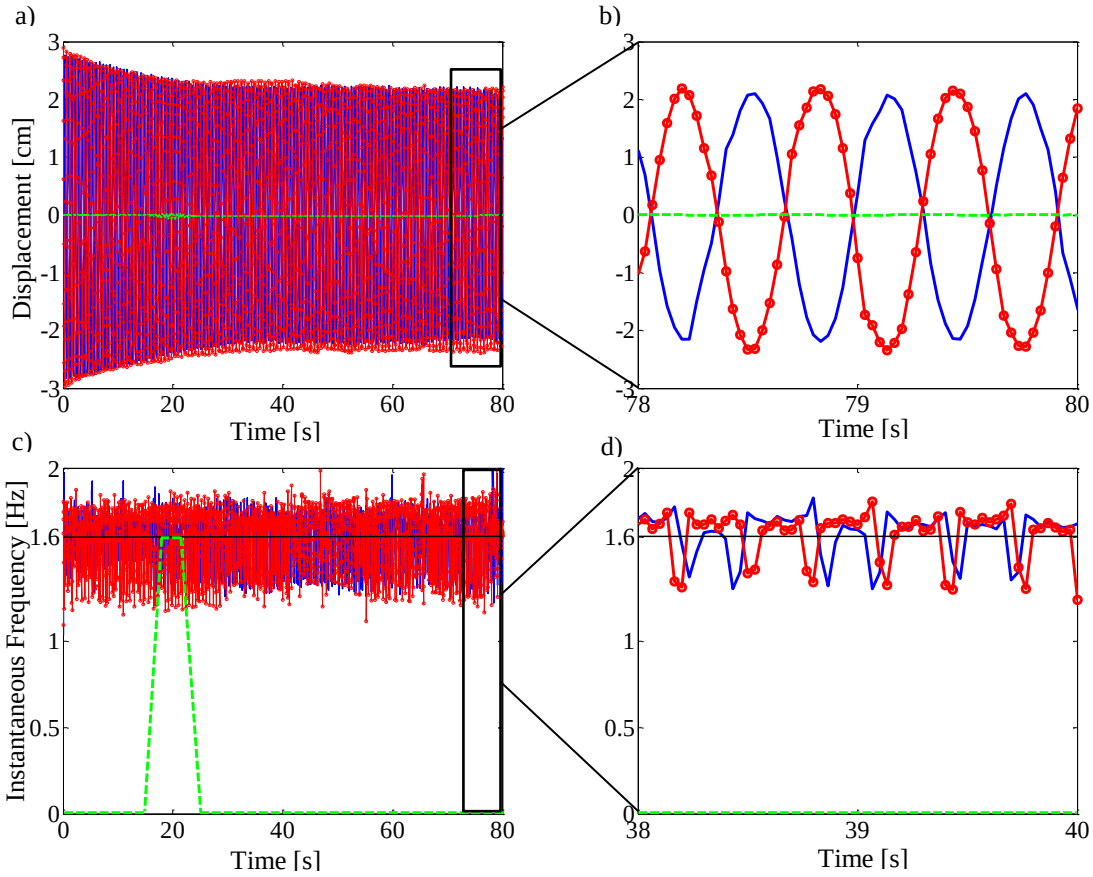

Source: Elaborated by the author.

initial set up frequency. This also occurs with the model in both cases, when van der Pol damping is present and when no damping is considered in the system. This corresponds to the frequency of oscillation of the third mode of vibration for such a system (see section 2.3 in chapter 2). The oscillation of the IFs reveals the presence of higher harmonics in the time-domain displacements, as well as some noise characteristics of the experimental data.

The error in the measurements of the displacements of m_1 and m_2 is about ±1 mm and corresponds in all cases to less than 2.3%. The error in the displacement of M is ±0.4 mm and corresponds to less than 1.4% for the in-phase synchronization experiment. However for

the anti-phase synchronization experiment it can be considerable, when compared with its amplitude, as *M* is static and then it generates some noise which is amplified when the IF is

Figure 3.11 – Experimental in-phase synchronization and their IFs. (a) and (b) In-phase synchronization of the system and zoom of the steady-state, respectively, for $\sigma = 0.068$ and ICs $\left[x_1(0)\ x_M(0)\ x_2(0)\right] = \left[1.35\ 0\ 1.33\right]$ [cm] and $x_i'(0) = 0$. (c) and (d) IFs for each mass and zoom at the steady-state, respectively. Solid blue line – m_1, red circle mark line – m_2, dashed green line – *M*.

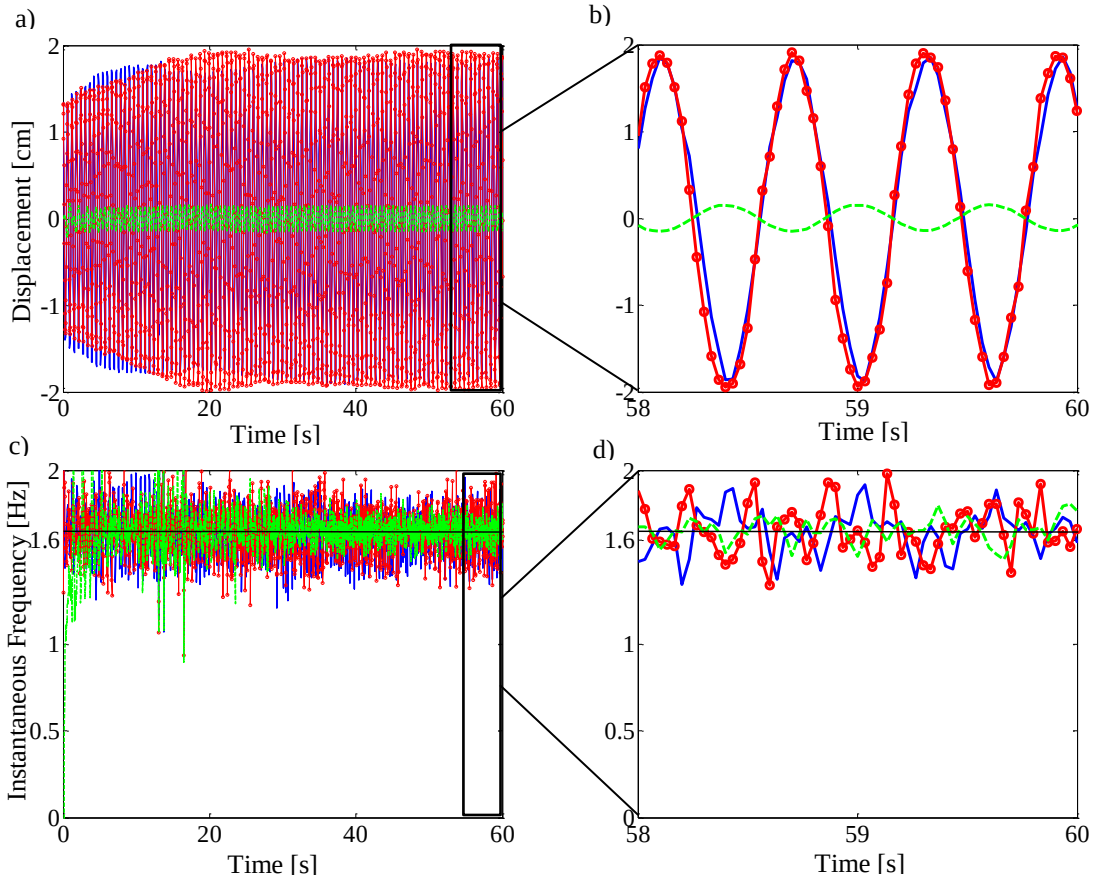

Source: Elaborated by the author.

calculated. However, comparing this value with amplitudes of m_1 and m_2, it is evident that *M* is static.

3.7 Conclusions

In this Chapter the IF concept has been introduced and applied to numerical simulations, as well as to in-phase, and anti-phase, experimental data. It has been shown that oscillation of the IF indicates the presence of higher harmonics in the signals and that the IF

oscillates around the value of the fundamental frequency of the signal. An analytical expression relating the IF of a signal and its higher harmonics has been found. The software Tracker® has been introduced and its main features of interest in this work have been described. It has been shown that when the system synchronizes in anti-phase, the frequency of oscillation of the metronomes is equal to their frequency of oscillation before they have been coupled in the system (their natural frequencies). It has also been also shown that, for in-phase synchronization, the three masses oscillate at the same frequency, which is higher than the frequencies of oscillation of the metronomes when they are placed on a rigid base. This has been shown to be valid for both simulations and experimental results.

In the next chapter the relationship between initial conditions and the final synchronization state is investigated.

4 BASINS OF ATTRACTION FOR SYNCHRONIZATION OF THE MODEL

4.1 Introduction

In chapter 2 it has been shown that the model in Figure 2.4 can capture the qualitative behaviour of two coupled metronomes. In chapter 3 a method to analyse the final synchronization state of the system has been studied and an experimental methodology to collect experimental data based on videos has been introduced. The aim of this chapter is to investigate how the ICs affect the final synchronization state. This is illustrated by using the model in Figure 2.4 by means of the concept of *basins of attraction* (THOMPSON; STEWART, 2002). Some experimental results are also presented and discussed. The whole work is focused on in-phase or anti-phase synchronization.

In this work basins of attraction describe the set of initial conditions which after some time leads the system to one of the two final synchronization states. Its name comes from the study of dynamical systems which, given a set of initial conditions, tends to stable limit cycles (e.g. stable oscillations) known as attractors (see e.g (BALANOV, 2009, p. 95)). In this chapter they are two-dimensional maps relating the initial displacements of the metronome masses to the two final synchronization states of interest. Basins of attraction have not used extensively in the study of synchronization of metronomes. The motivation to study such maps comes from the research conducted by Peña Ramirez (2013), in his doctoral thesis, who used a map while investigating in-phase and anti-phase synchronization of two oscillator.

4.2 Basins of Attraction for Several Damping and Mass Ratios

The study in Chapter 2 suggests that the key parameters for the synchronization of the model in Figure 2.4 are the damping ratio μ and the mass ratio σ. Then, for a given pair of parameters and for a given set of ICs, it is possible to determine the final synchronization state of the model in Figure 2.4 by numerically integrating equations (2.11). There are six ICs, three for the initial displacements of m_1, m_2 and M, and their corresponding initial velocities. If all the velocities are considered to be zero and the initial displacement of M is set to zero, only the initial displacements for m_1 and m_2 need to be considered.

Two different cases are considered. In the first case six basins of attraction are shown for six different values for μ, while the mass ratio is set so that $\sigma = 0.1$. In the second case, five basins of attraction are shown for five different values for the mass ratio σ while the damping ratio is set so that $\mu = 0.1$. In this study similar oscillators are considered, which represents the case when the natural frequencies of each metronome are equal.

Figure 4.1 shows the basins of attraction for a range of non-dimensional initial displacements for m_1 and m_2 when the damping parameter increases from $\mu = 0.01$ up to $\mu = 0.5$. There is a coloured pixel for each combination of initial conditions. A light green pixel represents in-phase synchronization for the specific combination, and a dark blue pixel represents anti-phase synchronization, the lighter the damping the longer the time necessary to obtain synchronization and therefore the greater the computational work to assign a colour to a given pixel.

To provide a sense of the computational work necessary to obtain each pixel of one basin of attraction, numerical simulations of the time-domain synchronization of the system are presented for two different values of damping, using initial conditions leading the system to obtain in-phase and anti-phase synchronization. Figures 4.2a and 4.2b show the in-phase and anti-phase synchronization of the system for $\mu = 0.1$ and $\sigma = 0.1$ and ICs $\left[x_1(0)\ x_M(0)\ x_2(0)\right] = [1\ 0\ 3\ ]$ for in-phase, and $\left[x_1(0)\ x_M(0)\ x_2(0)\right] = [1\ 0\ \text{-}3\ ]$ for anti-phase synchronization. For these specific ICs, the system reaches both types of synchronization in almost the same short period of time. Using the same ICs corresponding with each type of synchronization and the same mass ratio but using a tenth of the damping previously used $\mu = 0.01$, it can be seen in Figures 4.3a and 4.3b that the time the system takes to synchronize could be increased between 7 and 9 times the time for synchronization to be achieved with a higher damping. Additionally, each basin of attraction is composed of 101x101 pixels, leading to a 10201 pixels two dimensional map. After some simulations, one notice that because of the system is symmetric only half of this number of simulations need to be conducted.

Figure 4.1a shows the basins of attraction for $\mu = 0.01$, a damping ratio which is nearly six times the experimental value found in Appendix 2 for the metronomes. Figure 4.1b shows the basins of attraction for $\mu = 0.1$, ten times the damping ratio used in Figure 4.1a. The results in

Figure 4.1 – Basins of attraction showing when the system is attracted to either in-phase or anti-phase synchronization state for six different damping values μ and for a constant mass ratio $\sigma = 0.1$. The horizontal axis are initial positions for m_1 and the vertical axis are initial positions for m_2, when $\hat{x}_M = 0$ and $\hat{x}_i' = 0$. (a) $\mu = 0.01$, (b) $\mu = 0.1$, (c) $\mu = 0.2$, (d) $\mu = 0.3$, (e) $\mu = 0.4$, (f) $\mu = 0.5$. Green (light) pixels – in-phase synchronization, blue (dark) pixels – anti-phase synchronization.

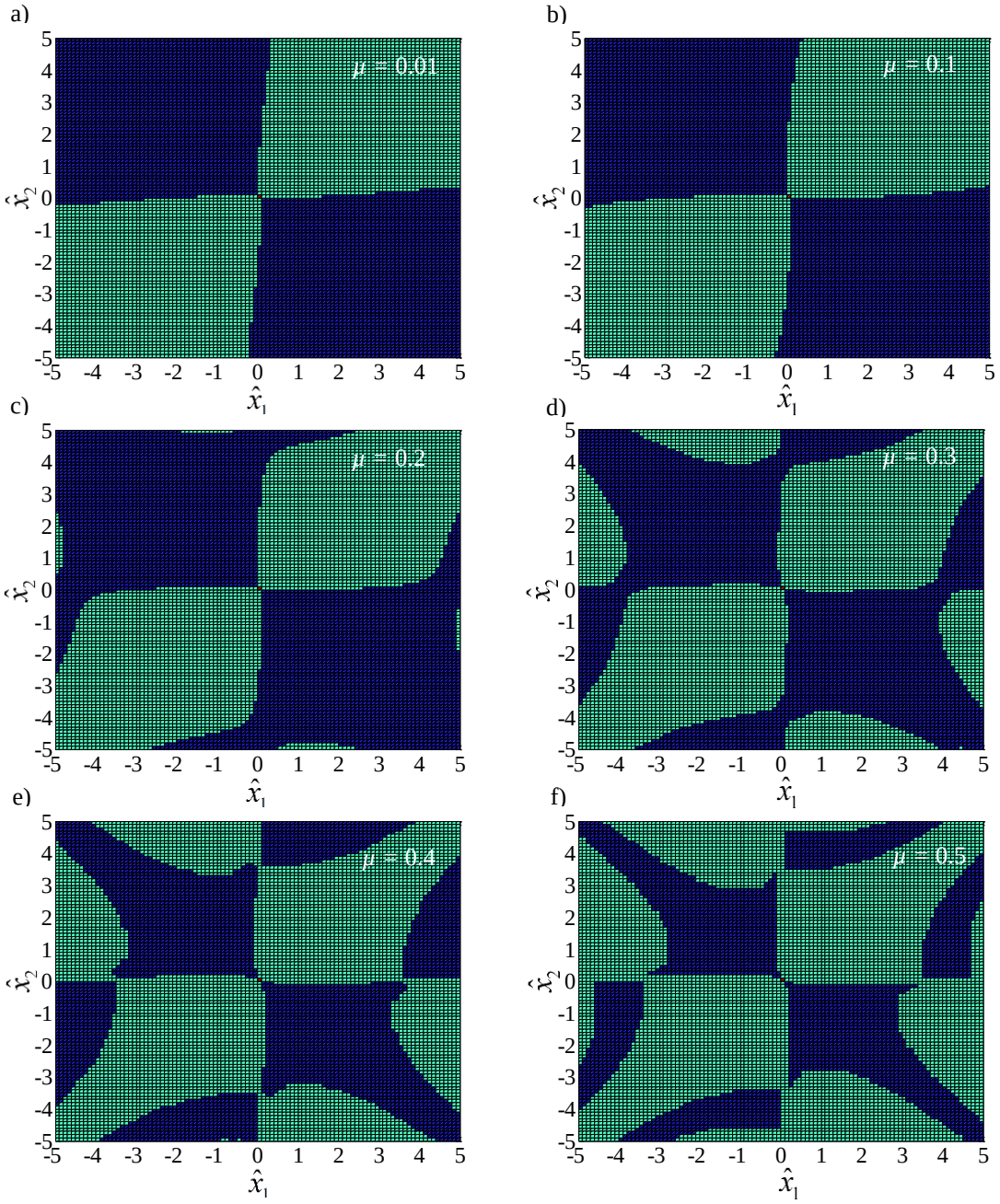

Source: Elaborated by the author.

Figure 4.2 – In-phase and anti-phase synchronization for $\mu = 0.1$ and $\sigma = 0.1$. a) In-phase synchronization of the 3DOF system and zoom of its initial and final states for ICs $\left[x_1(0)\ x_M(0)\ x_2(0)\right] = \left[1\ 0\ 3\right]$ [cm] and $x_i'(0) = 0$. b) Anti-phase synchronization of the system for ICs $\left[x_1(0)\ x_M(0)\ x_2(0)\right] = \left[1\ 0\ -3\right]$ [cm] and $x_i'(0) = 0$. Solid blue line – m_1, red line – m_2, dashed green line – M.

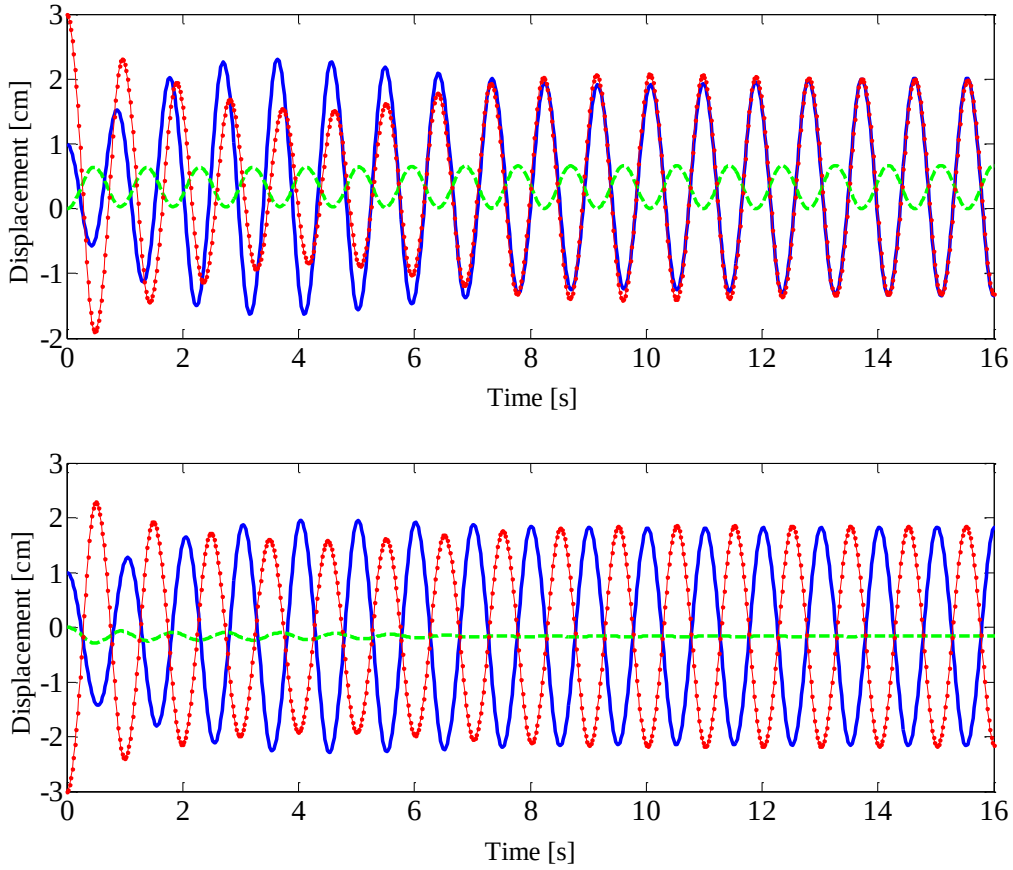

Source: Elaborated by the author.

Figures 4.1a and b are roughly separated by the horizontal and the vertical axes, suggesting that, when $\sigma = 0.1$ and the system has small damping, the final synchronization state generally depends on the sign of the initial displacements. It can be seen that ICs with the same sign generally lead to in-phase synchronization, while ICs with a different sign generally lead to anti-phase synchronization. Note that both figures are very similar; showing that for this range of damping ratios the influence of the ICs in the final synchronization state do not suffer significant changes when $\sigma = 0.1$. It will be seen that the experiments described in this chapter the mass and damping parameters correspond to $\sigma = 0.068$ and $\mu = 0.017$.

The basins of attraction for the experiments are therefore expected to be similar to those presented in Figure 4.1a.

Figure 4.3 – In-phase and anti-phase synchronization for light damping $\mu = 0.01$ and $\sigma = 0.1$. a) In-phase synchronization of the system and zoom of its initial and final states for ICs $\left[x_1(0)\ x_M(0)\ x_2(0)\right] = [1\ 0\ 3\ ]$ [cm] and $\dot{x}_i(0) = 0$. b) Anti-phase synchronization of the system and zoom of its initial and final states for ICs $\left[x_1(0)\ x_M(0)\ x_2(0)\right] = [1\ 0\ -3\ ]$ [cm] and $x_i'(0) = 0$. Solid blue line – m_1, red line – m_2, dashed green line – M.

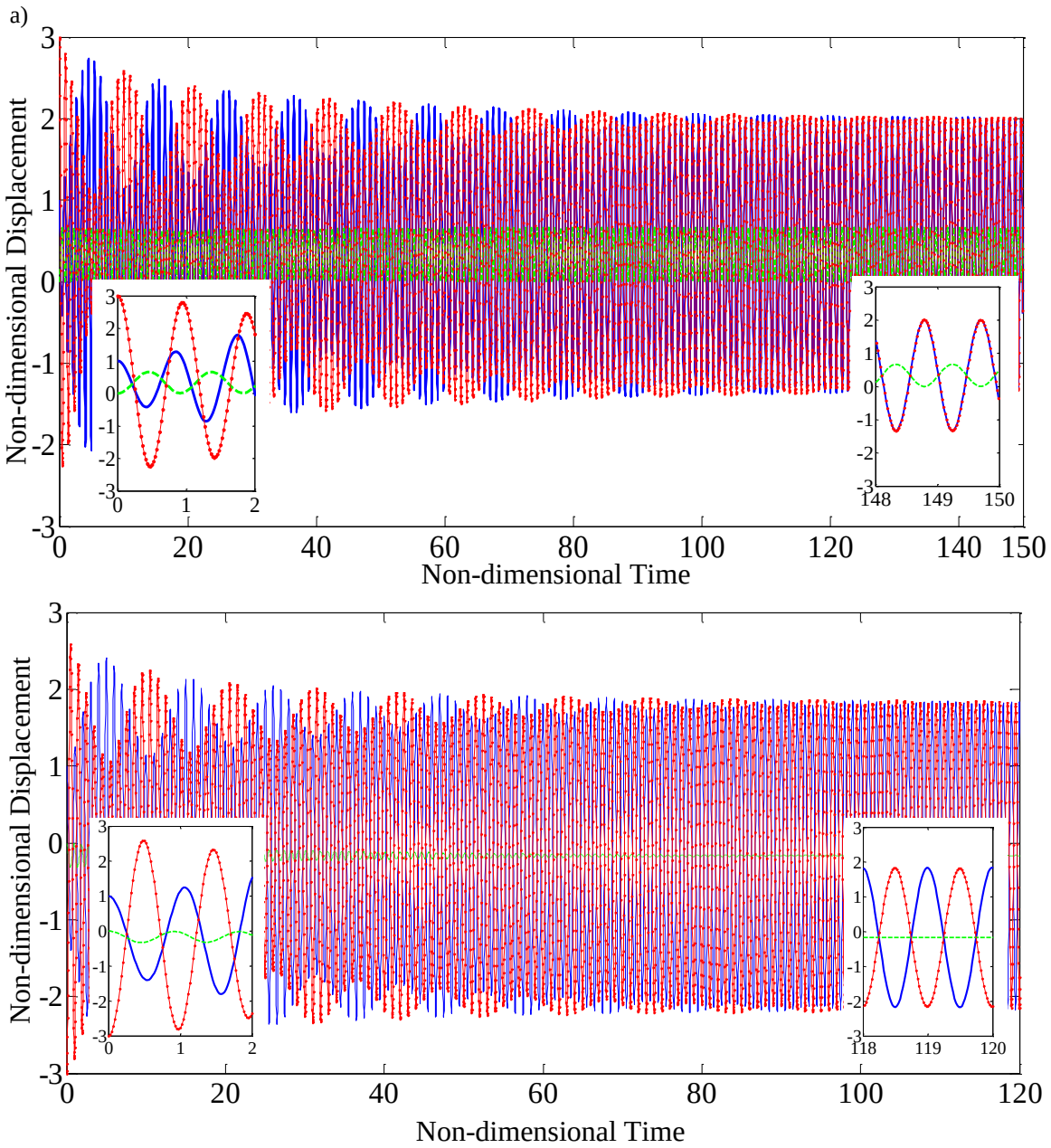

Source: Elaborated by the author.

An increase of the damping in the system causes the system to bias so that it synchronizes more often in anti-phase than in-phase, as shown for example in Figure 4.1c. By further increasing the damping in the system, this process is reversed and for the same range

of ICs the system reaches in-phase synchronization more often than anti-phase synchronization, as shown in Figure 4.1d, e and f. This suggest that in-phase synchronization is easier to obtain for large damping values, when $\sigma = 0.1$ (there is an exception when $\mu = 0.3$ although the difference between both synchronization states is not large). Note also the increasing complexity of the basins of attraction as the damping values is increased.

Figure 4.4 shows the ratios between the number of ICs leading to in-phase (IP) and anti-phase (AP) synchronization for the parameters used in the basins of attraction of Figure 4.1. Each ratio corresponds to one map with specific damping value. The letters in the horizontal axis correspond to the labels of each figure in Figures 4.1. The ratios IP/AP in Figure 4.4 shows

Figure 4.4 – Ratios between the number of IC leading to anti-phase (AP) to the number of IC leading to in-phase (IP) final synchronization states for $\sigma = 0.1$ and the damping values $\mu = 0.01$, $\mu = 0.1$, $\mu = 0.2$, $\mu = 0.3$, $\mu = 0.4$, and $\mu = 0.5$. The letters in the horizontal axis correspond to the labels of each figure in Figures 4.1.

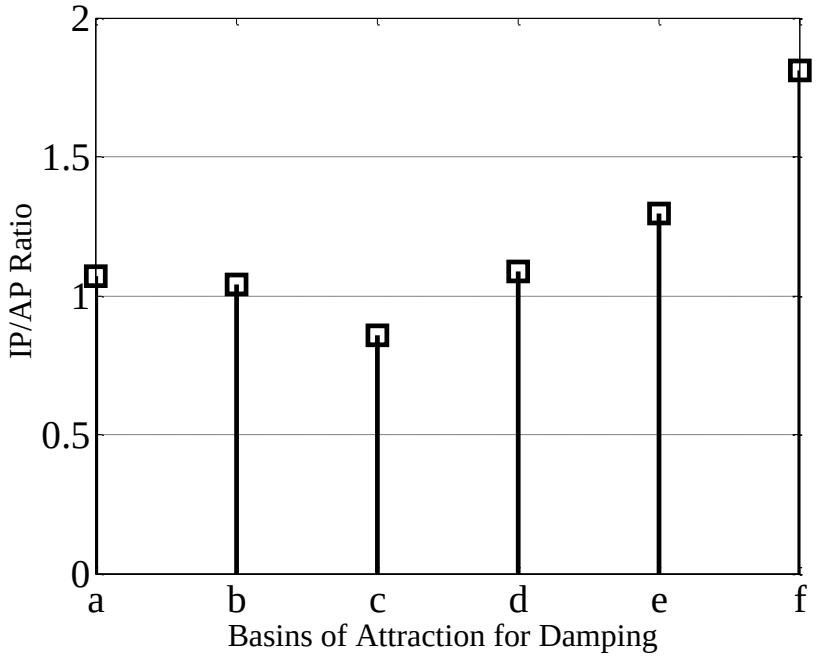

Source: Elaborated by the author.

that for this mass ratio, in-phase synchronization is more common, although for small damping values the difference between both synchronization states is very small. For high damping values the difference increases and in-phase synchronization is more common than the anti-phase state.

Figure 4.5 shows the basins of attraction for five different values of the mass ratio σ while $\mu = 0.1$ is constant. These values for σ are equivalent to a base mass M equal to 50, 20, 10, 5 and 1 times larger than m, corresponding with the mass ratio values $\sigma = 0.02$, $\sigma = 0.05$, $\sigma = 0.1$, $\sigma = 0.2$ and $\sigma = 1$, respectively. Figure 4.5a shows that, for this level of damping and for a large base mass compared to the metronomes, anti-phase synchronization is achieved more often than in-phase synchronization. There is also an interesting feature in the basin of attraction shown in Figure 4.5a for the set of ICs near the origin. For a base mass of 20 or 10 times larger than m, the in-phase and anti-phase synchronized states occur almost equally often as shown in Figures 4.5b and c. When M is 5 times larger than m, the anti-phase state starts to become more common once more, and is even more dominant when $M = m$. Figure 4.6 shows the ratios between the number of ICs leading to in-phase synchronization to the number of ICs leading to anti-phase synchronization. These simulations suggest that for light damping the anti-phase synchronization state is more common than the in-phase state. The lighter the base, compared to the metronome mass, the more dominant the anti-phase state becomes.

Figure 4.5 – Basins of attraction showing when the system is attracted to either in-phase or anti-phase synchronization state for five different mass ratio values σ and for a constant damping $\mu = 0.1$. The horizontal axis are initial positions for m_1 and the vertical axis are initial positions for m_2, when $\hat{x}_M = 0$ and $\hat{x}_i' = 0$. (a) $\sigma = 0.02$, (b) $\sigma = 0.05$, (c) $\sigma = 0.1$, (d) $\sigma = 0.2$, (e) $\sigma = 1$. Green (light) dots – in-phase synchronization, blue (dark) dots – anti-phase synchronization.

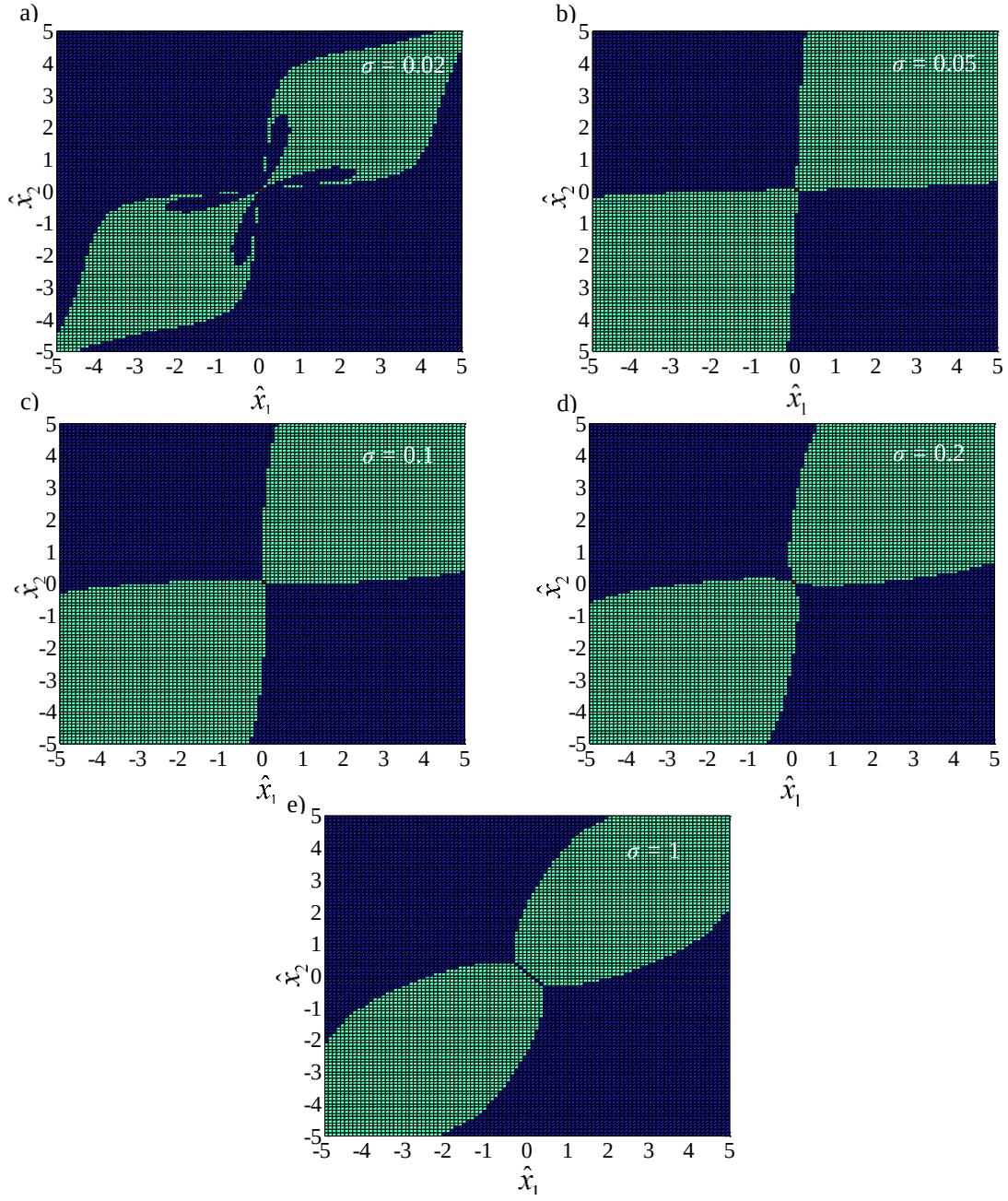

Source: Elaborated by the author.

Figure 4.6 – Ratios between the number of IC leading to anti-phase (AP) to the number of IC leading to in-phase (IP) final synchronization states for $\mu = 0.1$ and the mass ratios $\sigma = 0.02$, $\sigma = 0.05$, $\sigma = 0.1$, $\sigma = 0.2$, and $\sigma = 1$. The letters in the horizontal axis correspond to the labels of each figure in Figures 4.5.

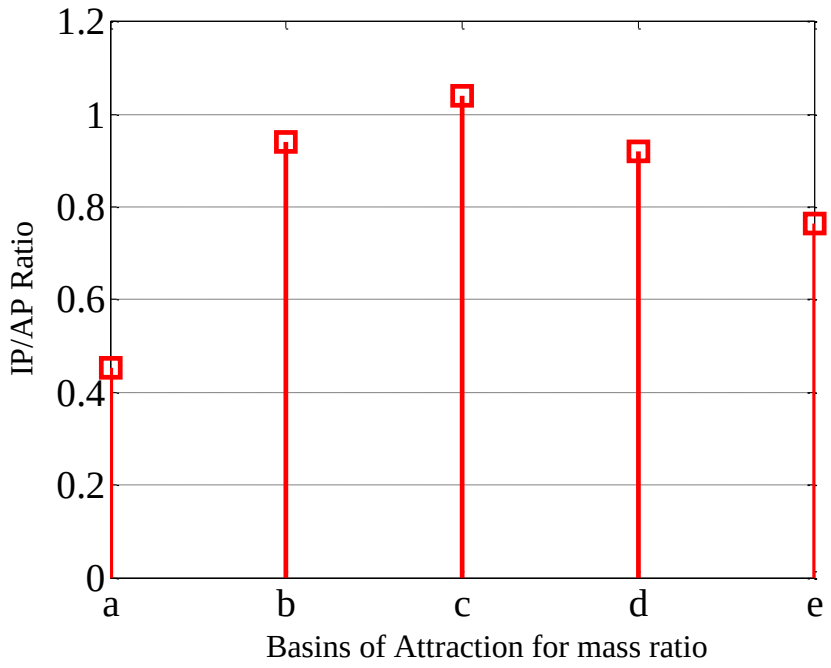

Source: Elaborated by the author.

4.3 Some Experimental Results

In the previous sections the relationship between ICs, parameters and the final synchronization state of the model for two coupling metronomes on a mobile base has been studied. It has been shown that, depending on the chosen values for the mass ratio and damping, one of the two final synchronization states of interest can be more or less dominant for a certain range of ICs. This section discusses two types of experimental results; the first one involves experiments in which the system achieves an expected final synchronization state from its ICs, called *typical* experiments, the seconds involves experiments in which the system achieves a final synchronization state different to the one expected.

Typical experiments occur when the ICs of an experiment are favourable to one of the synchronization states and the final state of the system is this one. The other cases are the second type of experiments shown in this section. It has been observed for the model results in the basins of attraction that, in general when the system is set with ICs with the same sign,

it is more likely for the system to reach in-phase synchronization, and when the ICs have different sign its more likely for the system to synchronizes in anti-phase.

The parameters used in the typical experiments are a mass ratio $\sigma = 0.1$ and an internal

Figure 4.7 – Typical experimental in-phase synchronization for $\sigma = 0.1$. a) In-phase synchronization of the system and zoom of its initial and final states for large ICs $\left[x_1(0)\ x_M(0)\ x_2(0)\right] = \left[2.3\ 0\ 2.2\right]$ [cm] and $\dot{x}_i(0) = 0$. b) In-phase synchronization of the system and zoom of its initial and final states for a combination of large and small ICs $\left[x_1(0)\ x_M(0)\ x_2(0)\right] = \left[2.3\ 0\ 1.46\right]$ [cm] and $\dot{x}_i(0) = 0$. Solid blue line – m_1, red circle mark line – m_2, dashed green line – M.

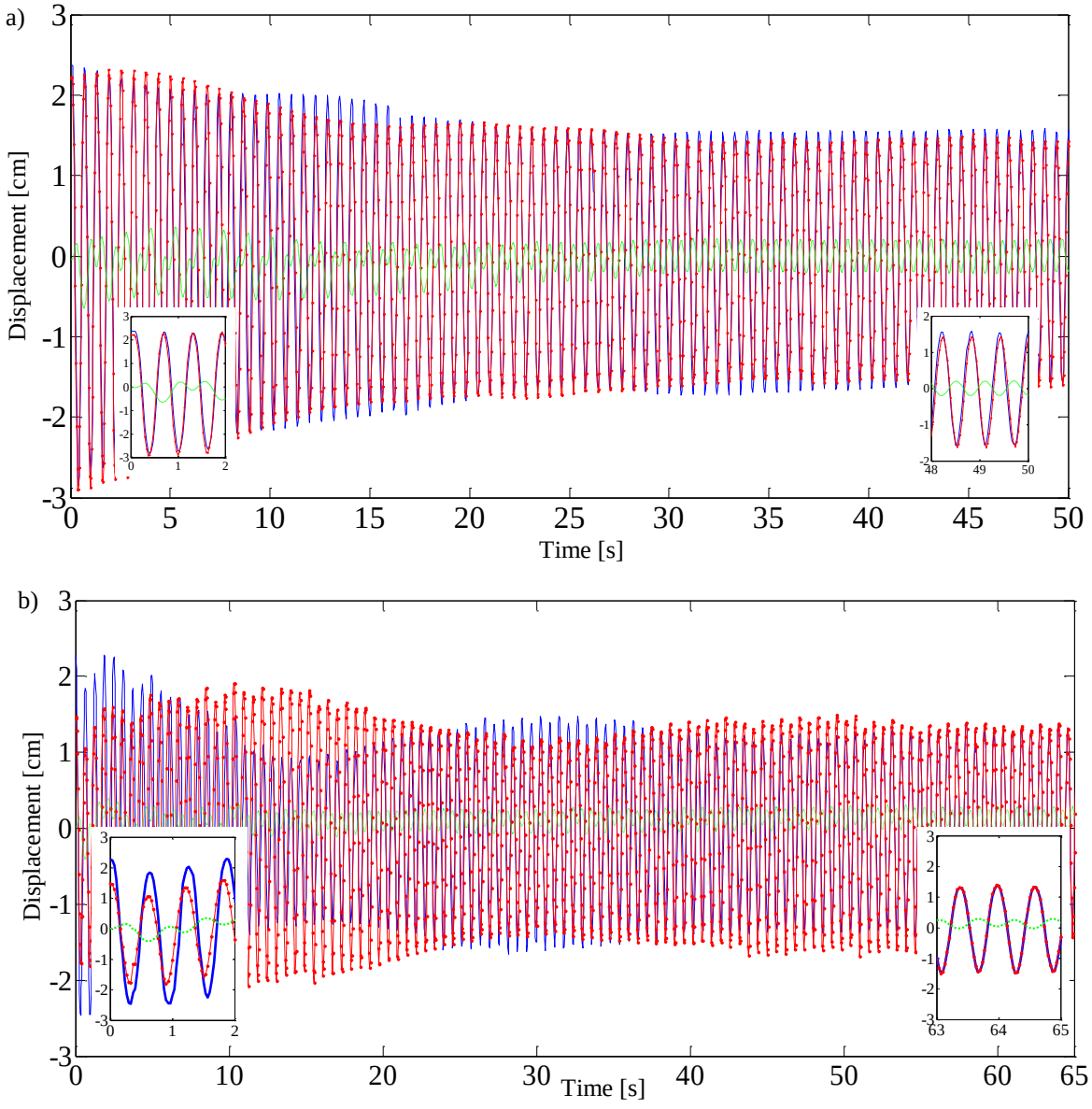

Source: Elaborated by the author.

damping of the metronomes approximated to $\mu = 0.017$ (see Appendix 2), the metronomes of the system in Figure 2.1 have been set at 192bpm (1.6Hz). For these parameters, the basins of attraction which are more similar to the experiments, are those of Figure 4.1a. Figure 4.7a shows the time-domain synchronization of typical experiments for a pair of positive large ICs $\left[x_1(0)\ x_M(0)\ x_2(0)\right] = \left[2.3\ 0\ 2.2\right]$ [cm] and $\dot{x}_i(0) = 0$ This leads to in-phase synchronization, as expected from the basins of attraction. Figure 4.7b shows the time-domain experimental synchronization of the system for combination of positive large and small ICs $\left[x_1(0)\ x_M(0)\ x_2(0)\right] = \left[2.3\ 0\ 1.46\right]$ [cm] and $\dot{x}_i(0) = 0$. This also leads to in-phase synchronization. Figures 4.8a and c shows their respective IFs with their corresponding zooms in Figures 4.8b and d.

Figure 4.8 –IFs for the typical in-phase experiments in Figures 4.7 (a) and (b). IFs for each mass in the experiments in Figures 4.7a and 4.7b and zoom at the steady-statse, respectively. Solid blue line – m_1, red circle mark line – m_2, dashed green line – M.

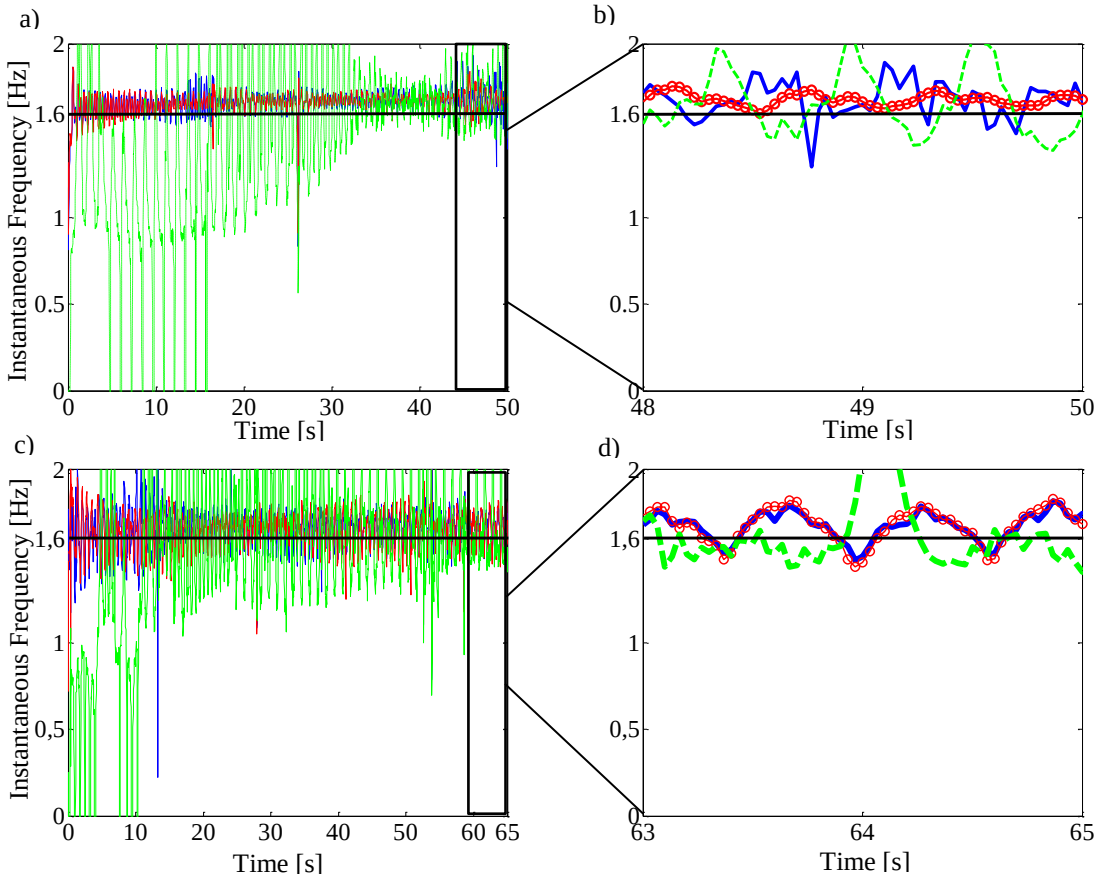

Source: Elaborated by the author.

Figure 4.9 – Typical experimental anti-phase synchronization for $\sigma = 0.1$. a) Anti-phase synchronization of the system and zoom of its initial and final states for two small ICs. $\left[x_1(0)\ x_M(0)\ x_2(0)\right] = [\text{-}1.7\ 0\ 1.2\ ]$ [cm] and $\dot{x}_i(0) = 0$. b) Anti-phase synchronization of the system and zoom of its initial and final states for a combination of short and large ICs $\left[x_1(0)\ x_M(0)\ x_2(0)\right] = [1.6\ 0\ \text{-}2.6\ ]$ [cm] and $\dot{x}_i(0) = 0$. Solid blue line – m_1, red circle mark line – m_2, dashed green line – M.

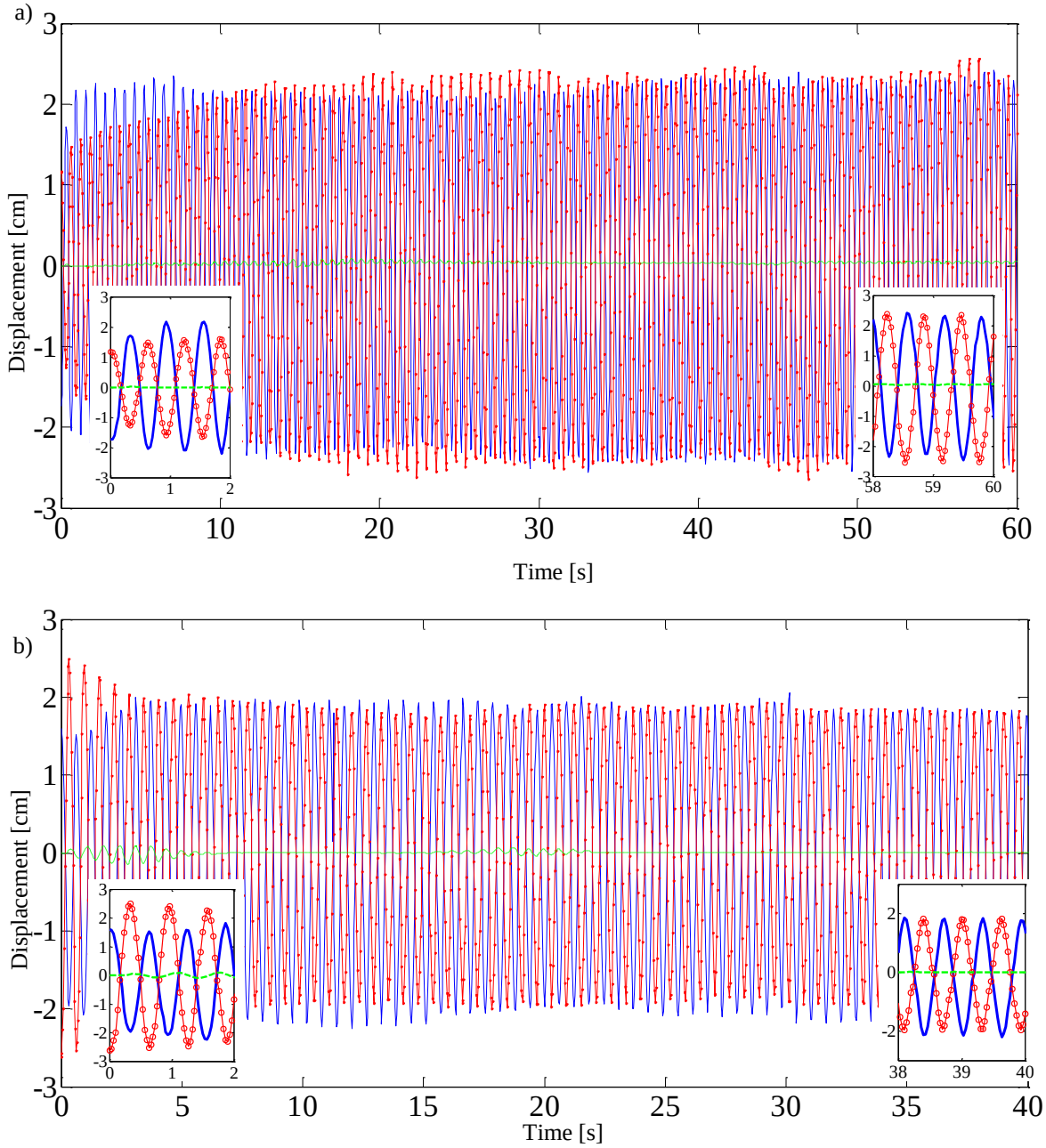

Source: Elaborated by the author.

Figure 4.9a shows a typical experimental result for a pair of small positive and negative ICs $\left[x_1(0)\ x_M(0)\ x_2(0)\right] = [\text{-}1.7\ 0\ 1.2\ ]$ [cm] and $\dot{x}_i(0) = 0$, leading to an expected

anti-phase synchronization. Figure 4.9b shows a typical anti-phase synchronization result for a combination of small positive and large negative ICs $\left[x_1(0)\ x_M(0)\ x_2(0)\right]=[1.6\ 0\ -2.6\ ]$ [cm] and $\dot{x}_i(0)=0$. Figures 4.10a and c shows their respective IFs with their corresponding zooms in Figures 4.10b and d. Note that the IF is higher for in-phase synchronization than for anti-phase synchronization as discussed in chapters 2 and 3.

Figure 4.10 – IFs for the typical in-phase experiments in Figures 4.9. (a) and (b) IFs for each mass in the experiments in Figures 4.9a and 4.9b and zoom at the steady-state, respectively. Solid blue line – m_1, red circle mark line – m_2, dashed green line – M. The IF for M do not appears in the zooms as its mean value is zero. Note that the motion of M tends to zero in the time-domain figures for anti-phase synchronization.

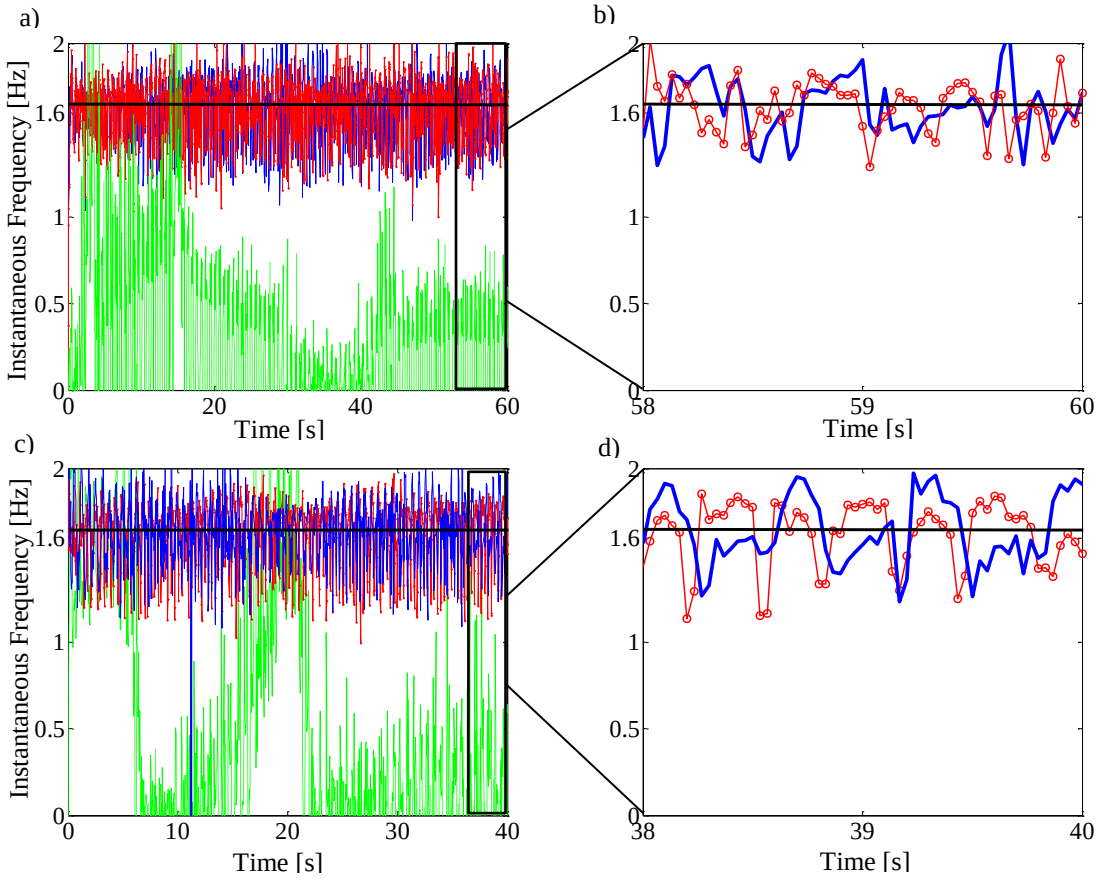

Source: Elaborated by the author.

The second type of experiments is experiments which have ICs favourable to one of the two final synchronization states, but reaches the other synchronization state. Figure 4.11 shows two experimental results in which the system in Figure 2.1 has been set so that the initial displacements of the metronomes have different signs but its final synchronization is in-phase, for this case the new mass ratio is $\sigma=0.068$ and the internal damping of the

metronome is approximately $\mu = 0.017$ (see Appendix 2), the metronomes have been set at 192bpm (1.6Hz).

Figure 4.11a shows the in-phase synchronization of the system in Figure 2.1 when the ICs are

Figure 4.11 – Experimental in-phase synchronization when the ICs are favourable to anti-phase synchronization for $\sigma = 0.068$. a) In-phase synchronization of the system and zoom of its initial and final states for ICs $\left[x_1(0)\ x_M(0)\ x_2(0)\right] = [1.4\ 0\ -3\ ]$ [cm] and $\dot{x}_i(0) = 0$. b) In-phase synchronization of the system and zoom of its initial and final states for ICs $\left[x_1(0)\ x_M(0)\ x_2(0)\right] = [2.8\ 0\ -1.35\ ]$ [cm] and $\dot{x}_i(0) = 0$. Solid blue line – m_1, red circle mark line – m_2, dashed green line – M.

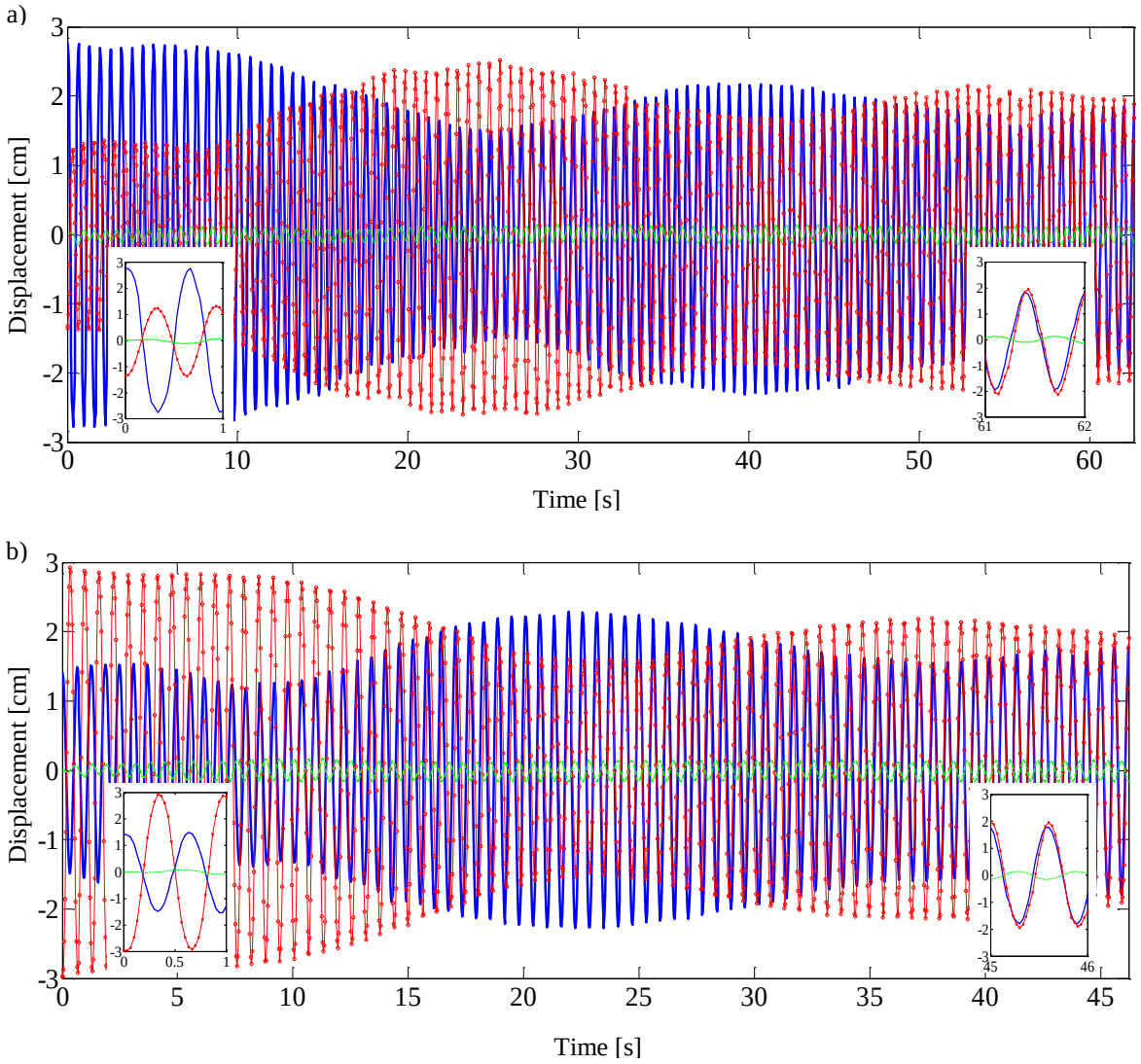

Source: Elaborated by the author.

$\left[x_1(0)\ x_M(0)\ x_2(0)\right] = [1.4\ 0\ -3\ ]$ [cm] and $\dot{x}_i(0) = 0$, and zooms of its initial and final states. Figures 4.11b shows the in-phase synchronization when the ICs are

$\left[x_1(0)\ x_M(0)\ x_2(0)\right]=\left[2.8\ 0\ -1.35\right]$ [cm] and $\dot{x}_i(0)=0$ and zooms of its initial and final states. In both figures the sign of the ICs are different to the final synchronization state. Figures 4.12a and c shows their respective IFs with their corresponding zooms in Figures 4.12b and d.

Figure 4.12 –IFs for the experiments in Figures 4.11. (a) and (b) IFs for each mass in the experiments 4.11a and 4.11b and zoom at the steady-states, respectively. Solid blue line – m_1, red circle mark line – m_2, dashed green line – M.

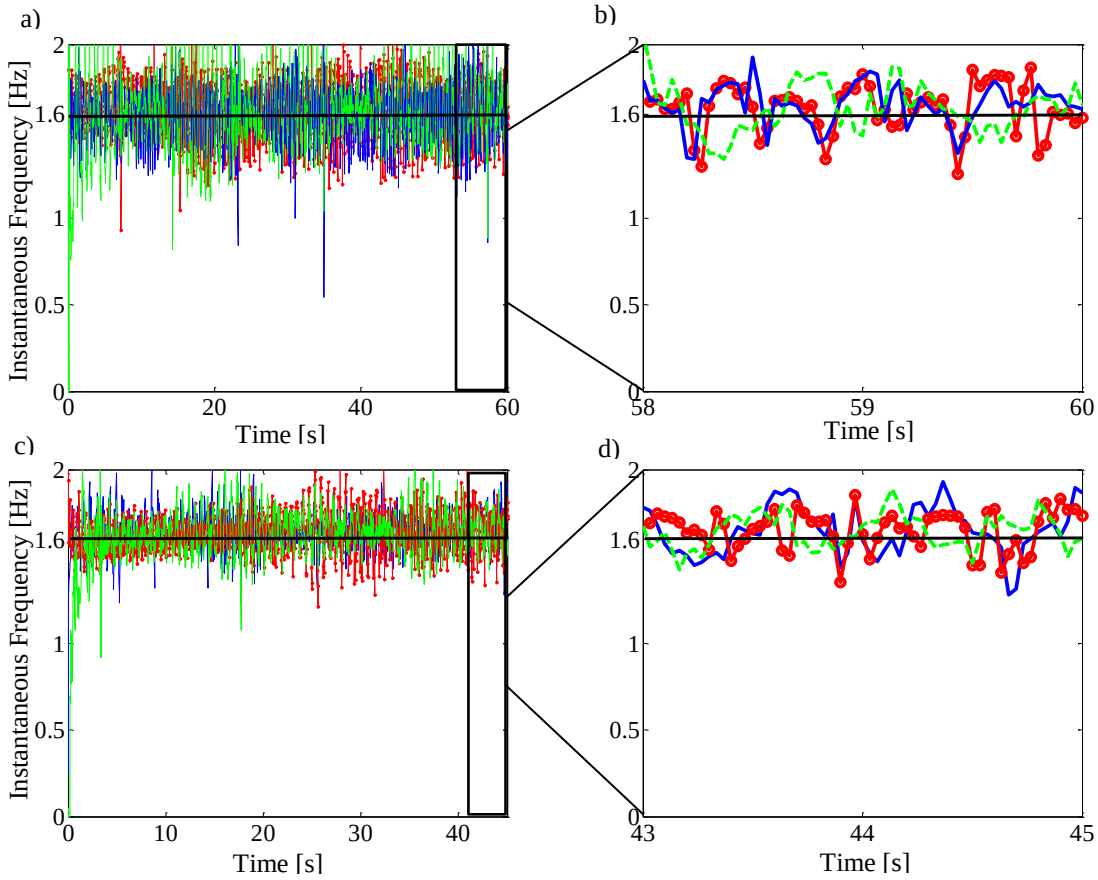

Source: Elaborated by the author.

Comparing Figures 4.7, 4.9 and Figure 4.11, it can be seen that the beating behaviour is grater in Figures 4.11a and b than in the others. That is because one of its ICs is large $\left(x_2(0)=\pm 3\right)$ compared with those used in Figures 4.7, 4.9. The mass with the larger initial displacement supplies a large amount of energy to the system. This energy passes from one mass to the other, forward and backward, up to the point that the transient motion is damped out and the synchronization state is achieved. Therefore some of the causes of the high

beating behaviour seem to be the large initial displacement of one of the masses compared to the displacement of the other mas and the light damping present in the metronomes.

Although the difference in energy supplied by each metronome to the system, causing a longer transient, does not explain why the final synchronization state is different to the expected from ICs with different sign, these results suggest this could be a relevant factor for further research relating to ICs and final synchronization states. Note that stiffness and damping also have an effect on the synchronization process, and that in this work some assumptions have been made. Stiffness is assumed to be linear, while a pendulum shows a softening stiffness characteristic. The internal damping of the metronome has been assumed to be of the van der Pol type, while it actually shows a friction characteristic with an impulse at certain time instants (see Appendix 2). Finally, the damping produced by the friction between the soda cans and the ground has been neglected. Those parameters could also affect the final synchronization state of the actual system and probably will change the basins of attraction when they are included in the model. The introduction of these parameters in the model could be of interest for further investigations into synchronization, relating parameters and ICs with the final synchronization states.

4.4 Conclusions

The model in Figure 2.4 has been used to investigate the way in which the initial conditions affect the final synchronized state of the system – whether the metronomes oscillate in-phase or in anti-phase. From numerical simulations, it has been found that for a mass ratio of $\sigma \leq 0.1$ and considering similar oscillators, ICs with the same sign generally lead to in-phase synchronization, while ICs with a different sign generally lead to anti-phase synchronization, when damping is light $\mu < 0.1$. Increasing the damping but maintaining the same mass ratio results in a bias so that the system synchronizes more often in anti-phase than in-phase. By further increasing the damping in the system, this process is reversed and for the same range of ICs the system reaches anti-phase synchronization more often than in-phase synchronization.

It has also been found that for a damping value of $\mu = 0.1$ and for a base mass ranging from 1 to 50 times the metronome masses results in the situation where, in general, the anti-phase synchronization state is more common than in-phase synchronization.

Two types of experimental results showing typical results and other interesting results have been presented. Comparison between these results suggest that large ICs supply an amount of energy to the system which takes long to be dissipated by the internal damping of the metronomes, causing a notable beat phenomenon in the motion of the masses of the system that can be a factor which help to change the expected final synchronization state. This is mentioned as a possible avenue further investigation.

Although the aim of this work was to study a simplified model for synchronization of two metronomes, it would be expected that more accurate basins of attraction could be obtained if damping with the ground and nonlinear stiffness are included in the model. A constant friction oscillator model for the escapement mechanism could also be considered in the investigation relating ICs and final synchronization states.

5. CONCLUSIONS

5.1 Summary of the Thesis

The main objective of this chapter is to present the main conclusions of the thesis and the recommendations for further works. The work done in each chapter is summarized. The condition to obtain in-phase and anti-phase synchronization of two metronomes on a mobile base has been investigated in this thesis. For this aim, a simplified lumped parameters model has been proposed. Its relationship with a previous pendulum model by Pantaleone (2002) has been shown.

Chapter 1 introduced the topic of synchronization from the first works of Huygens with pendulum clocks, it provide the historical background, the literature review and specify the main objectives and contributions to knowledge of the thesis.

In chapter 2 a simplified lumped parameters model to investigate in-phase and anti-phase synchronization of two metronomes on a mobile base has been proposed and its relationship with the previous model of Pantaleone (2002) has been showed. This model has been used to study undamped synchronization and synchronization when van der Pol damping is included, both for similar and slightly different metronomes. Analytical expressions for the frequencies of oscillation of the undamped system when in-phase and anti-phase synchronization is achieved are shown, for similar and slightly different metronomes. In Appendix A, a detailed description of the escapement mechanism which drives the metronomes and two models to represent it are presented. The reasons on why the van der Pol oscillator has been chosen to model this system where also described.

In chapter 3 the instantaneous frequency method has been introduced and later has been applied to determine the final synchronization state of the system from both, numerical and experimental data obtained from simulations, based on the simplified lumped parameters model of chapter 2, and experiments with two metronomes on a mobile base, respectively. The relationship between the instantaneous frequency of a signal and the presence of higher harmonics in such a signal has been shown. The methodology used to collecting experimental data from videos and the main features of the software have been described.

In appendix B an approximation of the experimental damping value of a metronome has been shown. It has been calculated based on a comparison between the experimental and the theoretical envelopes of the time-domain displacements.

In chapter 4 the relationship between initial conditions, parameters and final synchronization state has been investigated by means of the concept of basins of attraction, which are two-dimensional coloured maps. The axes of the maps correspond with the initial positions of the metronomes and a colour was designed to each synchronization state of interest, so that for a given pair of initial positions, a coloured pixel was set in the map. Firstly, the relationship between the final synchronization states and the ICs while the damping is changed has been investigated. Secondly, this relationship has been investigated when the ratio between the metronome mass to the base mass changes. Experimental results related to this investigation have been shown. In chapter 5, the summary of the thesis, the main conclusions and the recommendations for further work are shown.

5.2 Main Conclusions

From the investigation conducted with the proposed model and the experiments with two metronomes oscillating in a mobile base can be concluded that:

- It has been shown that a relationship between the proposed lumped parameters model and the previous pendulum model of Pantaleone exists. It has also been shown that, for the undamped system, synchronization can be achieved provided that the ICs correspond exactly with their 2^{nd} and 3^{rd} normal modes of vibration.

- It has been shown that key parameters relating to synchronization of metronomes are the damping ratio and the mass ratio.

- From experimental measurements and using the instantaneous frequency concept, it has been shown that the frequency of oscillation of the metronomes increases when the system synchronizes in-phase, and maintains constant when the system synchronizes in anti-phase. A fact predicted from the normal modes analysis of the undamped proposes model.

- It has been estimated that the experimental damping of a metronome is light and is in the range $0.001 < \mu < 0.005$ based on a perturbation method called Two Timing.

- It has been shown that oscillation of the IF of a signal reveals the presence of higher harmonics in such a signal, and that the IF oscillates around the value of the fundamental frequency of the signal. An analytical expression relating the IF of a signal and its higher harmonics has been found.

The investigation about the relationship between the initial conditions and the key parameters, to obtain in-phase and anti-phase synchronization of metronomes by means of numerical simulations, has been shown that:

- For a mass ratio of $\sigma = 0.1$ and considering similar oscillators, ICs with the same sign generally lead to in-phase synchronization, while ICs with a different sign generally lead to anti-phase synchronization, when damping is light $\mu < 0.1$. Increasing the damping but maintaining the same mass ratio results in a bias so that the system synchronizes more often in anti-phase than in-phase. By further increasing the damping in the system, this process is reversed and for the same range of ICs the system reaches in-phase synchronization more often than anti-phase synchronization.

- For a damping value of $\mu = 0.1$ and for a base mass ranging from 1 to 50 times the metronome masses results in the situation where, in general, the anti-phase synchronization state is more common than in-phase synchronization.

Finally it is important to remark that the non-contact method used in this work to collect data from experiments opens the possibility to investigate in more detail the relationship between initial conditions and the final synchronization states of the system without need to invest in sophisticated devices to obtain the time histories of the pendulums.

5.3 Recommendations for further work

In this thesis a simplified 3DOF has been proposed to investigate in-phase and anti-phase synchronization of two metronomes on a mobile base. The system has been modelled as 3

masses coupled by linear springs and van der Pol damping and their motion have been restricted to the horizontal. Further works can:

1. To include in the model nonlinear stiffness, instead of the linear used in this work since the pendulums presents stiffness with softening characteristics.

2. To improve the model for the nonlinear damping force using the more accurate model of Andronov and Chaikin (1937) described in appendix 1, for which it is necessary to solve the equations motion twice per cycle and add their solutions several times to obtain a time history.

3. To take into account in the model the damping caused by the friction of the soda cans and the ground.

4. To investigate, both theoretically and experimentally, the relationship among the ICs, parameters and the range of difference of (or set up) natural frequencies leading to synchronization.

5. To investigate the relationship between initial conditions, parameters and the final synchronization state by means of basins of attraction for a bigger range of values for the parameters and for a model which includes the damping with the ground.

REFERENCES

ANDRONOW, A. A. CHAIKIN C. E. **Theory of Oscillations**. New Jersey: Princeton University, 1949.

BALANOV, A. JASON N. POSTNOV, D. SOSNOVTSEVA, O. **Synchronization From Simple to Complex**. Berlin: Springer-Verlag, 2009.

BARBETA, V. B, YAMAMOTO I, Desenvolvimento e utilização de um programa de análise de imagens para o estudo de tópicos da mecânica clássica. **Revista Brasileira de Ensino da Física**, São Paulo, v. 24, n. 2, 158-167, 2002.

BELL, A. E. **Christian huygens and the development of science in the seventeenth century**. London: Edward Arnold, 1950. 134 p.

BENNETT, M.; SCHATZ, M. F.; ROCKWOOD, H. WIESENFELD, K. Huygens's clocks, **Proceedings of the Royal Society of London**, London, v. A 458, p. 563-579, 2002.

BLEKHMAN, I. I. **Synchronization in science and technology**, New York: ASME, 1988.

BLEKHMAN, I.I. **Vibrational mechanics.** New York: World Scientific Publishing, 2000.

BLEKHMAN, I. I.; FRADKOV, A. L.; NIJMEIJER, H.; POGROMSKY, A.YU. On self-synchronization and controlled synchronization. **Systems & Control Letters**, Amsterdam, n. 31, p. 299-305, 1997.

BOASHASH, B. Estimating and interpreting the instantaneous frequency of a signal-part 1: fundamentals. **Proceedings of the IEEE**, Piscataway, v. 80, n. 4, p. 520-538, 1992.

BROWN, D. OSP User's Guide Chapter 16: Tracker. **Video analysis and modelling tool**. Version 4.94. [S. l.: s. n.], 2017. Avaliable: <http://www.opensourcephysics.org/items/detail.cfm?ID=7379>. Accessed: 07 Jul. 2017.

CHANPICHAI, N.; WATTANAKASIWICH, P. Physics of throwing basketball. **Thai. Journal of Physics**, Bangcok, n. 5, p. 358-60, 2010.

CZOLCZYNSKI, K. PERLIKOWSKI, P. STEFANSKI, A. KAPITANIAK T., Synchronization of self-excited oscillators suspended on elastic structure. **Chaos Solitons Fractals**, Kidlington, v. 32, p. 937–943, 2007. (CZOLCZYNSKI ET AL, 2007)

CZOLCZYNSKI, K.; PERLIKOWSKI, P.; STEFANSKI, A.; KAPITANIAK T. Clustering and synchronization of n Huygens' clocks. **Physica A**, Amsterdam, v. 388, p. 5013-5023, 2009.

CZOLCZYNSKI, K.; PERLIKOWSKI, P.; STEFANSKI, A.; KAPITANIAK T. Huygens' odd sympathy experiment revisited. **International Journal of Bifurcation and Chaos**, Singapore, v 21, p. 1-15, 2011.

DEN HARTOG, J. P. **Mechanical vibrations**. New York: Dover, 1985.

DILÃO, R. Antiphase and in-phase synchronization of nonlinear oscillators: The Huygens' clocks system. **Chaos**, Melville, v. 19, n. 023118, p. 1-5, 2009.

DUNN, R.; HIGGIT, R. **Finding longitude.** Collins: HarperCollins, 2014.

ELLICOT, J. An account of the influence which two pendulum clocks were observer to have upon each other. **Philosophical Transactions**, London, v. 41, p. 126-128, 1739.

ELLICOT, J. Further observations and experiments concerning the two clocks above mentioned. **Philosophical Transactions**, London, v. 41, p. 128-135, 1753.

ELLIS, W. On sympathetic influence between clocks. **Monthly Notices of the Royal Astronomical Society**, Oxford, v. 33, p. 480-484, 1873.

ENNS, R. H. MCGUIRE, G. C. **Nonlinear physics with *mathematica* for scientist and engineers**. Boston: Birkhaser. 2001.

FIGLIOLA R.S, BEASLEY D.E. **Theory and design for mechanical measurements**. Danvers: John Wiley & Sons, 2011.

FELDMAN, M., **Hilbert transform applications in mechanical vibrations**. West Sussex: John Wyley & Sons, 2011a.

FELDMAN, M. Hilbert transform in vibration analysis. **Mechanical Systems and Signal Processing**, London, v. 25, p. 735–802, 2011b.

FIDLIN, A. **Nonlinear oscillations in mechanical engineering.** The Netherlands: Springer-Verlag, 2006.

GIL, S. REISIN H. D. RODRÍGUEZ, E. E. Using a digital camera as a measuring device. **American Journal of Physics,** Melville, v. 74, n. 9, 2006.

GINOUX, J-M. LETELLIER, C. Van der Pol and the history of relaxation oscillations: toward the emergence of a concept. **Chaos,** Melville, v. 22, p. 023120, 2012.

HUYGENS, C. Instructions concerning the use of pendulum-watches, for finding the longitude at Sea. **Philosophical Transactions**, London, n. 4, p. 937-976, 1669.

JOHANSSON, M. **The hilbert transform.** Sweden: Växjö University, 1999. Available: <fuchs-braun.com/media/d9140c7b3d5004fbffff8007fffffff0.pdf>. Accessed: 01 Mar. 2017.

KORTEWEG, D. J. Les Horloges sympathiques de Huygens, les phénomènes connexes et les oscillations principales et composées que présentent deux pendules fixés à un mécanisme à un seul degré de liberté. **Archives Néerlandaises d. Sciences ex. et nat**., [S. l.], Serie II, T. XI, p. 273–295, 1906.

LEITHOLD, L. **The Calculus 7.** New York: HarperCollins College, 1996.

LUENBERGER, D. G. **Introduction to dynamic systems**: theory, models and applications. New York: John Wiley & Sons, 1979.

MEIROVITCH, L. **Elements of vibration analysis**. Tokio: McGraw Hill, 1975.

MERRIAM-WEBSTER INC. **Dictionary**, Springfield: [s. n.], 2017. Avaliable: <https://www.merriam-webster.com/>. Accessed: 09 Mar. 2017.

MICKENS, R. E. **Truly nonlinear oscillations:** harmonic balance, parameter expansion, iteration and averaging method. New Jersey: World Scientific, 2010.

NAYFEH, A. H.; MOOK, D. T. **Nonlinear oscillations.** London: John Wiley & Sons, 2002.

PANTALEONE, J. Synchronization of metronomes. **Am. J. Physics**, Melville, v. 70, n. 10, p. 992-1000, 2002.

PEÑA RAMIREZ, J. **Huygens' synchronization of dynamical systems**: beyond pendulum clocks. 2013. 164 f. Thesis (Doctorate in Mechanical Engineering) – Eindhoven University of Technology, The Netherlands, 2013.

PIKOVSKY A., ROSEMBLUM M., KURTHS J. **Synchronization**: a universal concept in nonlinear science. Cambridge: Cambridge University Press, 2001.

POOK, L. P. **Understding pendulums.** London: Springer, 2011.

SENATOR, M. Synchronization of two coupled escapement-driven pendulum clocks. **Journal of Sound and Vibration**, London, v. 291, p. 566-603, 2006.

SIRISATHITKUL, C.; GLAWTANONG, P.; EADKONG1, T.; SIRISATHITKUL, Y. Digital video analysis of falling objects in air and liquid using Tracker. **Revista Brasileira de Ensino da Física**, São Paulo, v. 35, n.1, p. 1-6, 2013.

SOBEL, D. **Longitude.** New York: Penguin Books, 1995.

RUXU, DU. KONGHAN, XIE. **The mechanics of mechanical watches and clocks.** Berlin: Springer, 2013.

SHIN, K. HAMMOND, J. K., **Fundamentals of signal processing.** West Sussex: John Wyley & Sons, 2008.

STOKER, J. J. **Nonlinear vibrations in mechanical and electrical systems.** New York: Interscience, 1950.

STROGATZ, S.; STEAWARD, I. Coupled oscillators and biological synchronization, **Scientific American**, London, v. 269, p. 102-109 1993.

STROGATZ, S. H. **Nonlinear dynamics and chaos.** Cambridge: Perseus, 1994.

STROGATZ, S.; STEAWARD, I. **The emerging science of spontaneous order.** New York: Hyperon, 2003.

STROGATZ, S. H. **MAE5790-11 Averaging theory for weakly nonlinear oscillators**. Nonlinear dynamics and Chaos: Cornell University, 2016. Courses of study 2014-2015. Min. 50. Disponível em <https://cosmolearning.org/video-lectures/averaging-theory-for-weakly-nonlinear-oscillators/>. Acceso em: 05 ago. 2016.

TANDON, N.; CHOUDHURY, A. A review of vibration and acoustic measurement methods for the detection of defects in rolling element bearings. **Tribology International**, Kidlington, v. 32, p. 469–480, 1999.

THOMPSON, J. M. T.; STEWART, H. B. **Nonlinear dynamics and chaos.** West Suxess: John Wiley & Sons, 2002.

TRACKER. **Video analysis and modelling tool.** Version 4.94. Douglas Brown, Open Source Physics, 2016. Avaliable: <http://physlets.org/tracker/>. Accessed: 26 Sep. 2016.

ULRICHS, H. MANN, A. PARLITZ, U. Synchronization and chaotic dynamics of coupled mechanical metronomes. **Chaos**, Melville, v. 19, n. 043120, p. 1-6, 2009.

VAN DER POL, B. On relaxation-oscillations. **Philosophical magazine and journal of science,** London, v. 7, n. 2, p. 978-992, 1926.

VAN DER POL, B. Forced oscillators in a circuit with non-linear resistance. **Philosophical Magazine**, Abingdon, v. 3, p. 64–80, 1927.

VENKATESHAN S.P., **Mechanical Measurements**, 2nd Ed, John Wyley & Sons, West Sussex, UK, 2015.

VELJKO, V. **On the synchronization of metronomes**. 2012. Master (Dissertation) - Novi Sad University, Tecnical Sciences Faculty, Novi Sad, 2012. (In Serbian)

.

APPENDIX A – The Escapement Mechanism, a Model and the van der Pol Oscillator

The aim of this appendix is to describe the escapement mechanism driving the metronome as well as to describe the van der Pol oscillator to show how it can be used as a model for the metronome. Firstly the metronome, its escapement mechanism and the way in which it works is described and then the van der Pol oscillator is studied.

A1. The Escapement Mechanism

The escapement mechanism is the internal mechanism of metronomes, and mechanical clocks (including pendulum clocks), driving them to stable and nearly harmonic oscillations so that the number of oscillations can be counted. Metronomes emit a click, or beat, every half a cycle. Figure A.1 shows a *Wittner® Taktell-Piccolo (Serie 830)* metronome and its external components. The frequency of oscillation of such a metronome can be set from a range of 40 to 200 beats per minute (bpm) printed on the scale (p1) by adjusting the sliding weight (p3) on one of the grooves on the pendulum (p2) whose bob (p4) is at the bottom of the pendulum. As the metronome clicks twice per cycle the corresponding range in frequency is from $(40/2)(1/60\text{s}) = 0.33$ Hz to 1.67 Hz. The winding mechanism of the metronome provides between 30 to 40 minutes of oscillation which is a very long duration compared with the frequency of oscillation.

Figure A.2 shows the internal mechanism of the metronome as well as a zoom of the escapement mechanism inside a toothed casing. Potential energy is provided to the metronome by rotating the winding key (p5) which compresses the spiral torsional spring (p6). The spring transmits motion by means of a gear to the toothed shaft (p7), which is rigidly connected to the escapement gear (p8) sharing its rotational axis. The escapement gear (p8) teeth have a pointed shape with two angled faces as shown in a further zoom depicted in Figure A.3. The faces are used to transmit the motion from the escapement gear to the escapement pallets (p10) and (p11), which are rigidly connected to a perpendicular shaft (p9) that transmits the motion to the pendulum.

Figure A.1 – External components of a metronome. p1) Scale. p2) Pendulum. p3) Adjustable mass to set the oscillation frequency. p4) Pendulum bob. p5) Winding key.

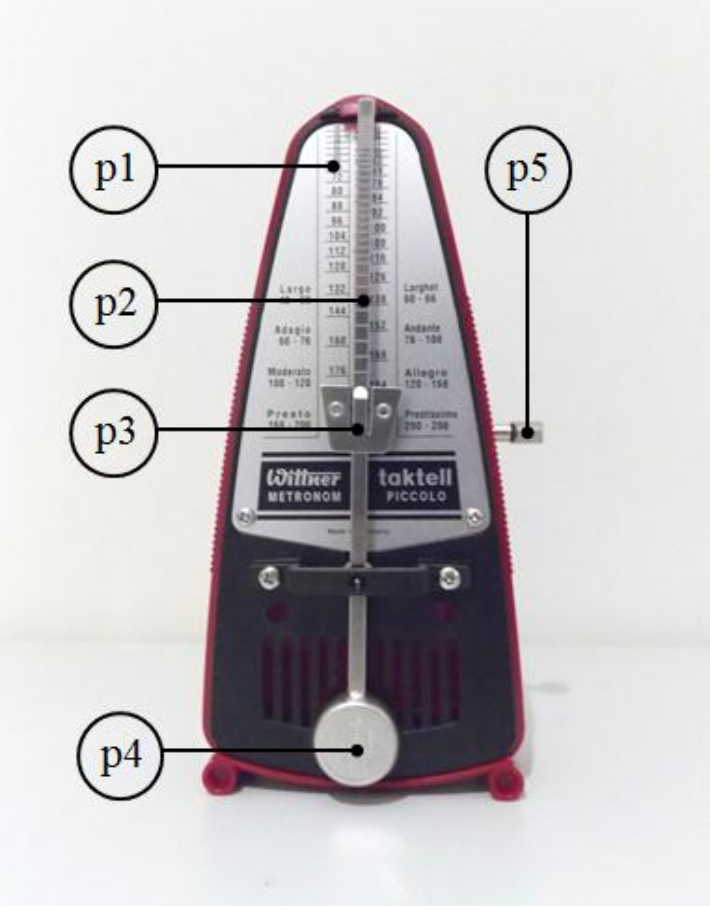

Elaborated by the author.

When the pendulum (p2) is oscillating, the perpendicular pallet shaft (p9) also rotates as well as the escapement pallets (p10) and (p11) in the same direction and with the same angular velocity as they are rigidly connected. A click is emitted once the escapement gear (p8) stops when the tip of one of its teeth hits the external large face of pallet (p10) (see the zoom of the escapement pallets in Figure A.3). A friction force occurs between them. The pendulum motion is counterclockwise up to the point at which the pendulum achieves its maximum angle (in its steady-state) and then it rotates clockwise passing through the vertical position. During this part of the oscillation there is just a friction force between the escapement gear tooth and the pallet (p10). When the pendulum is in a position near to half the maximum height, the right face of the escapement gear tooth comes into contact with the lateral angled face of the escapement pallet (p10) (see Figure A.3) giving it an impulse and creating a clockwise torque, supplying energy to the pendulum. Then the tooth ‘escapes’ for

Figure A.2 – Internal mechanism of a metronome with a zoom of the escapement mechanism. p6) Spiral torsional spring (inside its toothed casing). p7) Toothed shaft. p8) Escapement gear. p9) Pallet shaft. p10) and p11) first and second escapement pallet, respectively.

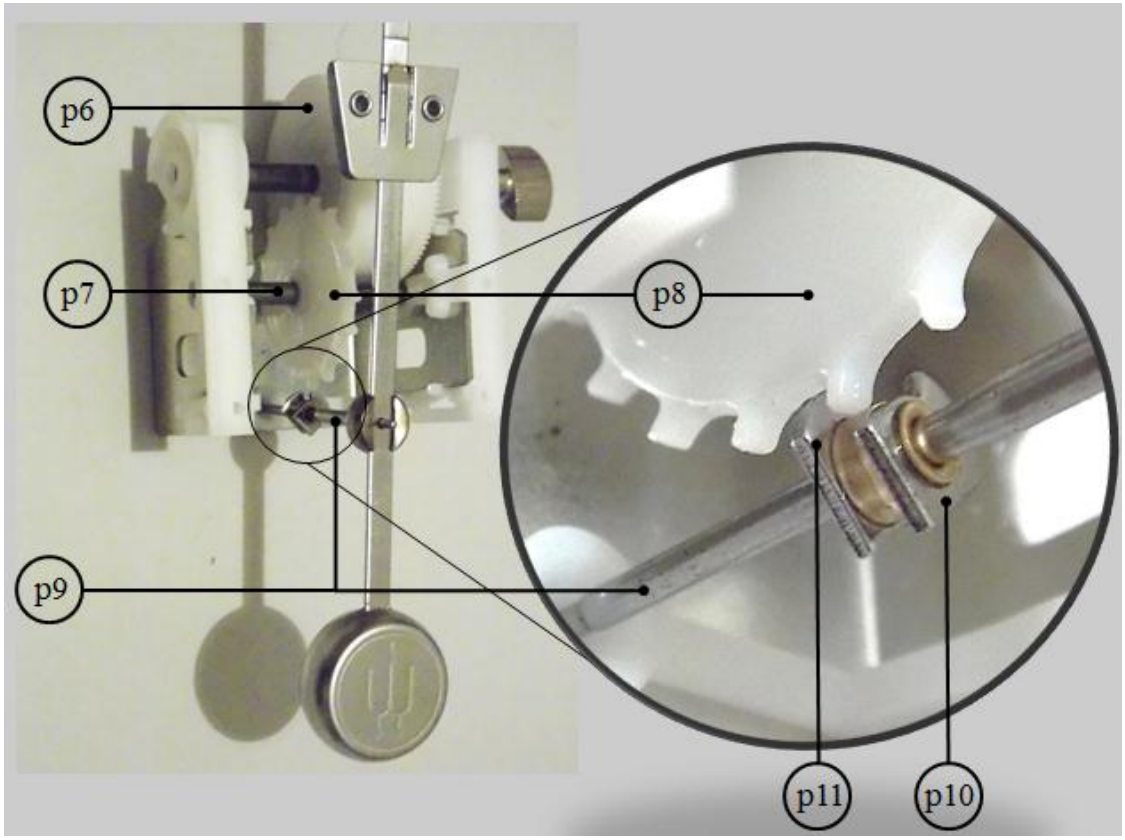

Elaborated by the author.

an instant and then is stopped again by the escapement pallet (p11) when its tip hits the internal large face of pallet (p11) and a click is emitted. Friction occurs again but this time between the escapement gear tooth and the internal large face of pallet (p11). The motion continues until the pendulum achieves its maximum negative angle then it turns counterclockwise. The pendulum then passes through the vertical position again. When it passes a position which is nearly half of its maximum positive angle the left face of the escapement gear tooth comes into contact with the lateral angled face of the escapement pallet (p11) giving it an impulse. This creates a counterclockwise torque which adds to the motion of the pendulum. The escapement gear tooth 'escapes' but immediately after, the next tooth gear hits the external large face of pallet (p11) creating friction and then damping the motion. This process is repeated over and over during the time the spring has potential energy. The metronome is always driven by its escapement mechanism to steady and almost harmonic oscillations (Avoiding initial impulses which could damage the system).

Figure A.3 – Upper photograph: zoom of a tooth of the *Escapement gear* (p8). Lower photograph: zoom of the first (p10) and the second (p11) escapement pallets.

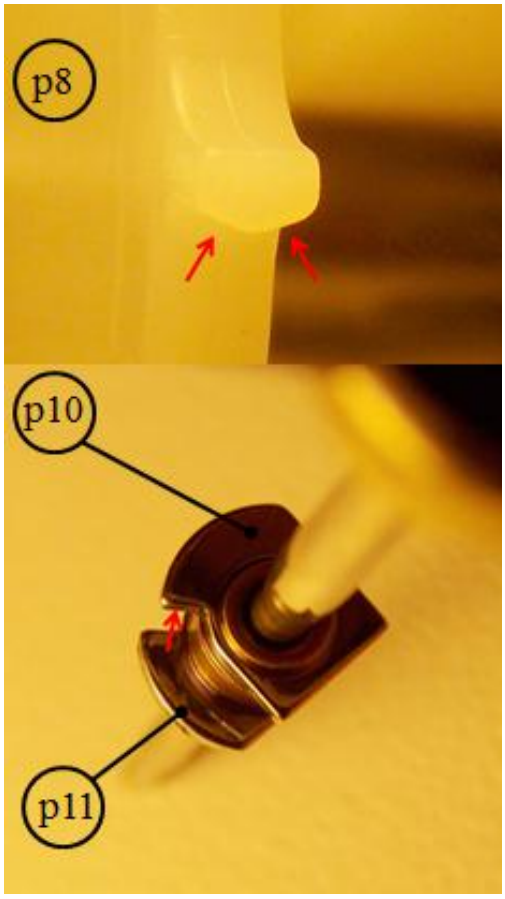

Elaborated by the author.

A2. A Model for the Escapement Mechanism

In 1937 Andronov and Chaikin (1949) presented in a nice way a very interesting model for clocks. In this section part of this work is reproduced with the aim of providing a model for the escapement mechanism which takes into account its main features. The main advantages and disadvantages for its use in the study of the synchronization phenomenon are then discussed.

A2.1 Model description

The escapement mechanism of a metronome described in the last section can physically be modelled as an oscillatory system (the pendulum) with friction, produced by the tips of the gear teeth and the external large face of the pallets, which receives energy (by means of impulses) at certain instants of its cycle. Firstly, neglecting the impulses and

assuming the approximation $r\sin\theta \approx r\theta = x$ (with an error about 5.5% for an angle of 40º) where r is length of the pendulum, θ its angle from the vertical and x its horizontal displacement for "small" angles; the maximum measured angle described by a metronome at the steady-state in these experiments is 32.1 º. The free vibration of the oscillatory pendulum with friction can be represented as an oscillator with linear stiffness and constant friction, as shown in Figure A.4. This kind of friction is always opposite to the motion, so that its absolute value is constant but it changes in sign, being opposite to velocity (see Figure A.5). The equation of motion for this system is given by

$$m\ddot{x} + kx = \pm f \tag{A1}$$

Figure A.4 – SDOF linear oscillator with constant friction. *O* is the origin of the oscillator when no friction is in the system and x_0 is the amplitude at which stiffness equals the friction force.

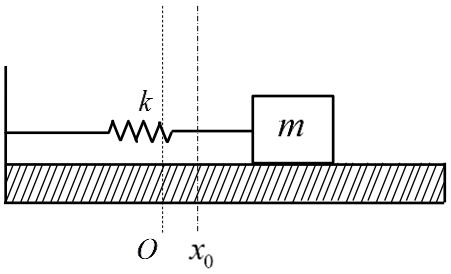

Elaborated by the author.

Figure A.5 – Behaviour of constant friction respect to velocity. It is constant in absolute value but opposite in sign to the velocity.

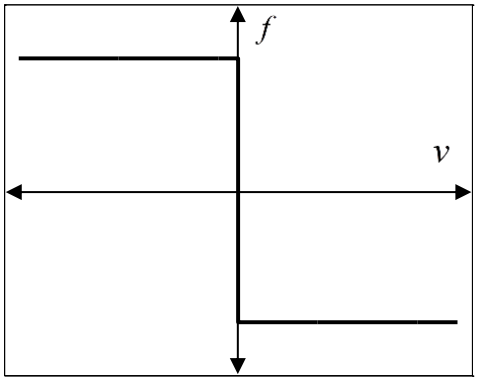

Elaborated by the author.

where f is the friction force whose sign always opposes the velocity, m the mass of the pendulum and k the stiffness. Defining the friction force as $f = kx_0$ where x_0 is the constant

position at which the friction and the stiffness forces are in equilibrium, two equations are obtained

$$\begin{aligned} \ddot{x} + \omega_n^2 \left(x - x_0 \right) = 0 \qquad & \text{for } \dot{x} < 0 \\ \ddot{x} + \omega_n^2 \left(x + x_0 \right) = 0 \qquad & \text{for } \dot{x} > 0 \end{aligned} \tag{A2a, b}$$

where $\omega_n = \sqrt{k/m}$. Note that the system cannot be described by a single equation. Instead the motion is obtained by piecing together two halves of the motion of harmonic oscillators with equilibrium positions at distances $\pm x_0$ from the equilibrium position with no friction (ANDRONOV; CHAIKIN, 1949). To obtain the phase portrait v is set to $\dot{x}$, using $\frac{dv}{dt} = \frac{d}{dx}\left(\frac{dx}{dt}\right)v = \frac{dv}{dx}v$ and substituting it into equations (2a and b) leads to

$$\begin{aligned} v dv = -\omega_n^2 \left(x - x_0 \right) dx \qquad & \text{for } v < 0 \\ v dv = -\omega_n^2 \left(x + x_0 \right) dx \qquad & \text{for } v > 0 \end{aligned} \tag{A3a, b}$$

Integrating both sides results in

$$\begin{aligned} \frac{\left(x - x_0 \right)^2}{R_1^2} + \frac{v^2}{\omega_n^2 R_1^2} = 1 \qquad & \text{for } v < 0 \\ \frac{\left(x + x_0 \right)^2}{R_2^2} + \frac{v^2}{\omega_n^2 R_2^2} = 1 \qquad & \text{for } v > 0 \end{aligned} \tag{A4a, b}$$

which are half-ellipses with centers at $\pm x_0$ from the non-frictional equilibrium position respectively, R_1 and R_2 are constants of integration. If the parameters are chosen so that $\omega_n = 1$, then the paths in the phase portrait are spirals obtained by joining together half-circles with centers at $\pm x_0$ from the non-frictional equilibrium positions as shown in Figure A.6. The section $-x_0 < x < x_0$ is the displacement range of equilibrium positions.

Eqs (4a and b) describes the free oscillation of the system with friction. The characteristic impact, that puts energy into the system and then generate the clicks, still has not been modelled. To model this, the following convenient assumptions are made: 1. The system is impacted once per cycle instead of twice and the impact occurs at the position $-x_0$ when the

Figure A.6 – Phase portrait for a SDOF oscillator with linear stiffness and constant friction for suitable units leading to spiral paths formed by joining together half circles. In general the paths are formed by halves of ellipses. The section from $-x_0 < x < x_0$ is a segment of equilibrium positions.

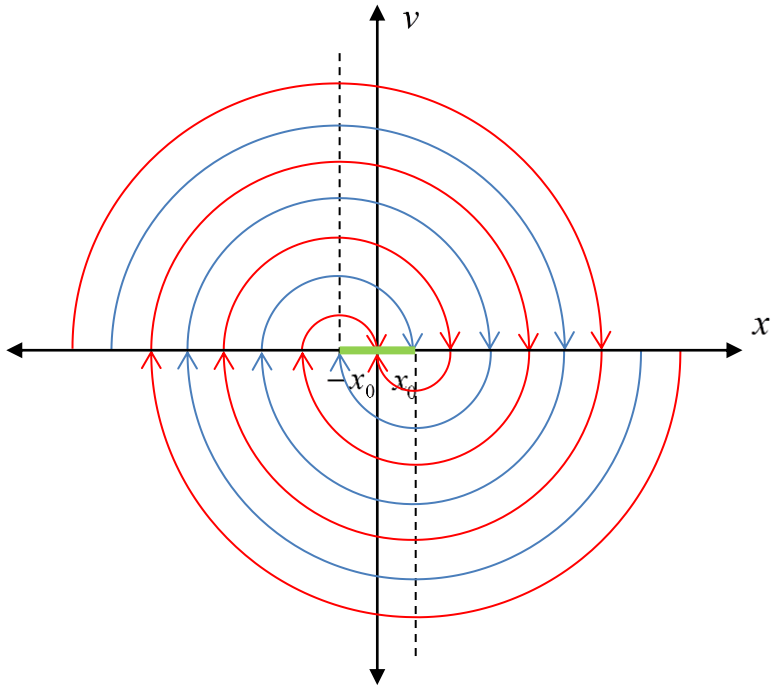

Elaborated by the author.

system moves from negative to positive displacement. This makes it easier to conduct the analysis and does not changes the behavior of the system. 2. The impact follows the *energy law* $mv_1^2 - mv_0^2 = \text{constant}$ and generates an instantaneous change in velocity $\Delta v = v_1 - v_0$, where v_0 and v_1 are the velocities before and after the impact. The energy law can be written as $v_1^2 - v_0^2 = h^2$ where h is a constant, then the change in velocity produced by the impact is given by $\Delta v = \sqrt{v_0^2 + h^2} - v_0$. Figure A.7 shows the relationship between v_0 and Δv. It can be seen that the greater the initial velocity in each cycle, the smaller the increase in velocity, Δv gradually tends to a constant value.

The phase portrait for this system is shown in Figure A.8. If the motion is started at $(-A_0, 0)$ it describes an upper circle of radius R_0 with center at $(-x_0, 0)$, then at $-x_0$ after the impact, describes a circle of radius R_1 with the same center and from the energy law $R_1^2 - R_0^2 = h^2$ (See Figure A.8). Next it cuts the horizontal axis at $(A_1, 0)$ where $A_1 = R_1 - x_0$ from the origin.

Figure A.7 – Relationship between the initial velocity v_0 before the impact and the change in velocity Δv produced by the impact in the escapement mechanism of a metronome. In this plot $h = 1$.

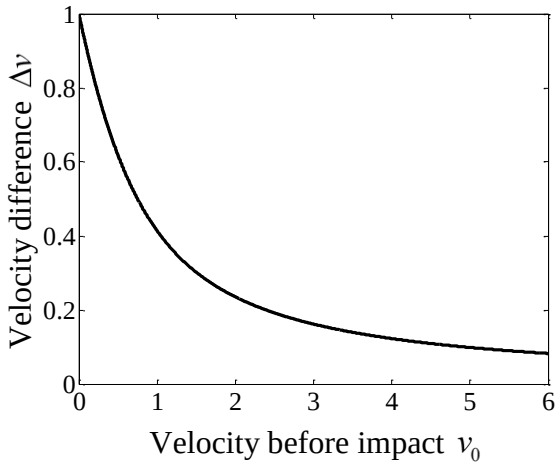

Elaborated by the author.

Figure A.8 – Phase portrait for a model of metronome (also a pendulum clock) consisting on a SDOF oscillator with linear stiffness and constant friction being hit once a cycle. The central shading area comprehends the ICs for which the system never achieves a periodic motion being is damped out, the horizontal section on this shading area correspondas to the segment of equilibrium positions. ICs outside the shadown area gradually lead to a stable periodic motion (external red line) after several cycles (internal thin black and ble lines).

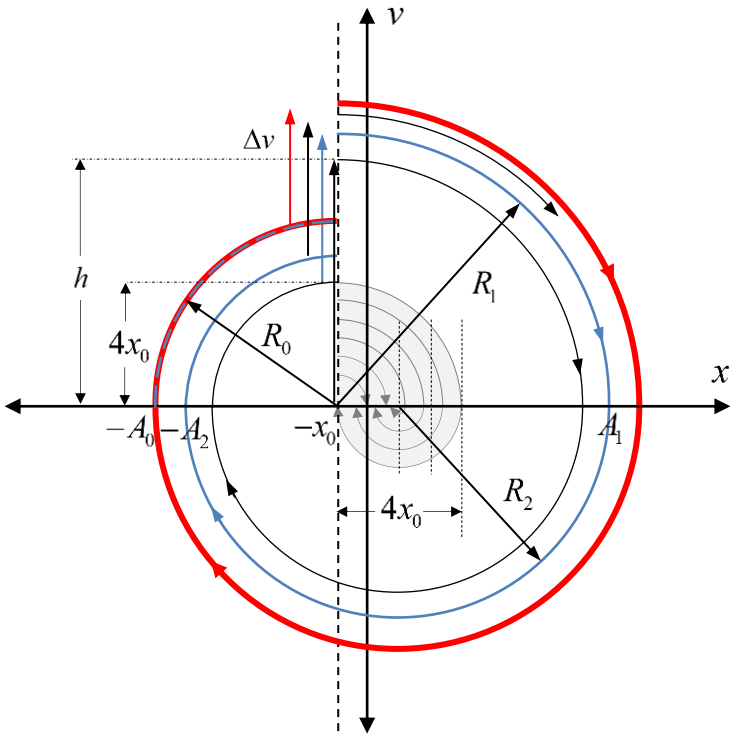

Elaborated by the author.

Then it describes a lower circle of radius $R_2 = R_1 - 2x_0$ center at $(x_0, 0)$ and cuts the negative horizontal axis at $(-A_2, 0)$ where $A_2 = R_1 - 3x_0$ from the origin. So the energy law can be written as

$$(A_2 + 3x_0)^2 + (A_0 + x_0)^2 = h^2 \tag{A5}$$

For periodic motion $A_2 = A_0$, substituting this into Eq. (5) leads to

$$A_0 = \frac{h^2}{8x_0} - x_0 \tag{A6}$$

For periodic motion it is necessary that $A_0 > x_0$, hence $h > 4x_0$, for lower values of *h* the initial position $(-A_0, 0)$ will lie on the segment of equilibrium states. This imposes a condition on the energy source demanding it to be proportional to x_0. The external thick red line in Figure A.8 is the steady periodic motion of the metronome composed by segments of circles and a section of length Δv at $x = -x_0$ (ANDRONOV; CHAIKIN, 1949).

*A*2.2 *Discussion*

The previous model contains the important features of the escapement mechanism: friction, an impact which puts energy into the system, and most importantly the existence of a stable periodic oscillation and the need of a special initial position (or *impulse*) to start the oscillation. This model, with constant friction, needs two equations to describe the motion of a SDOF system, therefore the motion in one cycle is obtained by piecing together the solutions of each equation. Additionally, it is not clear how to introduce into the equations the energy law to model the impact. These issues make the task of modelling more difficult, especially for a more complex system to study the synchronization of two metronomes on a mobile base where many cycles are needed to achieve synchronization. In the next section the van der Pol oscillator is introduced as an alternative approximation model for the escapement mechanism.

A3. The van der Pol Oscillator

The aim of this section is to study the main features of the van der Pol oscillator and to discuss why it can be used as an approximate model for a metronome. Moreover, the advantages and disadvantages of its use for this purpose are also discussed. Firstly the van der Pol oscillator is explained and secondly the advantages and disadvantages are discussed.

A3.1 Main features of the van der Pol oscillator

A mechanical model for the van der Pol oscillator is a SDOF system with linear stiffness and nonlinear damping, which is its main characteristic. The van der Pol damping depends on both velocity and position, so that when the amplitude of oscillation is large the damping is positive and energy is dissipated from the system, but when the amplitude of oscillation is small the damping becomes negative and energy is supplied to the system. This characteristic of the positive and negative damping with the restoring and the inertial forces leads the oscillator to a stable oscillation with defined amplitude and frequency, regardless the initial conditions (ICs) used to start the system oscillation. This is the behaviour of the metronome driven by an escapement mechanism. The stable oscillation is called a *limit cycle*.

The damping force of the van der Pol oscillator can be represented as a sum of a negative and a positive damping force (DEN HARTOG, 1975)

$$f_d = -\left(c - bx^2\right)\dot{x} \tag{A7}$$

where c [Ns/m] and b [Ns/m^3] are linear and nonlinear viscous damping coefficients respectively. Note that a positive damping force (dissipation) depends on the square of the mass position, while a negative damping force has the usual form for linear viscous damping. The position at which $f_d = 0$ is given by $l_0 = \sqrt{c/b}$ and Eq. (7) can be written as

$$f_d = c\left(\left(\frac{x}{l_0}\right)^2 - 1\right)\dot{x} \tag{A8}$$

Then the equation of motion for a van der Pol oscillator is given by

$$m\ddot{x} + c\left(\left(\frac{x}{l_0}\right)^2 - 1\right)\dot{x} + kx = 0 \tag{A9}$$

The non-dimensional equation of motion for a van der Pol oscillator is given by

$$\hat{x}'' + \mu\left(\hat{x}^2 - 1\right)\hat{x}' + \hat{x} = 0 \tag{A10}$$

where $\hat{x} = x/l_0$ is the non-dimensional displacement, $\hat{x}' = d\hat{x}/d\tau$ the non-dimensional velocity and $\hat{x}'' = d^2\hat{x}/d\tau^2$ the non-dimensional acceleration, $\tau = \omega_n t$ and $\mu = c/\omega_n m$ is the non-dimensional damping term which controls the nonlinearity in the oscillator and $\hat{f}_d = \mu\left(\hat{x}^2 - 1\right)\hat{x}'$ the non-dimensional van der Pol damping force. When $\mu \ll 1$ the motion can be considered harmonic and for harmonic motion μ is the ratio between the maximum negative damping (input force) and the maximum stiffness force. This can be seen as follows, letting $x = X\sin\omega_n t$ and $\dot{x} = \omega_n X\cos\omega_n t$, the maximum negative damping is $c\dot{x}_{\max} = cX\omega_n$ while the maximum stiffness (or inertia force) is given by $kx_{\max} = kX = m\omega_n^2 X$. Then μ can be written as

$$\mu = \frac{max\ input\ force}{max\ stiffness\ force} = \frac{c}{\omega_n m} \tag{A11}$$

When the oscillation is harmonic it is also possible to find the final amplitude of the stable oscillation by considering energy (DEN HARTOG, 1975). For oscillations with amplitudes smaller than the final amplitude, the damping force supplies energy into the system, while for oscillations with amplitudes greater than the final one the damping force dissipates energy. When the system oscillates at its final stable amplitude, the energy dissipated and the energy which has been supplied to the system during a cycle are equal. The work done by the damping force over a cycle is then zero, i.e

$$\int \hat{f}_d d\hat{x} = \int_0^{2\pi} \hat{f}_d \hat{x}' d\tau = \int_0^{2\pi} \mu\left(1 - \hat{x}^2\right)\hat{x}'^2 d\tau = 0 \tag{A12}$$

with harmonic motion $\hat{x} = \hat{X}\sin\tau$ and $\hat{x}' = \hat{X}\cos\tau$ then

$$\int_0^{2\pi} \mu\left(1 - \hat{X}^2\sin^2\tau\right)\hat{X}^2\cos^2\tau d\tau = 0 \tag{A13}$$

from which it can be seen that

$$\hat{X}^2 = \frac{\int_0^{2\pi} \cos^2\tau d\tau}{\int_0^{2\pi} \sin^2\tau\cos^2\tau d\tau} = \frac{\pi}{\frac{1}{4}\pi} = 4 \tag{A14}$$

Both integrals can be solved by a graphical method (STROGATZ, 2014, 2015, *MAE5790-11*). Figure A.9a shows the plot for $\cos^2\tau$ in a cycle. The integral in Eq. (14) is the area below the curve in Figure A.9a. This area is equivalent to half the area of the whole rectangle, so the result of this integral is $(1/2)(2\pi)(1) = \pi$. In the same way the area below the curve in Figure A.9b is the resultant value of $\int_0^{2\pi} \sin^2\tau\cos^2\tau d\tau$ and is half of the area of this rectangle $(1/2)(2\pi)\left(\frac{1}{4}\right) = \frac{\pi}{4}$. Consequently

$$\hat{X} = 2 \qquad \text{or} \qquad X = 2x_0 \tag{A15}$$

so the stable final amplitude of oscillation for the van der Pol oscillator is twice the amplitude at which damping force is null.

Figure A.9 – Plots of (a) $\cos^2\tau$ and (b) $\cos^2\tau\sin^2\tau$ in a cycle for graphical integration.

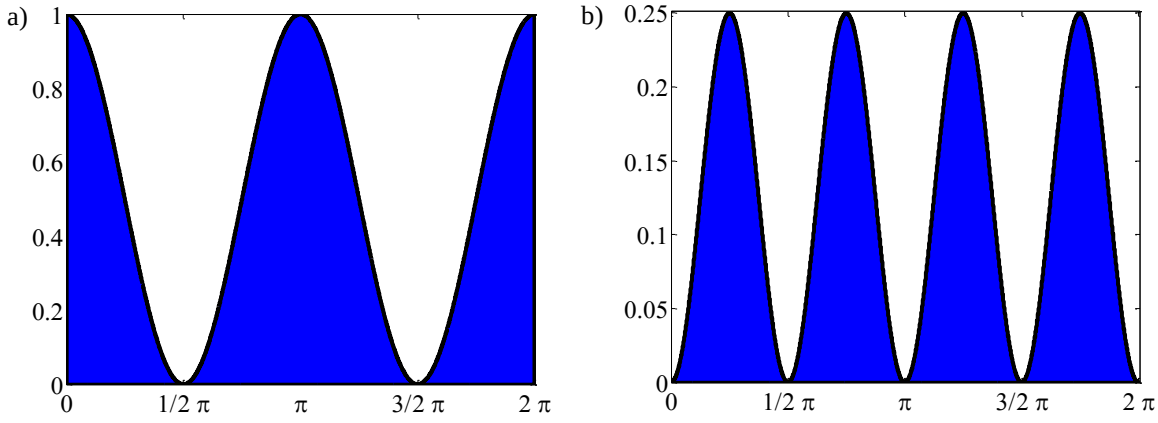

Source: Elaborated by the author.

Figure A.10 shows the time-domain displacement and the phase portrait of a van der Pol oscillator obtained by numerical integration for two different damping values. In the case of

Figure A.10 – Time-domain displacement of a van der Pol oscillator and for two different damping values and its corresponding phase portraits. (a) and (b) displacement and phase portrait for ICs $\hat{x}_0 = -0.2$, $\hat{x}_0' = 0$ and $\mu = 0.1$. (c) and (d) displacement and phase portrait for ICs $\hat{x}_0 = 3$, $\hat{x}_0' = 0$ and $\mu = 10$.

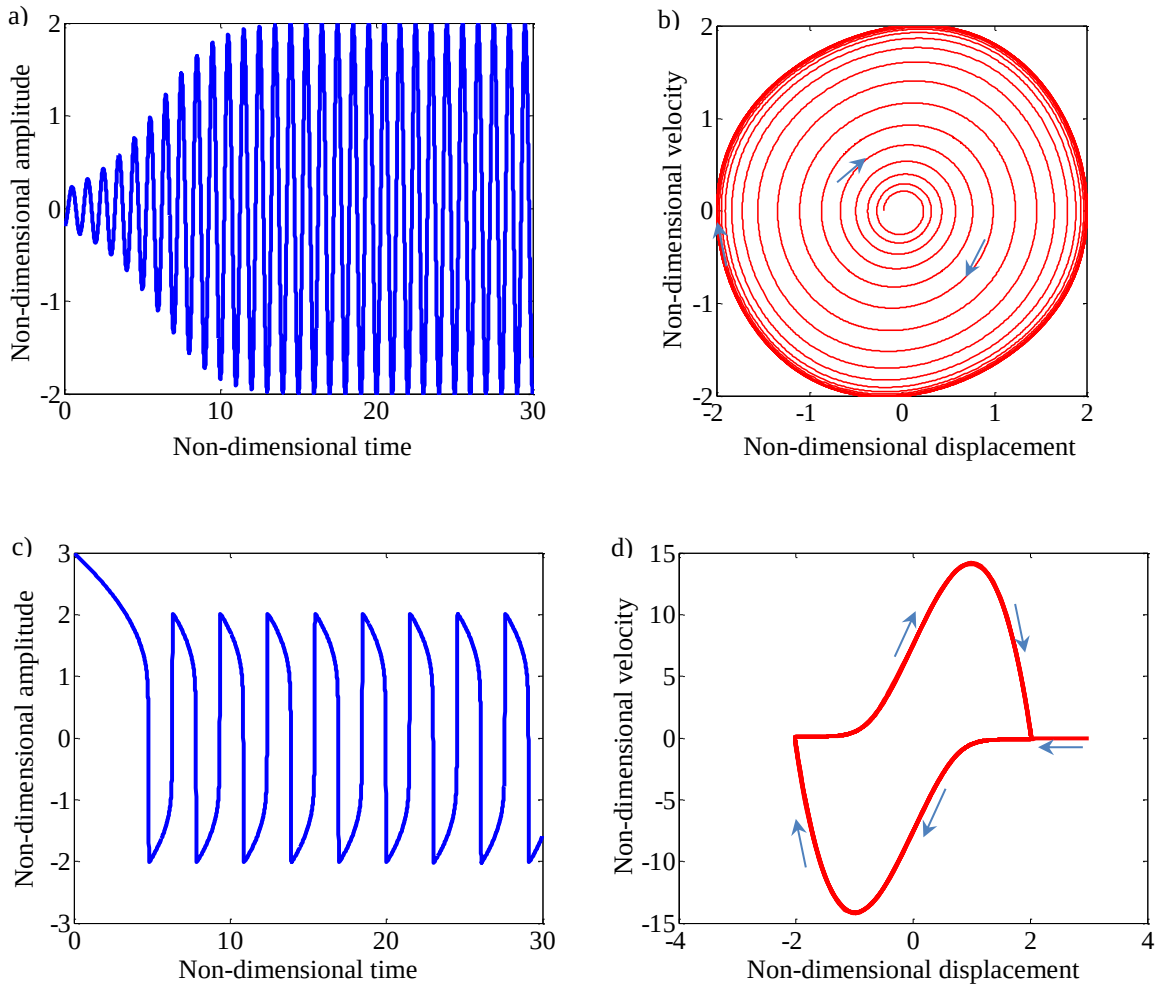

Source: Elaborated by the author.

small damping $\mu = 0.1$ (Figures A.10a and A.10b) it can be seen that the system is taken from its IC to a stable oscillation, or *Limit cycle*, with non-dimensional amplitude of 2. For small values of damping (Eq. 11) the stiffness forces dominate the oscillation so the frequency of oscillation is given by $\omega_n \approx \sqrt{k/m}$. The non-dimensional time in the figures is defined as t/T_n where $T_n = 2\pi/\omega_n$. Figure A.10c shows the time-domain displacement of the van der Pol system for high values of damping. It can be seen that the system is driven to a stable oscillation too, but the frequency of oscillation changes because the damping force is large compared to the stiffness force and then the damping dominates the oscillation. From Eq. (10) it can be seen that the system dissipates energy from a non-dimensional amplitude of between 1 and 2. Below amplitude of 1 a large amount of energy is supplied to the system. For $\mu \gg 1$

the system response passes quickly from the non-dimensional amplitude 1 to amplitude near to −2. It then it changes slowly until it reaches a displacement of −1 and then it quickly passes to a displacement of almost 2, from which slowly passes to 1 and the processes is repeated over and over (see Figure A.10c). At the beginning of the 20th century van der Pol, working with electrical circuits with a similar system response to that in Figure A.10c, found that for high values of μ the period of this oscillation is determined by the duration of a capacitor discharge in a RC circuit (VAN DER POL, 1926; GINOUX, 2012), which is usually called *relaxation time*. This is the reason why these kinds of oscillations are known as *relaxation oscillations*. Figure A.10d shows the phase portrait of the van der Pol oscillator when $\mu \gg 1$. It can be seen that the large damping force distorts the phase portrait driving the system to high velocities.

Figure A.11 – Non-dimensional energy input and energy dissipated as function of amplitude for a SDOF van der Pol oscillator performing harmonic oscillations whit $\mu = 1/2\pi$. The intersection point is the steady amplitude. Solid blue line – energy in, red dashed line – energy dissipated.

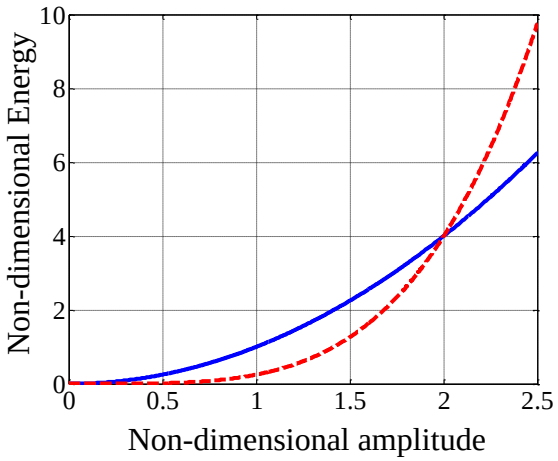

Elaborated by the author.

Figure A.11 shows the non-dimensional energy input and dissipated per cycle, of a van der Pol oscillator, with respect to non-dimensional amplitude for harmonic oscillations. Energy input is given by $\mu \hat{X}^2 \int_0^{2\pi} \cos^2 \tau d\tau$ and energy dissipated is given by $\mu \hat{X}^4 \int_0^{2\pi} \sin^2 \tau \cos^2 \tau d\tau$. It can be seen that both lines intersect at the stable amplitude $\hat{X} = 2$. Figure A.11 shows the case $\mu = 1/2\pi$.

Of interest in this work are oscillations produced by the van der Pol oscillator with small damping values to model the escapement mechanism.

*A*3.2 *Discussion*

Comparing the escapement mechanism model given by Andronov and Chaikin (1937) and the van der Pol oscillator the following differences can be noted:

1. The former dissipates energy by means of friction, in the same way as in the real escapement mechanism, while the latter dissipates energy by mean of viscous damping.
2. The former supplies energy to the oscillation by two instantaneous kicks (in fact one in the simplified model) at defined positions and dissipates energy during the rest of the cycle. The latter puts energy into the system in a whole range of positions near the origin and dissipates energy in the rest of the cycle (at the ends). Therefore it is not necessary for the ICs to be of a certain magnitude to start the oscillation, contrary to what occurs with the real escapement mechanism.

When the escapement mechanism is represented by a van der Pol oscillator it has some important advantages:

1. The system can be represented by a unique equation for all the time it oscillates so it is not necessity to solve twice the equation of motion for each cycle.
2. The system exhibits the main characteristic of the metronome: after a transient it achieves a steady oscillation with defined amplitude, in other words a limit cycle.

The second advantage is the main feature of the escapement mechanism and combined with simplicity of using just an equation to describe the whole system for all time, the van der Pol equation is considered to be able to represent the escapement mechanism for the purpose of studying the synchronization phenomenon.

APPENDIX B – Experimental Approximation to the Damping Ratio for a Metronome

The aim of this appendix is to determine experimentally a range of values for the damping ratio of a metronome. The method used in this appendix consist of first, to find an expression relating the slow variation of the amplitude of the van der Pol oscillator, and then to find the range of values for the damping ratio which best fit the experimental decrement of the amplitude of the metronome and its further steady-state. It is known from Appendix 1 that the escapement mechanism of a metronome dissipates energy by means of friction between some of its internal parts and friction produces a linear decrement of the amplitude in time. It is also know that the van der Pol oscillator shows an exponential decrement of its amplitude. Therefore some differences between the experimental and the theoretical behaviours exist but it will be seen that the damping ratio can be determine satisfactorily between certain range.

B1. Slow-varying Amplitude and Phase for the van der Pol Oscillator

In this section a method called *Two - Timing* presented in (STROGATZ, 1994, p. 218) is shown to find an expression which relates damping ratio and the slow-variation of the amplitude of the van der Pol oscillator. Then it is compared with the experimental decrement of the amplitude in the oscillation of a metronome, obtained with Tracker® software, to find the values for μ which more approximates the experimental data.

The non-dimensional equation of motion for a van der Pol oscillator has been introduced in Eq. (10) of Appendix A and is given by

$$\hat{x}'' + \mu\left(\hat{x}^2 - 1\right)\hat{x}' + \hat{x} = 0 \tag{B1}$$

Letting the non-dimensional time τ as the fast time scale (order $O(1)$) and $S = \mu\tau$ the slow time scale. Functions of the slow time *S* are considered to be constant respect to the fast time τ. It means that the envelope (a function of *S*) keeps nearly constant while one

oscillation occurs (at a fast time scale τ)[1]. Expanding the solution $x(\tau,\mu)$ in power series of μ gives

$$\hat{x}(\tau,\mu)=\hat{x}_0(\tau,S)+\mu\hat{x}_I(\tau,S)+O(\mu^2) \tag{B2}$$

where the subscripts 0 and I means terms $O(1)$ and $O(\mu)$ respectively. Only the two first terms of Eq. (2) are taken into account since terms of order μ^2 are very small. Using chain rule the time derivative of Eq. (2) can be written as

$$\hat{x}'=\frac{\partial\hat{x}(\tau,\mu)}{\partial\tau}=\frac{\partial\hat{x}(\tau,S)}{\partial\tau}+\mu\frac{\partial\hat{x}(\tau,S)}{\partial S} \tag{B3}$$

where $\mu=(\partial S/\partial\tau)$. Substituting Eq. (2) into Eq. (3) and collecting powers of μ, the velocity and acceleration expressions are given by[2]

$$\hat{x}'=\frac{\partial\hat{x}_0}{\partial\tau}+\mu\left(\frac{\partial\hat{x}_0}{\partial S}+\frac{\partial\hat{x}_I}{\partial\tau}\right) \tag{B4a}$$

$$\hat{x}''=\frac{\partial^2\hat{x}_0}{\partial\tau^2}+\mu\left(\frac{\partial^2\hat{x}_I}{\partial\tau^2}+2\frac{\partial}{\partial S}\frac{\partial\hat{x}_0}{\partial\tau}\right) \tag{B4b}$$

Substituting Eqs (4a, b) into Eq. (1), the van der Pol equation becomes

$$\frac{\partial^2\hat{x}_0}{\partial\tau^2}+\hat{x}_0+\mu\left(\hat{x}_I+\frac{\partial^2\hat{x}_I}{\partial\tau^2}+2\frac{\partial}{\partial S}\frac{\partial\hat{x}_0}{\partial\tau}+\frac{\partial\hat{x}_0}{\partial\tau}\left(\hat{x}_0^2-1\right)\right)=0 \tag{B5}$$

Two equations are obtained from Eq. (5)

Fast time scale $O(1)$: $$\frac{\partial^2\hat{x}_0}{\partial\tau^2}+\hat{x}_0=0 \tag{B6a}$$

Slow time scale $O(\mu)$: $$\frac{\partial^2\hat{x}_I}{\partial\tau^2}+\hat{x}_I=-2\frac{\partial}{\partial S}\frac{\partial\hat{x}_0}{\partial\tau}-\frac{\partial\hat{x}_0}{\partial\tau}\left(\hat{x}_0^2-1\right) \tag{B6b}$$

The solution for Eq. (6a) is harmonic and can be written as

$$\hat{x}_0=r(S)\cos\left(\tau+\phi(S)\right) \tag{B7}$$

[1] See e.g. Figure 1 at.
[2] The detailed calculation of the approximate expressions for velocity and acceleration can be found at section 3 of this appendix.

where $r(S)$ and $\phi(S)$ are the slow-varying amplitude and phase of x_0. This solution comprised a slow-varying amplitude with fast oscillation the phase of which slowly change. To find $r(S)$ and $\phi(S)$ Eq. (7) is substituted into Eq. (6b) leading to

$$\frac{\partial^2 x_I}{\partial \tau^2} + x_I = -2\left[\dot{r}\sin(\tau+\phi) + r\dot{\phi}\cos(\tau+\phi)\right] + r\sin(\tau+\phi)\left[r^2\cos^2(\tau+\phi) - 1\right] \qquad \text{(B8)}$$

terms proportional to $\sin(\tau+\phi)$ and $\cos(\tau+\phi)$ are called *resonant terms*, they lead to solutions of the form $\tau\sin(\tau+\phi)$, known as secular terms, which grows to infinity and then are to be avoid. Using a trigonometric identity in the second term of Eq. (8), all the secular terms appears and Eq. (8) can be written as

$$\frac{\partial^2 x_I}{\partial \tau^2} + x_I = \left(2\dot{r} + \frac{r^3}{4} - r\right)\sin(\tau+\phi) + 2r\dot{\phi}\cos(\tau+\phi) + \frac{r^3}{4}\sin 3(\tau+\phi) \qquad \text{(B9)}$$

to avoid secular terms it is firstly necessary that $2r\dot{\phi} = 0$, then the ***slow-varying phase*** is given by

$$\boxed{\phi(S) = \text{constant}} \qquad \text{(B10)}$$

And secondly that

$$2\dot{r} + \frac{r^3}{4} - r = 0 \qquad \text{(B11)}$$

Equation (10) sets that for $\mu \ll 1$, the phase evolution is very slow so that it can be considered as constant. Separating the time variables from amplitude variables on Eq. (11) leads to

$$\int dS = \int \frac{8}{r\left(4 - r^2\right)} dr \qquad \text{(B12)}$$

and using partial fractions, Eq.(12) can be written as

$$\int dS = \int \left(\frac{2}{r} - \frac{1}{r-2} - \frac{1}{r+2}\right) dr \qquad \text{(B13)}$$

after integration of Eq. (13) leads to

$$C_1 - T = \ln\left(r^2 - 4\right) - \ln\left(r^2\right) \qquad \text{(B14)}$$

rearranging Eq. (14) leads to

$$r^2\left(1+Ce^{-T}\right)=4 \tag{B15}$$

where $C=-e^{C_1}$ is a constant. Solving for $r(T)$ the ***slow-varying amplitude*** is given by

$$r(S)=\frac{2}{\sqrt{1+Ce^{-S}}}=\frac{2}{\sqrt{1+Ce^{-\mu\tau}}} \tag{B16}$$

where *C* can be found by means of the ICs $\hat{x}(0)$ e $\hat{x}'(0)$ and is given by

$$C=\frac{4}{r_0^2}-1,\ \text{with}\ r_0=\sqrt{\hat{x}(0)^2+\hat{x}'(0)^2} \tag{B17}$$

and the oscillatory solution given by Eq. (7) leads to

$$x_0(\tau,S)=r(S)\cos(\tau+\phi)=\frac{2}{\sqrt{1+Ce^{-\mu\tau}}}\cos(\tau+\phi) \tag{B18}$$

where ϕ is constant. Hence the first order approximation given by Eq. (2) can be written as

$$x(\tau,\mu)\approx\frac{2}{\sqrt{1+Ce^{-\mu\tau}}}\cos(\tau+\phi)+O(\mu) \tag{B19}$$

Figure B.1 shows the time-domain displacement of a van der Pol oscillator obtained by means of numerical simulation of Eq, (1) (in blue) and its slow-varying amplitude obtained with Eq. (16) (in red).

Figure B.2 shows the experimental horizontal displacement of a metronome with $\text{ICs}=\left[\hat{x}_0,\ \hat{x}_0'\right]=\left[-3.8,\ 0\right]$ and the slow-varying amplitude for the same ICs obtained with Eq. (16) for $\mu=0.01$, $\mu=0.001$ and $\mu=0.002$. The metronome is oscillating at 200 bpm or (1.67 Hz) and the non-dimensional time in the figure corresponds to the time in seconds divided by the period of oscillation of the metronome. The non-dimensional amplitudes corresponds to twice the displacement divided by the maximum displacement at the steady-state, this comes from analogy with the amplitude of the van der Pol oscillator at the steady-state, which is equals two for light damping. Note that the value $\mu=0.0017$, obtained by eye, fits very well to the decrement in amplitude and the later stable amplitude described by the metronome. It can be seen that the experimental damping for the metronome is in the range $0.001<\mu<0.005$.

Figure B.1 – Time-domain displacement of the van der Pol oscillator obtained by means of numerical integration and slow-varying amplitude obtained by means of an analytical approximation, both for $\mu = 0.01$ and for ICs $\text{ICs} = [\hat{x}_0,\ \hat{x}'_0] = [4,\ 0]$. Oscillatory blue line – time-domain displacement of the van der Pol oscillator. Solid red envelope – slow-varying amplitude.

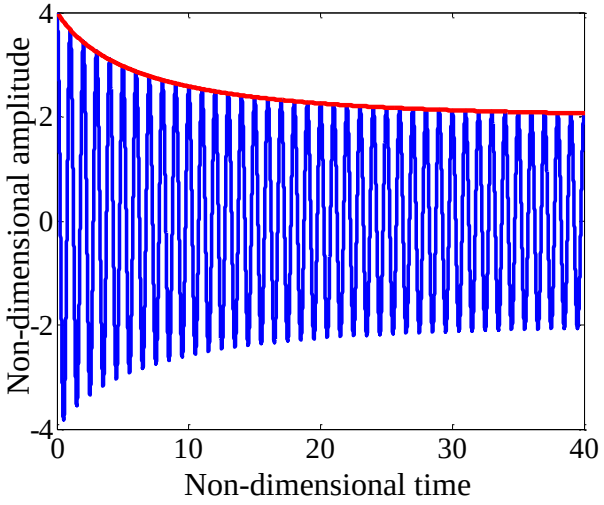

Source: Elaborated by the author.

Figure B.2 – Experimental time-domain displacement of a metronome obtained with Tracker® and three different slow-varying amplitudes corresponding to three different damping ratio values for $\text{ICs} = [\hat{x}_0,\ \hat{x}'_0] = [-3.8,\ 0]$. Slow-varying amplitude for $\mu = 0.001$ – dashed internal green line, for $\mu = 0.005$ - dotted external cyan line, for $\mu = 0.0017$ - solid middle red line. Characteristic decrement of the escapement mechanism with friction – dashed-dotted black straight lines.

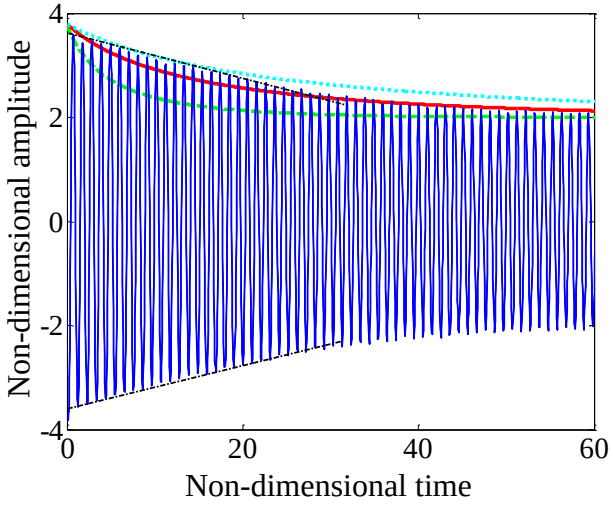

Source: Elaborated by the author.

Figure B.3 shows the damped oscillation of a metronome at 1.67 Hz. It can be seen the linear decrement of its amplitude, characteristic of an oscillating system with friction. In Figure B.3 the metronome has been set to oscillate inclined, in this position the escapement mechanism cannot put energy in the system and only its occurs friction between a tooth of the escapement

Figure B.3 – Experimental damped oscillation in time-domain of an inclined metronome at 1.67 Hz, obtained with Tracker®, showing its linear decay characteristic of a system damped by means of friction.

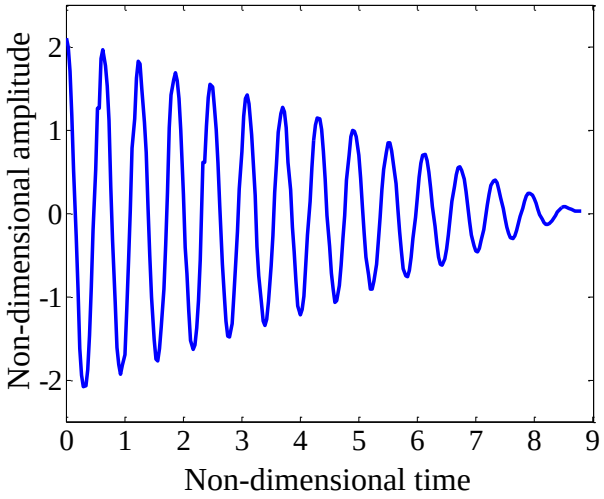

Source: Elaborated by the author.

Figure B.4 – Picture of a metronome oscillating inclined, damped by means of the friction between its internal pieces, during the data collecting with Tracker®.

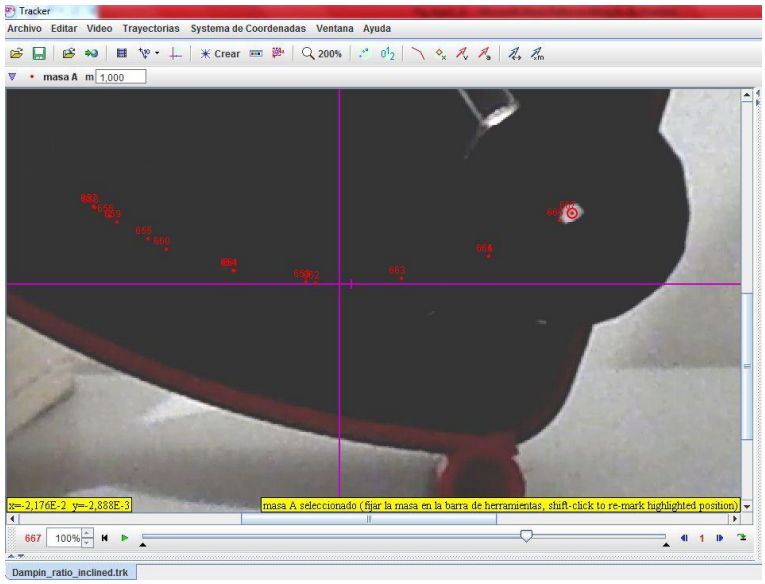

Source: Elaborated by the author.

gear (p8) and the pallet (p11) in Figure A.2. Figure B.4 shows a picture of the inclined metronome during the data collecting process. The next section shows the mathematical calculation of the expressions for velocity and acceleration used in this section.

B2. Additional Notes: Expression for Velocity and Acceleration

The expression for velocity Eq. (4a) is obtained from the chain rule

$$\hat{x}' = \frac{\partial \hat{x}(\tau, S)}{\partial \tau} = \frac{\partial \hat{x}}{\partial \tau}\frac{\partial \tau}{\partial \tau} + \frac{\partial \hat{x}}{\partial S}\frac{\partial S}{\partial \tau} \tag{B20}$$

considering that and $S = \mu\tau$ then

$$\hat{x}' = \frac{\partial \hat{x}(\tau, S)}{\partial \tau} = \frac{\partial \hat{x}}{\partial \tau} + \mu\frac{\partial \hat{x}}{\partial S} \tag{B21}$$

Substituting Eq. (2) into Eq. (21) leads to

$$\hat{x}' = \frac{\partial \hat{x}_0}{\partial \tau} + \mu\left(\frac{\partial \hat{x}_0}{\partial S} + \frac{\partial \hat{x}_I}{\partial \tau}\right) \tag{B22}$$

which is the expression for velocity Eq. (4a). The acceleration can be written as

$$\hat{x}'' = \frac{\partial \hat{x}'(\tau, S)}{\partial \tau} = \frac{\partial \hat{x}'}{\partial \tau}\frac{\partial \tau}{\partial \tau} + \frac{\partial \hat{x}'}{\partial S}\frac{\partial S}{\partial \tau} \tag{B23}$$

then

$$\hat{x}'' = \frac{\partial \hat{x}'(\tau, S)}{\partial \tau} = \frac{\partial \hat{x}'}{\partial \tau} + \mu\frac{\partial \hat{x}'}{\partial S} \tag{B24}$$

The first term of the right hand of Eq. (24) leads to

$$\frac{\partial \hat{x}'}{\partial \tau} = \frac{\partial}{\partial \tau}\left[\frac{\partial \hat{x}_0}{\partial \tau} + \mu\left(\frac{\partial \hat{x}_0}{\partial S} + \frac{\partial \hat{x}_I}{\partial \tau}\right)\right] = \frac{\partial^2 \hat{x}_0}{\partial \tau^2} + \mu\left(\frac{\partial}{\partial \tau}\frac{\partial \hat{x}_0}{\partial S} + \frac{\partial^2 \hat{x}_I}{\partial \tau^2}\right) \tag{B25}$$

The second term of the right hand of (24) leads to

$$\mu\frac{\partial \hat{x}'}{\partial S} = \mu\frac{\partial}{\partial S}\left[\frac{\partial \hat{x}_0}{\partial \tau} + \mu\left(\frac{\partial \hat{x}_0}{\partial S} + \frac{\partial \hat{x}_I}{\partial \tau}\right)\right] = \mu\frac{\partial}{\partial S}\frac{\partial \hat{x}_0}{\partial \tau} + O\left(\mu^2\right) \tag{B26}$$

Substituting Eq. (25) and (26) into Eq. (24) and avoiding terms of order μ^2 leads to

$$\hat{x}'' = \frac{\partial^2 \hat{x}_0}{\partial \tau^2} + \mu\left(\frac{\partial^2 \hat{x}_I}{\partial \tau^2} + 2\frac{\partial}{\partial S}\frac{\partial \hat{x}_0}{\partial \tau}\right) \tag{B27}$$

which is the expression for acceleration Eq. (5.4b).